

Aus der Klinik und Poliklinik für Psychiatrie und Psychotherapie

Klinik der Ludwig-Maximilians-Universität München

Vorstand: Prof Dr. med. Peter Falkai

**Cell-based monitoring and multiplexing of ERBB receptor activity, antagonist
selectivity and pathway responses.**



Dissertation

zum Erwerb Doktorgrades der Naturwissenschaften

an der Medizinischen Fakultät der

Ludwig-Maximilians-Universität zu München

vorgelegt von

Jan Peter Wintgens

aus

Aachen

2020

Mit Genehmigung der Medizinischen Fakultät
der Universität München

Betreuer: Prof. Dr. rer. nat. Moritz Rossner
Zweitgutachter(in): Prof. Dr. rer. nat. Axel Imhof
Mitbetreuung: Dr. Michael C. Wehr
Dekan: Prof. Dr. med. dent. Reinhard HICKEL
Tag der mündlichen Prüfung: 30.09.2020

Eidesstattliche Versicherung

Wintgens, Jan Peter

Hiermit erkläre ich an Eides statt,

dass ich die vorliegende Dissertation mit dem Thema

Cell-based monitoring and multiplexing of ERBB receptor activity, antagonist selectivity and pathway responses.

selbständig verfasst, mich außer der angegebenen keiner weiteren Hilfsmittel bedient und alle Erkenntnisse, die aus den Schrifttum ganz oder annähernd übernommen sind, als solche kenntlich gemacht und nach ihrer Herkunft unter der Bezeichnung der Fundstelle nachgewiesen habe.

Ich erkläre des weiteren, dass ich die hier vorgelegte Dissertation nicht in gleicher oder in ähnlicher Form bei einer anderen Stelle zur Erlangung eines akademischen Grades eingereicht wurde.

München den 3. März 2021

Ort, Datum

Jan Wintgens

Unterschrift des Doktoranden

“The right understanding of any matter and a misunderstanding of the same matter do not wholly exclude each other.”

— Franz Kafka

Abstract

Background: Schizophrenia is a severe mental disorder that manifests in positive and negative symptoms, and cognitive deficits. The disturbance of synchronous network activity that is maintained by the balanced interplay between excitatory pyramidal neurons and inhibitory interneurons is implicated in schizophrenia. At the molecular level, an activated Neuregulin-ERBB4 pathway impacts on disrupting the excitation-inhibition (E/I) balance. Conversely, decreasing enhanced ERBB4 activity may restore the E/I balance.

Results: In a cell-based assay using the split TEV technology, we screened FDA-approved drugs that antagonize ERBB4 activity. Spironolactone was recovered as best candidate from the screen and was validated to reduce phosphorylation levels of ERBB4 using biochemistry. Together with the findings from electrophysiology and mouse behavior studies, we concluded that spironolactone improves the E/I balance by decreasing ERBB4 phosphorylation. However, spironolactone is not selective for ERBB4 among the ERBB family. To address selectivity, a universal RTK adapter suitable for cell-based high-throughput screening assays was designed. The clustered SH2(GRB2) domain adapter increased the comparability of RTK assays and allowed to better assess compound selectivity across targets.

Outlook: Using RNA barcode reporters we can monitor the activity of multiple targets and pathways simultaneously. Using such a multiplexing approach, we will be able to profile compound actions in early drug discovery.

Table of Contents

Eidesstattliche Versicherung	3
Abstract	5
List of Abbreviations.....	7
List of Publications.....	9
Introduction	10
Genetics of Schizophrenia.....	11
Theories for the pathoetiology of schizophrenia	12
Neurodevelopmental causes of Schizophrenia	14
Predictive coding and the disconnection hypothesis	14
The excitation inhibition balance	16
The NRG1-ERBB4 Pathway.....	19
The ERBB family is a subfamily of receptor tyrosine kinases	21
The split TEV protein complementation Assay.....	22
Zusammenfassung.....	25
Summary	27
Research Article I.....	28
Research Article II.....	61
Perspective and discussion.....	98
Multiplexed assays for profiling receptor activities and physiological signaling.....	99
Agonist treatment of the ERBB family and HTR2A	100
Antagonist treatment of the ERBB family and HTR2A	102
Pathway sensor responses to antagonist treatments	104
Discussion	105
Bibliography	108
Acknowledgment.....	117

List of Abbreviations

Brain derived neurotrophic factor (BDNF)

cAMP response element (CRE)

Concatenated SH2 domains from GRB2 SH2(GRB2)

Dopamine receptor 2 (DRD2)

Early growth response protein 1 promoter (EGR1p)

Epidermal growth factor (EGF)

Epidermal growth factor receptor (EGFR)

Erb-b2 receptor tyrosine kinase 2 (ERBB2)

Erb-b2 receptor tyrosine kinase 3 (ERBB3)

Erb-b2 receptor tyrosine kinase 4-(ERBB4)

Excitation inhibition balance (E/I balance)

G protein coupled receptors (GPCRs)

GAL4-VP16 (GV)

Genome-wide association studies (GWAS)

Growth factor receptor-bound protein 2 (GRB2).

High-throughput screening (HTS)

Inhibitory concentration of 50% (IC₅₀)

Mitogen-activated protein kinase (MAPK)

Neuregulin (NRG)

Neuregulin 1 (NRG1)

N-methyl D-aspartate (NMDA)

Parvalbumin positive (PV-positive) interneurons

Phosphatidylinositol 3-kinase regulatory subunit alpha (PIK3R1)

Phosphotyrosine (p-Tyr) motifs

Phosphotyrosine-binding (PTB) domain

Protein complementation assays (PCA)

Protein-protein interaction (PPI)

SHC-transforming protein 1 (SHC1)

Single-nucleotide polymorphisms (SNPs)

Src homology 2 (SH2) domain

TEV-specific cleavage site (tcs)

Upstream activating sequence (UAS)

α -amino-3-hydroxy-5-methyl-4-isoxazolepropionic acid (AMPA)

List of Publications

Wehr MC, Hinrichs W, Brzózka MM, ... Wintgens JP, et al (2017) Spironolactone is an antagonist of NRG1-ERBB4 signaling and schizophrenia-relevant endophenotypes in mice. EMBO Mol Med.

Wintgens JP, Rossner MJ, Wehr MC (2017) Characterizing dynamic protein-protein interactions using the genetically encoded split biosensor assay technique split TEV. Methods Mol Biol 1596:219–238.

Wintgens JP, Wichert SP, Wehr MC et al (2019) Monitoring activities of receptor tyrosine kinases using a universal adapter in genetically encoded split TEV assays. Cell Mol Life Sci. PMID: 30623207

Introduction

Schizophrenia is a mental syndrome that influences feelings, behavior, and cognition of a person. The symptoms can be classified into three groups. 1) Positive symptoms, like hallucinations and delusions; 2) negative symptoms, such as anxiety and loss of motivation; and 3) cognitive impairment, including memory function and attention span. The symptoms typically appear gradually, starting in adolescence and, in most cases, never resolve (van Os and Kapur, 2009). The prevalence in the world's population is between 0.3% and 0.7% (Saha et al., 2005). Schizophrenia is a complex disease, meaning that a genetic burden contributes together with environmental factors to the outbreak and severity. This complexity is represented in the "Two-Hit" hypothesis of schizophrenia (shown in figure T1) (Bayer et al., 1999). It states that there is first a hit of neurodevelopmental alterations based on the genetic load, leaving the neuronal circuitry vulnerable to the second hit of environmental factors later in life (Insel, 2012; Rapoport et al., 2012). There is some evidence of neurobiological alterations in schizophrenia like reduced connectivity (Schmitt et al., 2011) and thinner cortical structures (Shaw et al., 2007). However, unlike the neuronal degeneration in Alzheimer's disease or the specific lesion in the substantia nigra in Parkinson's, schizophrenia does not have a single neurobiological cause (Maynard et al., 2001). Instead, the pathological mechanisms remain mostly unclear and are subject to current research and hypotheses. Despite scientific progress and knowledge about schizophrenia, new treatments, especially of the negative and cognitive symptoms, have not been developed in the past years (Insel, 2012).

„Two hit“ model of schizophrenia

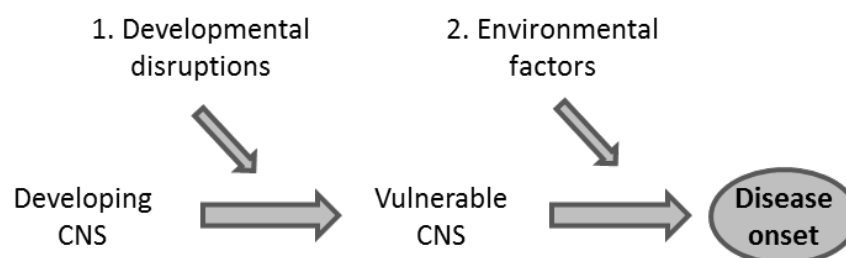


Figure T1: Two Hit Model of Schizophrenia suggests that disruptions in the first hit the development of the central nervous system (CNS) produce a vulnerability to the disorder but that the onset of symptoms in a vulnerable brain would be triggered by the second hit of environmental factors. Adapted from (Maynard et al., 2001).

Genetics of Schizophrenia

Schizophrenia has a high heritability of around 60-80% as shown by twin and family studies (Lichtenstein et al., 2009; Sullivan et al., 2003). To study the genetic loci behind this heritability so called genome-wide association studies (GWAS) are conducted. In GWAS, a genome-wide set of genetic variants, specifically single-nucleotide polymorphisms (SNPs), in different individuals are observed and a case versus control comparison is made. The advantage of GWAS is that it is not hypothesis driven. The SNPs tested are spread all over the genome and do not necessarily lie in a coding region of a gene. The latest GWAS in schizophrenia identified 145 risk loci from a meta-analysis integrating the results from a study including up to 36,989 cases compared to 113,075 controls (Schizophrenia Working Group of the Psychiatric Genomics Consortium, 2014) and further 11,260 independent cases and 24,542 controls (Pardiñas et al., 2018). This means schizophrenia is a highly polygenic disease. As a biological marker is lacking the cohorts are grouped functionally with symptoms and science. This big aetiological heterogeneity is overcome by the high case numbers used in GWAS. The most relevant genetic factors are identified due to the large cohort numbers providing high statistical power. Therefore, a higher reproducibility than in the older more hypothesis driven genetic studies is achieved. In the loci presented are both, risk genes that have not been associated with schizophrenia before, and genes where an association to the disease has been discussed previously. Examples for the latter case are the dopamine D2 receptor (DRD2) and a subunit of the N-methyl D-aspartate (NMDA) type glutamate receptor called glutamate ionotropic receptor NMDA type subunit 2A (GRIN2A) (Pardiñas et al., 2018). The strongest genetic association involves major histocompatibility complex variations, arising from structurally diverse alleles in the complement component 4 (Schizophrenia Working Group of the Psychiatric Genomics Consortium et al., 2016). Additionally, the GWAS shows suggestive evidence by weaker genetic association for the Neuregulin 1 (NRG1)- erb-b2 receptor tyrosine kinase 4-(ERBB4) pathway that was one of the first pathways that has been connected to schizophrenia (Balu and Coyle, 2011; Mei and Nave, 2014; Schizophrenia Working Group of the Psychiatric Genomics Consortium, 2014). Additionally, ERBB4 is a druggable target in this pathway.

Theories for the pathoetiology of schizophrenia

An early theory about the neurobiological causes of schizophrenia symptoms is linked to the DRD2 risk gene and is called the dopamine theory. It was created on the basis of finding that an inhibition of DRD2 reduced positive symptoms in mice (Carlsson and Lindqvist, 1963). Other studies showed that the effects of antipsychotic drugs in the clinic correlated with their dopamine receptor affinity (Creese et al., 1976; Seeman and Lee, 1975). However, negative and cognitive symptoms could not be explained using this initial model.

As a general idea of the mechanisms and pathways behind the disease was lacking, the hypothesis was reverse engineered from the treatable targets, the dopaminergic mechanism in the brain (Meltzer and Stahl, 1976). This interpretation of evidence led to limitations in the hypothesis. The drugs used, in addition to their effect on dopamine, alters the signaling of other neurotransmitters (Davis et al., 1991). Additionally, the locus in the brain where the dopaminergic signaling was altered was not known at the time. Finally, the theory was only able to explain the positive symptoms of the disease. Nevertheless, the dominant theory strongly influenced the search for treatments towards the dopaminergic mechanisms in the prefrontal cortex (Schwartz et al., 2012). Subsequently, antipsychotic drugs form the mainstay in schizophrenia treatment today (Andrews et al., 2003).

With the dopamine theory as a basis, and its limitations apparent, the hypothesis has been extended by the glutamate theory. It was shown that antagonists of NMDA type glutamate receptors (NMDARs) , such as ketamine or phencyclidine, could induce all three symptom groups (Coyle, 2012; Javitt, 2010). While the dopaminergic transmitters are a regionally distinct system, NMDARs are expressed all over the brain. The glutamate theory therefore incorporates alterations connected to schizophrenia also in the cortex and subcortical regions. At first, a glutamatergic neurotransmission deficit was postulated. Over the years, the theory has been developed further and many glutamate receptors were linked to the theory; however, the primary involvement of dysfunctional NMDA receptor prevailed (Stone et al., 2007) a finding that is supported by the candidate risk gene GRIN2A, a NMDAR subunit (Pardiñas et al., 2018). Additionally, alterations to glutamatergic functioning were found in post-mortem studies. For example, expression of glutamate receptors, especially the levels of the subunit NMDAR1 in the superior frontal cortex as well as the superior temporal cortex

were shown to be reduced (Humphries et al., 1996; Sokolov, 2002). These findings have, however, been inconsistent. The problem seems not to be caused by the general expression level, but rather in an altered localization of the NMDA receptor (E. McCullumsmith et al., 2012; Hammond et al., 2014). This irregular trafficking could arise from changes that target proteins involved in the trafficking process itself, or the binding capacities between NMDARs and these auxiliary proteins (Funk et al., 2009).

The two theories do not contradict and could therefore both play a role in the neurological cause of schizophrenia. The activity of dopaminergic neurons is regulated by the projections of glutamatergic neurons to the dopamine nuclei in the midbrain. These nuclei, therefore are sensitive to both changes of the glutamatergic and dopaminergic signaling (Mcguire et al., 2008; Miller and Abercrombie, 1996).

Given the already discussed variety of loci found in the GWAS to be involved in Schizophrenia, and the complexity that arises from the aforementioned theories of pathoetiology it is unlikely that schizophrenia and its symptoms in all cases arise from a single cause (Horváth and Mirnics, 2015; Howes and Kapur, 2014).

Both theories are reverse engineered from findings that drugs induce or reduce symptoms of schizophrenia. This approach is relevant as it does show a druggable target of the disease immediately. As mentioned, most of the drugs used for schizophrenic patients are addressing the positive symptoms of the disease. The search for new druggable targets, especially for the other two symptom classes in schizophrenia shifted the attention to the neurological basis of the disease.

Neurodevelopmental causes of Schizophrenia

Schizophrenia today is seen as a neurodevelopmental disease (Insel, 2010). The variety of genetic alterations influences the development of the central nervous system (CNS) right from its start. For example, there is evidence for NMDAR alterations to play a role in various developmental issues in the CNS. The formation of dendritic spines and growth of dendritic trees is disrupted by NMDAR hypofunction (Monfils and Teskey, 2004; Sin et al., 2002). The myelination of axons is also affected, here by the alteration of NMDARs through neuregulin 1 (NRG1) and brain-derived neurotrophic factor (BDNF) (Lundgaard et al., 2013). This implies that white matter changes can be a consequence, not a cause, of diverging synaptic plasticity by modulations of the NMDA receptors. However, there is currently some debate whether myelination factors may also play an active role in eliciting schizophrenia (Raabe et al., 2018). This argumentation opens schizophrenia research up for neurogenetic connectivity studies. In bipolar disorder for example, descending connectivity from the prefrontal cortex and its selective failure has already been shown (Radua et al., 2013). Understanding the importance of NMDAR signaling in schizophrenia patients and in CNS development, a theory was developed, not only reverse engineered from the effects of different drugs, but also based on a top-down theory of how we perceive the world in general. This model integrates schizophrenia-relevant brain structures, such as the nucleus accumbens and prefrontal cortex, and was connected to the three symptom classes.

Predictive coding and the disconnection hypothesis

The disconnection hypothesis of schizophrenia is based on the idea that the brain is a statistical Bayesian organ. It generates hypotheses of what sensory input will be received and tests these against the sensory evidence. This paradigm has already been proposed by Helmholtz with the idea of unconscious interference (Helmholtz, 1866). Over time, the perspective has been developed to include the causes of our sensations as hierarchical Bayesian interference and the way these interferences generate beliefs and behavior (Clark, 2013; Dayan et al., 1995; Friston et al., 2006; Lee and Mumford, 2003).

Predictive coding means that higher levels of cortical hierarchies create predictions of representations and compare them to the representations coming from lower levels, a scheme is presented in figure T2. The representations from lower levels initially come from the sensory input. The difference between these two representations is manifested as

prediction error, which is associated with superficial pyramidal cells and their activity. The prediction error is transmitted back up in the hierarchy, to enable the generation of an updated higher representation, a process connected to deep pyramidal cells and their activity. This recursive transition leads to a shrinking of the prediction error until its suppression, with finally providing a hierarchical explanation of the sensory input at every level (Rauss and Pourtois, 2013).

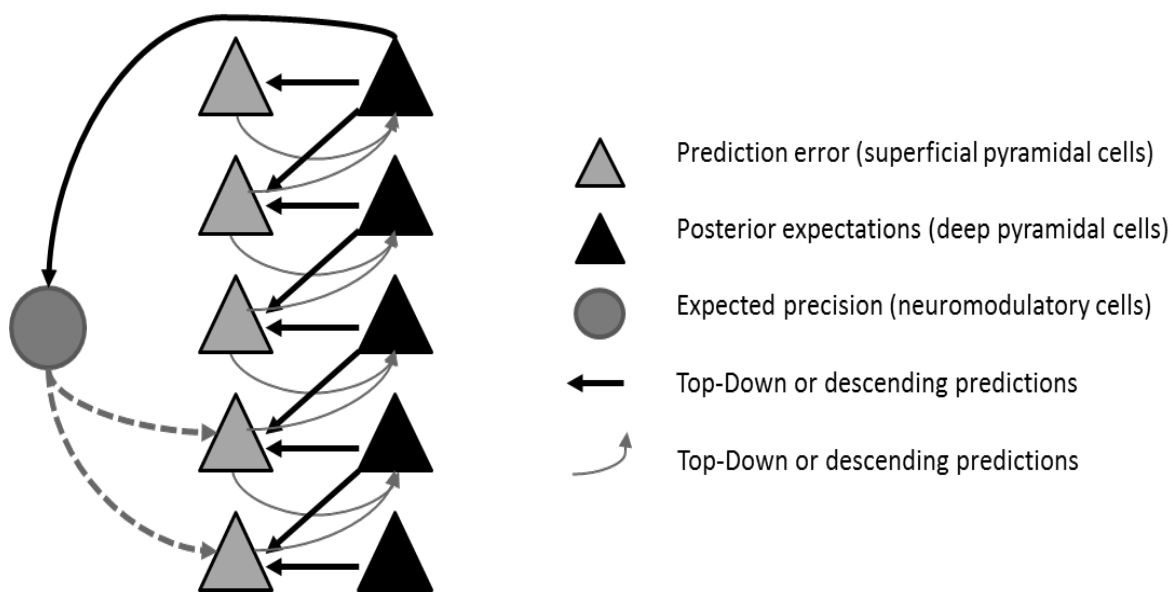


Figure T2: This figure summarizes the neuronal message passing that underlies predictive coding. The basic idea is that neuronal activity encodes expectations about the causes of sensory input, where these expectations minimize prediction error. Prediction error is the difference between (ascending) sensory input and (descending) predictions of that input. This minimization rests upon recurrent neuronal interactions between different levels of cortical hierarchies. Anatomical and physiological evidence suggests that superficial pyramidal cells (grey triangles) compare the representations (at each level) with top-down predictions from deep pyramidal cells (black triangles) of higher levels. This schematic shows a simple cortical hierarchy with ascending prediction errors and descending predictions. This graphic includes neuromodulatory gating or gain control (dotted lines) of superficial pyramidal cells that determines their relative influence on deep pyramidal cells encoding expectations (in the same level and the level above). Note that the implicit descending gain control rests on predictions of the precision of prediction errors at lower levels – and can be thought as mediating top-down attentional gain. Every top-down prediction is reciprocated with a bottom-up prediction error to ensure predictions are constrained by sensory information. Adapted from (Friston et al., 2016).

The recursive ascending and descending signaling is mostly mediated by NMDARs. The disconnection hypothesis combines the predictive coding approach with the importance of NMDAR signaling and the known defects observed in schizophrenia patients. The disconnection hypothesis specifically emphasizes the role of transmitters and proteins that modulate NMDAR localization. These modulations then lead to alterations in synaptic efficacy. For example, NMDAR conductivity may be altered via phosphorylation, subunit expression, and trafficking (Stephan et al., 2009). Importantly, the disconnection hypothesis describes the physiological consequences of NMDAR mediated plasticity and how these transfer into impairment of computation in the neuronal circuits (Friston et al., 2016).

The excitation inhibition balance

During predictive coding, coordination of activity of the individual brain regions, layers, and neurons is key (Miller and Cohen, 2001). This coordination is achieved by synchronous inhibition of pyramidal neurons (Gonzalez-Burgos et al., 2010), a process referred to as the excitation-inhibition balance (E/I balance). When excitation surpasses inhibition, activity will increase to the maximum, or when inhibition is induced by this maximum, network activity will lead to a balanced state. The same holds true for inhibition surpassing excitation, either quieting the circuit or sparking more excitation in the process, again leading to a balanced activity in the network (Sohal and Rubenstein, 2019). It was shown that in cortical layer 2/3 optimal tuning of E/I balance produced neuronal activity responses that are referred to as neuronal avalanches and optimized information processing in the network (Shew et al., 2011).

This crucial balance is mainly mediated by parvalbumin-positive (PV-positive) GABAergic interneurons (Cardin et al., 2009; Sohal et al., 2009) that themselves are connected to glutamatergic neurons as input and output. These connections form a so-called microcircuit shown in figure T3. This simplified version shows how a glutamatergic neuron excites a downstream glutamatergic neuron and an inhibitory neuron that subsequently can inhibit the activity of the second glutamatergic neuron. In reality, glutamatergic neurons receive input from a variety of inhibitory and excitatory neurons, which themselves are connected to a variety of functionally diverse neurons (Elert, 2014; He and Cline, 2019). The number of neurons involved in the E/I balance is highly regulated, as is the number of synapses on individual cortical pyramidal neurons (Hengen et al., 2013; Iascone et al., 2018).

Interneurons are important for the E/I balance that matures until adolescence, a timeframe correlating with the outbreak of schizophrenia (Insel, 2010). While there is little evidence coming from human adolescent post-mortem neuroanatomy, studies in nonhuman primate brains show that during early adulthood the refinement of circuits involves pruning of excitatory synapses, inhibitory circuit maturation, and continuous targeting of pyramidal dendrites by inhibitory input (Hashimoto et al., 2009; Lewis and González-Burgos, 2008; Rakic et al., 1986).

In summary, interneuron activity is crucial for the functioning of the neuronal network as it synchronizes excitatory neuronal activity through inhibition. The expression of the NMDA receptors, which are responsible for transmission of the glutamatergic signal are unchanged in Schizophrenia patients. Subsequently the focus of attention, as described in the disconnection hypothesis lies on mechanisms that modulate the E/I balance. One of the pathways that is able to alter NMDAR trafficking and is the NRG1-ERBB4 pathway (Mei and Nave, 2014).

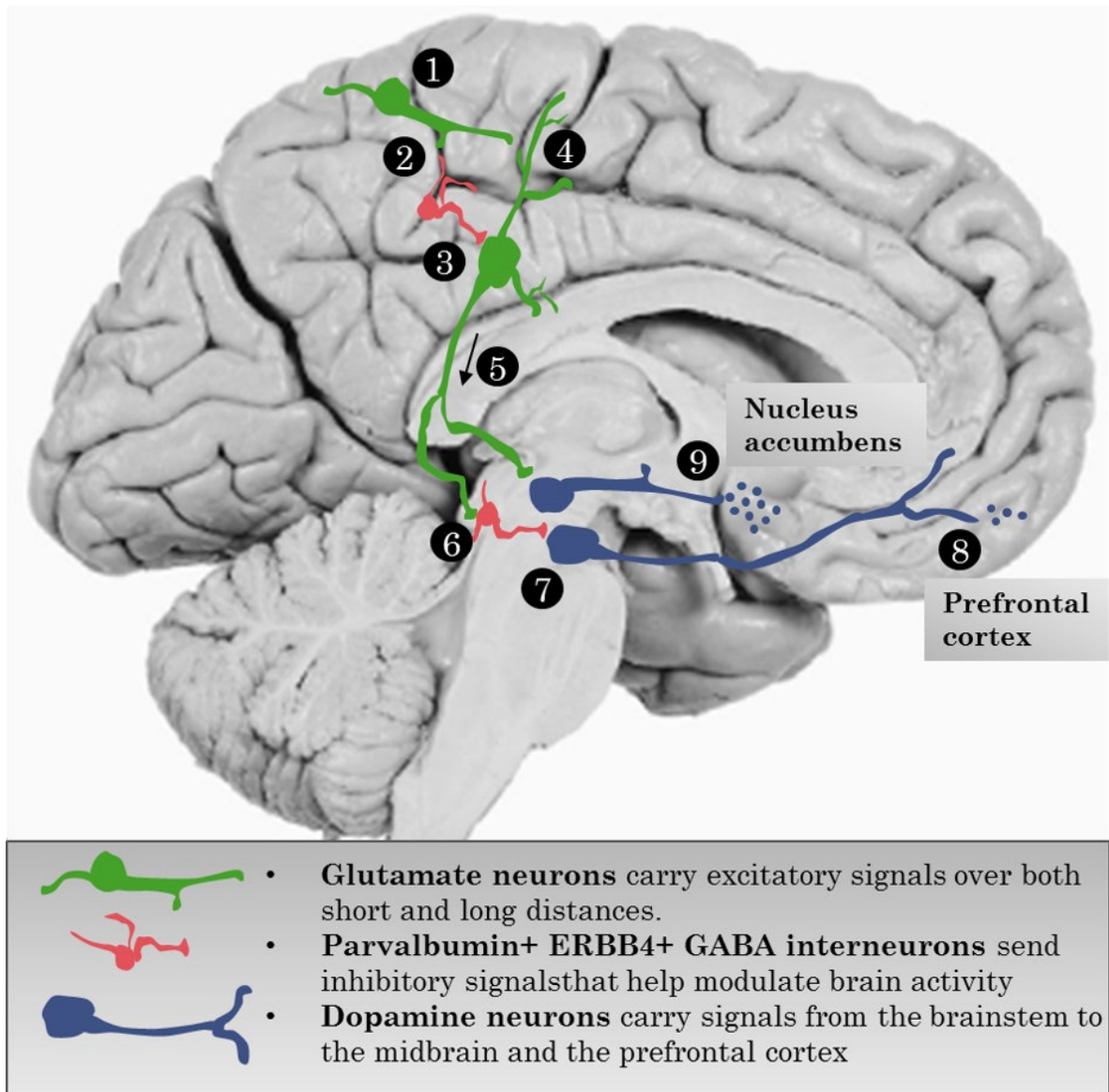


Figure T3: Example of a microcircuit and its impact on schizophrenia. (1) Principle neuron fires and generates electric pulse; signal arrives at synapse releasing glutamate (2); glutamate binds to receptor on GABAergic interneurons, in schizophrenia this connection is abnormal, decreasing the interneuron activity (3). (4) Activity of the second glutamate neuron is increased due to decreased GABAergic inhibition (5), at the synapses (6) too much glutamate is released, overstimulating a dopaminergic neuron. (7) GABA interneuron over inhibits a different dopaminergic neuron suppressing its activity. Resulting in (8) a decreased dopaminergic neuronal signal to the prefrontal cortex, leading to negative symptoms. (9) Hyperactive dopamine signaling in midbrain, leading to positive symptoms. Adapted from (Elert, 2014).

The NRG1-ERBB4 Pathway

The NRG1-ERBB4 Pathway is associated with several functions in the developing and matured brain. As it is specifically connected to synaptic maturation and plasticity it is connected to several psychiatric disorders, such as autism, bipolar disorder and schizophrenia (Kenny et al., 2014; Mei and Nave, 2014). The combination of NMDAR hypofunction only in PV interneurons and subsequent increase in glutamatergic signaling and how that influences the E/I balance brings the NRG1-ERBB4 pathway into focus for schizophrenia as seen in the disconnection hypothesis. Notably, ERBB4 is selectively expressed in PV interneurons (Fazzari et al., 2010; Vullhorst et al., 2009).

ERBB4 is a receptor tyrosine kinase (RTK) and together with EGFR, ERBB2 and ERBB3 belongs to the ERBB sub-family of RTKs (Lemmon and Schlessinger, 2010). NRG1 is a trophic factor that contains an epidermal growth factor (EGF) like domain and belongs to the neuregulin family that acts on the ERBB family as ligands for activation (Britsch, 2007). RTKs and their signaling will be described in more detail later in this introduction.

It has been shown that ERBB4, when activated, associates with NMDA receptors leading to an internalization of both receptors. Subsequently, NMDAR, but not α -amino-3-hydroxy-5-methyl-4-isoxazolepropionic acid (AMPA) receptor, currents are downregulated (Vullhorst et al., 2015). NRG1 acutely dampens the excitability of ErbB4-expressing interneuron by depolarizing the firing threshold (Janssen et al., 2012). Additionally, ERBB4 splicing patterns are involved in the regulation of excitatory synapse formation onto PV interneurons (Chung et al., 2016, 2017, 2018). ERBB4 is specifically expressed in PV interneurons, while NRG1 maybe expressed both pre- and post-synaptic (Vullhorst et al., 2017) and personal communication with Markus Schwab) In agreement, NRG1 overexpression and NMDAR hypofunction in PV interneurons has been connected to schizophrenia symptoms recently (Bygrave et al., 2019; Kotzadimitriou et al., 2018). In an in vivo study on healthy subjects GABA concentrations were predicted by genetic variation in ErbB4 (Marenco et al., 2011).

In addition, an increased expression of NRG1 was found in schizophrenia patients in a number of postmortem studies (Hashimoto et al., 2004; Law et al., 2006; Weickert et al., 2012).

In line with these findings, a hyperphosphorylation of ERBB4 was also found in postmortem brains in schizophrenia patients (Hahn et al., 2006). Furthermore, increased expression of the

ERBB4-JM-a-CYT-1 variant carrying a PI3K-recruitment domain has also been detected in schizophrenics (Silberberg et al, 2006; Law et al, 2007, 2012), supporting the notion that the NRG1-ERBB4 signaling is elevated in patients. Nrg1-ErbB4 signaling is also increased during neuronal activity linked to limbic seizure (Tan et al., 2012) and spontaneous seizures are increased when ErbB4 is lost in PV Interneurons promoting kindling progression (Li et al., 2012b; Tan et al., 2012). All these findings show that the NRG1-ERBB4 pathway is regulating NMDAR function and hence plays a role in the E/I balance.

NRG1-ERBB4 signaling also plays a role in the development of the brain, specifically in different stages of circuit development in the cortex (Mei and Nave, 2014). The migration of interneurons during the development of the cortex is regulated by NRG1 (Flames et al., 2004; Li et al., 2012a). ErbB4 mutant mice show reduced amounts of GABAergic interneurons in the cortex, it is however unclear if genesis and/or survival of those interneurons are changed. Synapse formation in cortical circuits is also connected to NRG-ERBB signaling. The generation and maturation of excitatory synapses signaling on to GABAergic interneurons is promoted (Abe et al., 2011; del Pino et al., 2013; Ting et al., 2011). Transgenic mice with increased Nrg1 expression show schizophrenia relevant behavioral deficits, such as hyperactivity, decreased sensorimotor gating, impaired social interaction, and reduced cognitive functions (Deakin et al., 2009, 2012; Kato et al., 2010). Schizophrenia risk genes are known to cause overlapping behavioral and synaptic plasticity phenotypes both at gain and loss function, as exemplified for transcription factor 4 (TCF4), which is one of the best replicated risk genes for schizophrenia (Badowska, 2015; Brzózka et al., 2010). Likewise, reduced and elevated NRG1 levels in cortical projection neurons lead to reduced synaptic plasticity and impaired inhibitory neurotransmission, arguing that NRG1 levels need to be maintained at an optimal level to guarantee a balanced excitatory and inhibitory neurotransmission (Agarwal et al., 2014).

In summary, these findings suggest that the NRG1-ERBB4 risk pathway plays a role in schizophrenia pathophysiology, likely by influencing PV interneuronal signaling and thus altering the E/I balance.

Elucidating the mechanisms regulated by the NRG1-ERBB4 pathway is not only central to understanding the basis of schizophrenia but will be also useful for the treatment of the disease, as ERBB4 as a receptor is a druggable target. It is for example speculated, that treatments to increase NMDAR function, e.g. by decreasing ERBB4 activity, could reduce

oxidative stress and boost the function of PV interneurons and therefore might be beneficial for schizophrenia (Powell et al., 2012). In mouse studies it has been shown that endophenotypes caused by increased NRG1 levels are reversible in adult animals. This indicates that NRG1-ERBB4 signaling could principally function as a target for pharmacological intervention in patients (Luo et al., 2014; Yin et al., 2013). As impaired NRG1-ERBB4 signaling is implicated in all three symptom classes of schizophrenia (Agarwal et al., 2014; Luo et al., 2014), a pharmacological intervention might be beneficial through optimizing the E/I balance.

In general, the need to explore new targets and develop directed therapies for schizophrenia is high (Nestler and Hyman, 2010). Many Pharma companies have withdrawn from research on severe mental disorders due to the complex nature and the still limited mechanistic understanding of these diseases (Margraf and Schneider, 2016). As already mentioned current medication is mostly targeting the positive symptoms of schizophrenia (Insel, 2012). Additionally, drug development campaigns for drugs targeting the negative symptoms have failed, for example the clinical trials for bitopertin (Bugarski-Kirola et al., 2017). One of the options could be to use drug repurposing, where already approved drugs are monitored for additional or different usage, presenting a swift way towards clinical application (Insel, 2012; Lencz and Malhotra, 2015). In conclusion, there is a need to develop better and more specific assays to find drugs and monitor their efficacy and side effects.

The ERBB family is a subfamily of receptor tyrosine kinases

There are 58 receptor tyrosine kinases known in humans, the kinases can be divided into 20 sub families, one of which is the ERBB sub family (Lemmon and Schlessinger, 2010). RTKs are, together with G protein coupled receptors (GPCRs), one of two most important drug targets in human cells (Santos et al., 2017). When RTKs are stimulated, they dimerize as homo or hetero dimers restricted to their sub family. Dimerization leads to a kinase domain-mediated cross phosphorylation of the phosphotyrosine (p-Tyr) motifs present in the cytoplasmic receptor. Upon phosphorylation, an adapter is recruited binding to those phosphorylated p-Tyr motifs. To bind, the adapter needs a Src homology 2 (SH2) domain or a phosphotyrosine-binding (PTB) domain (Yaffe, 2002). There are 120 different SH2 domains in 110 different proteins, making this the largest class of p-Tyr recognition domains (Liu et al., 2006), with the most important ones for the ERBB family being Phosphatidylinositol 3-kinase regulatory

subunit alpha (PIK3R1), SHC-transforming protein 1 (SHC1), and Growth factor receptor-bound protein 2 (GRB2). The specificity of binding between different receptors and adapters is important for the initiation of specific downstream signaling and correlates to the selectivity of receptor activity (Davis et al., 2011). This specificity is caused by the interplay between the amino acid residues sequence flanking the tyrosine of the p-Tyr motif and the residues in the SH2 domain itself. Their interaction and non-covalent binding define the binding strength and therefore the selectivity of binding between different sequences (Tinti et al., 2013). Apart from its impact in schizophrenia, the ERBB sub family is known to be involved in, amongst other diseases, breast cancer and non-small cell lung cancer. The ERBB family is also critical for development, as exemplified by the heart deficiency observed in *ErbB4* full knockout mice that are not vital. To date, many inhibitors that are selective for the sub family, such as lapatinib, have been developed (Davis et al., 2011). However, these inhibitors are not selective for a single family member causing side effects due to the wide range of physiological functions the different ERBBs exert in the body. Despite the importance of RTKs in various diseases, only 3% of marketed drugs target kinases (Santos et al., 2017). The development of a cell-based assay system that robustly and sensitively assesses the selectivity of RTKs may therefore contribute to the development of better medicines.

The split TEV protein complementation Assay

A protein fragment complementation assay (PCA) measures a protein-protein interaction (PPI), such as the recruitment of an adapter by a receptor or the dimerization of two receptors. PCAs are cell-based and genetically encoded, allowing the assessment of the interaction in its natural cellular environment. In a PCA, a reporter protein is split, and each part is covalently bound to the two proteins to be studied for an interaction. These interaction partners under study are termed bait and prey. Upon interaction of the two candidate proteins, the two moieties of the reporter protein functionally complement and thus regains activity. This activity is then translated into a stable and quantifiable read out. The first PCA experiment described used a split β -galactosidase (Rossi et al., 1997), followed by analogous approaches for GFP and luciferase (i.e. firefly, Renilla, Gaussia). This direct read out of split reporter activity was extended by fusing an artificial transcription factor to one moiety of the split reporter. Once this reporter complements, the transcription factor is cleaved off and migrates to the nucleus to induce a reporter gene of choice, such as a fluorescent protein or a luciferase. This

approach enables the signal indicating an occurred protein-protein interaction to be enhanced. The split ubiquitin and the split TEV (shown in figure T4) approach are the most renowned examples of this approach (Wehr and Rossner, 2016). The split TEV technique has previously been used to monitor dynamic PPIs in both the cytosol and at the membrane in a robust, sensitive, and reproducible manner (Wehr et al., 2008, 2006). The split TEV system was used to monitor receptor tyrosine kinase activity in both the publications shown below.

The split TEV method uses the functional complementation of two previously inactive fragments of the tobacco etch virus (TEV) protease (Wehr et al., 2006). The moieties have been termed NTEV and CTEV, and they are each fused to one of the interaction candidate proteins. The artificial transcription factor GAL4-VP16 (GV) is fused to NTEV via a TEV-specific cleavage site (tcs) in between. When the two candidate proteins interact, the TEV protease regains its activity, cleaving off GV at tcs, and therefore enabling GV to migrate to the nucleus. Here, GV binds to clustered upstream activating sequences (UAS). Upon binding of GV to UAS, the transcription of the firefly luciferase reporter gene is initiated. Independently, a *Renilla* luciferase is co-expressed under the control of the constitutive thymidine kinase promoter to monitor transfection efficiencies and simple off target effects, such as toxicity.

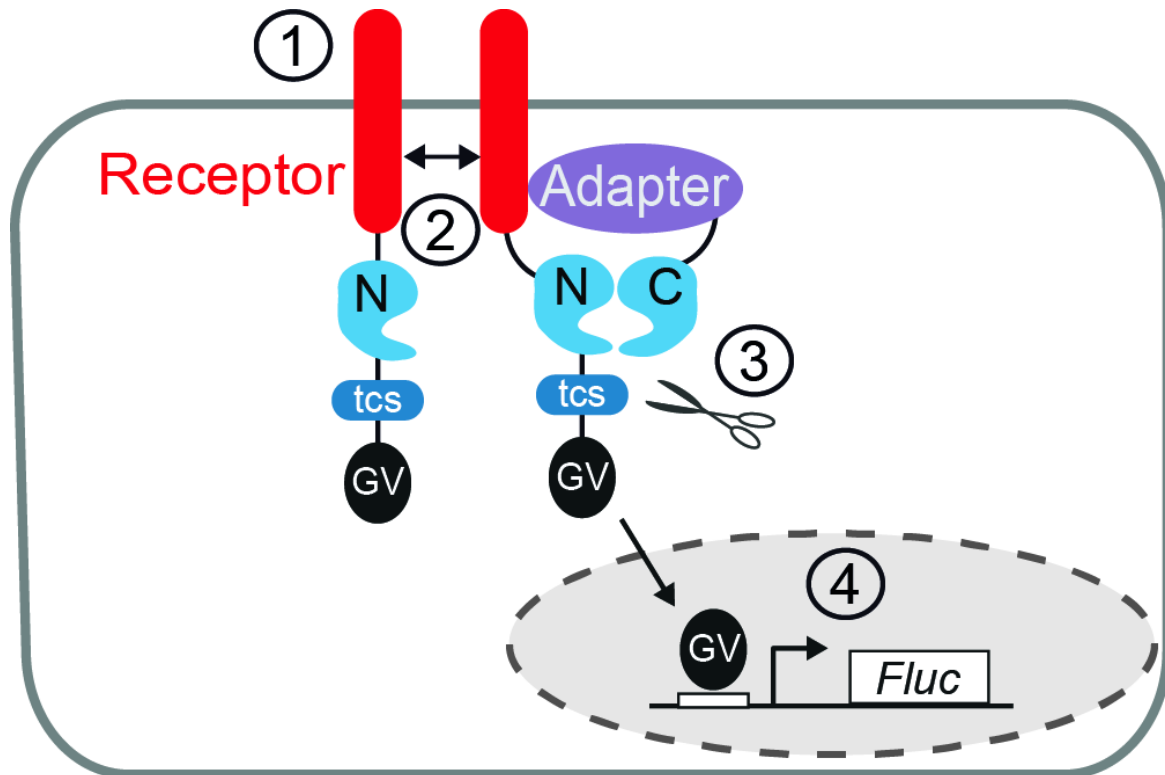


Figure T4: Design of a versatile split TEV recruitment assay for receptor tyrosine kinases. Scheme of the split TEV recruitment assay for receptor tyrosine kinases (RTKs). RTKs are fused to an NTEV moiety along with a TEV protease cleavage site (tcs) and an artificial co-transcriptional activator GAL4-VP16 (GV). Adapter proteins are fused to CTEV. Upon activation by a specific ligand (1), the RTK dimerizes, is cross-phosphorylated by the kinase domains at Tyr residues, providing docking sites for adapter proteins that bind to phosphorylated tyrosines (2). The ligand-induced interaction between RTK and adapter causes the NTEV and CTEV moieties to form a reconstituted TEV protease (2). Reconstituted TEV protease cleaves at tcs to release GV (3). Liberated GV migrates to the nucleus and initiates expression of firefly luciferase (Fluc) (4). From (Wintgens et al., 2019).

Zusammenfassung

Schizophrenie ist eine psychische Erkrankung deren Symptome in Positivsymptome, Negativsymptome und kognitive Defizite aufgeteilt werden. Schizophrenie ist eine komplexe neurologische Entwicklungsstörung, bei der genetische Variation genauso wie Umwelteinflüsse beim Ausbruch im jugendlichen Alter eine Rolle spielen. Schizophrenie hat eine Erblichkeit von circa 80%, neueste GWAS Daten suggerieren hier eine hohe Polygenität. Störungen in der synchronisierten Inhibition von pyramidal Neuronen durch einen überaktiven NRG1-ERBB4 Signalweg führen zu einem Ungleichgewicht der Erregung und Hemmung (E/H-Balance), was mit den kognitiven Störungen in Verbindung gebracht werden kann. In diesem Sinne wäre zu erwarten, dass eine Hemmung der ERBB4 Aktivität die E/H-Balance und damit die kognitiven Störungen wiederherstellen würde.

Veröffentlichung 1: Deshalb haben wir die NIH Clinical Collection (727 FDA-zugelassene Medikamente) mithilfe der zellbasierten split TEV Technologie durchsucht und Spironolakton als ERBB4 Inhibitor identifiziert. In der ersten Veröffentlichung dieser kumulativen Thesis zeige ich, wie ich zur Validierung des Top-Hits Spironolakton beitragen konnte. Im Detail, habe ich die Inhibition der Dimerisierung der ERBB Rezeptorfamilie getestet (Figs 3E, F and EV 4A-J). Des weiteren konnte ich zeigen, dass gekürzte ERBB4 Rezeptoren, die keine intrazelluläre Domäne haben, nicht von Spironolakton inhibiert werden können (Fig. EV3 A-C). Zusätzlich war es mir, durch Western Blot Technologie, möglich zu zeigen, dass Spironolakton die Phosphorylierung von ERBB4 in kultivierten humanen Zellen reduziert (Fig. 4 A, B). Zusammen mit den Ergebnissen der elektrophysiologischen Experimenten und Maus Verhaltensstudien kann auf einen Einfluss auf die E/H-Balance durch ERBB4 Phosphorylierungsreduktion geschlossen werden. Dies führt zu einer Verbesserung der Schizophrenie relevanten Verhaltensphänotypen in Mäusen.

Veröffentlichung 2. Spironolakton inhibiert allerdings nicht selektiv nur ERBB4 in der ERBB Familie (Wehr et al. 2017 Fig. 3F). Diese Selektivität ist schwer zu testen, wenn man verschiedene Bindungspartner miteinander vergleichen muss. Daher habe ich einen universalen RTK Adapter entwickelt, um die Selektivität von bekannten RTK Inhibitoren zu messen und Dosis-Wirkungs-Messungen in einem zellbasierten Hochdurchsatzscreen zu vergleichen. Ich konnte zeigen, dass ein künstlicher SH2 Domänen Adapter (SH2(GRB2)) das Signal-Rausch-Verhältnis verschiedener RTK Messungen verbessert, und so zu erhöhter Robustheit und Flexibilität der Messung beiträgt. Zusammengefasst war es mir möglich die split TEV Technologie im Feld der RTK Aktivierungsmessung zu verbessern und für eine Applikation mit multiparametrischen parallelen Messungen zu öffnen. In dieser Veröffentlichung habe ich fast alle Experimente selbst durchgeführt und zu allen Abbildungen beigetragen. Den universalen Adapter konnten wir mithilfe eines RNA Barcodes zum simultanen Messen von mehreren Assays mit Hilfe der Next-Generation-Sequenzierung nutzen. Zusätzlich reduziert dies die Anzahl an Proben und erhöht die Vergleichbarkeit der einzelnen Assays, was ein wichtiger Schritt in Richtung Hochdurchsatz Medikamenten Tests ist.

Zusammengefasst war der Inhalt meiner Arbeiten: in Veröffentlichung 1, dass ich zur pharmakologischen Validierung des NRG1-ERBB4 Signalwegs als ein Ziel für die bisher nicht therapierbaren kognitiven Defizite in der Schizophrenie beitragen konnte.

In Veröffentlichung 2 habe ich eine umfassende Reihe von Assays entwickelt, die in der Zukunft dabei helfen können neue Arzneimittel mit einer erhöhten Selektivität für ERBB4 zu entwickeln.

Summary

Schizophrenia is a severe mental disorder and its symptoms can be divided into positive and negative domains and treatment resistant cognitive deficits. Schizophrenia is a complex neurodevelopmental disease with both genetic variation and altered environmental cues playing a role in the outbreak around adolescence. Schizophrenia has a heritability of around 80%, newest GWAS data suggests that it is highly polygenic. Disturbance of synchronous inhibition of pyramidal neurons by an hyperactivated NRG1-ERBB4 pathway causes excitation-inhibition (E/I) imbalance and might be linked to cognitive deficits. In this vein, decreasing enhanced ERBB4 activity is expected to restore the E/I imbalance and cognitive deficits.

Study 1: Therefore, we screened the NIH Clinical Collection (727 FDA-approved drugs) using the cell-based split TEV technology and identified spironolactone to inhibit ERBB4 activation. In the first publication of this cumulative thesis I show how I contributed to the validation this top hit spironolactone. Specifically, I generated data sets testing the inhibition to other dimers formed by the ERBB family (Figs 3E, F and EV 4A-J). Further, I was able to show that truncated ERBB4 receptors that lack the intracellular domain, cannot be inhibited by spironolactone (Fig. EV3 A-C). In addition, using Western blotting, I was able to confirm that spironolactone reduces phosphorylation levels of ERBB4 in human cultured cells (Fig. 4 A, B). Together with the findings in electrophysiology and behavioral mouse studies, we can conclude that spironolactone alters the E/I balance by decreasing ERBB4 phosphorylation, leading to an improvement of schizophrenia-relevant behavioral phenotypes in mice.

Study 2. However, spironolactone is not selective for ERBB4 amongst the ERBB family (Wehr et al. 2017 Fig. 3F). This selectivity is hard to address technically when using various binding partners for dimerization and different adapters within the ERBB family. Hence, in the second study shown in this thesis, I designed a universal RTK adapter to measure and compare the selectivity of known RTK inhibitors in dose-response profiling and cell-based high-throughput screening (HTS) assays. I was able to show that the synthetic clustered SH2(GRB2) domain adapter increased signal-to-noise ratios of various RTK assays and thus enhanced the robustness and flexibility of the assays in general. In summary, I was able to establish an improved split TEV recruitment assay to monitor RTK activities, with the potential for its application of multiplexed assays that are run in parallel. In this publication, I performed nearly all experiments myself and contributed to all figures. This universal adapter also enables us to multiplex RTK measurements. Using an RNA barcode reporter, we can measure various assays simultaneously using next-generation sequencing as final readout. In addition, the number of samples needed is decreased and comparability among RTK dose-response assays is increased, an important step towards HTS compound profiling.

The general impact of my studies are: (i) I could contribute to the pharmacological validation of the NRG1-ERBB4 pathway as a target of the so far treatment-resistant cognitive deficits for schizophrenia; (ii) I developed a comprehensive set of assays that may help to develop compounds with enhanced selectivity for ERBB4 in the future.

Research Article I

Spironolactone is an Antagonist of NRG1-ERBB4 Signaling and Schizophrenia-Relevant Endophenotypes in Mice

Authors:

Michael C. Wehr^{1,#,*}, Wilko Hinrichs^{2,#}, Magdalena M. Brzózka¹, Tilmann Unterbarnscheidt^{2,3}, Alexander Herholt⁴, Jan P. Wintgens⁴, Sergi Papiol^{1,5}, M. Clara Soto-Bernardini², Mykola Kravchenko⁶, Mingyue Zhang⁶, Klaus-Armin Nave², Sven P. Wichert¹, Peter Falkai¹, Weiqi Zhang⁶, Markus H. Schwab^{2,3,7} & Moritz J. Rossner^{1,2,*}

Author Affiliations:

¹ Molecular and Behavioral Neurobiology, Department of Psychiatry, Ludwig Maximilian University of Munich, Nussbaumstr. 7, 80336 Munich, Germany

² Department of Neurogenetics, Max Planck Institute of Experimental Medicine, Hermann-Rein-Str. 3, 37075 Göttingen, Germany

³ Cellular Neurophysiology, Center of Physiology, Hannover Medical School, Carl-Neuberg-Str. 1, 30625 Hannover, Germany

⁴ Systasy Bioscience GmbH, Adams-Lehmann-Str. 56, 80797 Munich, Germany

⁵ Institute of Psychiatric Phenomics and Genomics (IPPG), Medical Center of the University of Munich, Nussbaumstr. 7, 80336 Munich, Germany

⁶ Laboratory of Molecular Psychiatry, Department of Psychiatry, University of Münster, Albert-Schweitzer-Campus 1/A9, 48149 Münster, Germany

⁷ Center for Systems Neuroscience (ZSN), Hanover, Germany

These authors contributed equally to this work.

SOURCE
DATATRANSPARENT
PROCESSOPEN
ACCESS

Spironolactone is an antagonist of NRG1-ERBB4 signaling and schizophrenia-relevant endophenotypes in mice

Michael C Wehr^{1,†,*} , Wilko Hinrichs^{2,†}, Magdalena M Brzózka¹, Tilmann Unterbarnscheidt^{2,3}, Alexander Herholt⁴, Jan P Wintgens⁴, Sergi Papiol^{1,5}, Maria Clara Soto-Bernardini², Mykola Kravchenko⁶, Mingyue Zhang⁶, Klaus-Armin Nave², Sven P Wichert¹, Peter Falkai¹, Weiqi Zhang⁶, Markus H Schwab^{2,3,7} & Moritz J Rossner^{1,2,**} 

Abstract

Enhanced NRG1-ERBB4 signaling is a risk pathway in schizophrenia, and corresponding mouse models display several endophenotypes of the disease. Nonetheless, pathway-directed treatment strategies with clinically applicable compounds have not been identified. Here, we applied a cell-based assay using the split TEV technology to screen a library of clinically applicable compounds to identify modulators of NRG1-ERBB4 signaling for repurposing. We recovered spironolactone, known as antagonist of corticosteroids, as an inhibitor of the ERBB4 receptor and tested it in pharmacological and biochemical assays to assess secondary compound actions. Transgenic mice overexpressing *Nrg1* type III display cortical *ErbB4* hyperphosphorylation, a condition observed in postmortem brains from schizophrenia patients. Spironolactone treatment reverted hyperphosphorylation of activated *ErbB4* in these mice. In behavioral tests, spironolactone treatment of *Nrg1* type III transgenic mice ameliorated schizophrenia-relevant behavioral endophenotypes, such as reduced sensorimotor gating, hyperactivity, and impaired working memory. Moreover, spironolactone increases spontaneous inhibitory postsynaptic currents in cortical slices supporting an ERBB4-mediated mode-of-action. Our findings suggest that spironolactone, a clinically safe drug, provides an opportunity for new treatment options for schizophrenia.

Keywords drug repositioning; NRG1-ERBB4; schizophrenia; spironolactone; split TEV assay

Subject Categories Neuroscience; Pharmacology & Drug Discovery

DOI 10.15252/emmm.201707691 | Received 13 February 2017 | Revised 26 June 2017 | Accepted 28 June 2017 | Published online 25 July 2017

EMBO Mol Med (2017) 9: 1448–1462

Introduction

Schizophrenia (SZ) is as severely debilitating neuropsychiatric disorder characterized by positive symptoms, that is, hallucinations and delusions, negative symptoms, that is, lack of motivation, and cognitive symptoms (Insel, 2010). Positive symptoms can frequently be ameliorated by treatment with dopamine receptor antagonists, but efficient treatment options for negative and cognitive symptoms are not available (Goff *et al*, 2011). Thus, there is a strong clinical need to develop and explore more target-directed therapies for SZ (Nestler & Hyman, 2010). Repurposing of existing drugs principally offers a fast track to the clinic and has been demanded for SZ (Insel, 2012; Lencz & Malhotra, 2015), also because many pharma companies withdrew from research on severe mental disorders (Margraf & Schneider, 2016). Genetic association studies have identified *NRG1* and its cognate receptor *ERBB4* as SZ risk genes, and altered NRG-ERBB4 signaling has been associated with positive, negative, and cognitive symptoms (Stefansson *et al*, 2002; Harrison & Law, 2006; Li *et al*, 2006; Nicodemus *et al*, 2006). Several postmortem studies revealed increased expression of *NRG1* in SZ patients (Hashimoto *et al*, 2004; Law *et al*, 2006; Weickert *et al*, 2012). Elevated expression of the *ERBB4*-JM-a-CYT-1 variant carrying a PI3K-recruitment domain has also been detected in SZ (Silberberg *et al*, 2006; Law *et al*, 2007, 2012). Moreover, ERBB4 was found to be

1 Molecular and Behavioral Neurobiology, Department of Psychiatry, Ludwig Maximilian University of Munich, Munich, Germany

2 Department of Neurogenetics, Max Planck Institute of Experimental Medicine, Göttingen, Germany

3 Cellular Neurophysiology, Center of Physiology, Hannover Medical School, Hannover, Germany

4 Systasy Bioscience GmbH, Munich, Germany

5 Institute of Psychiatric Phenomics and Genomics (IPPG), Medical Center of the University of Munich, Munich, Germany

6 Laboratory of Molecular Psychiatry, Department of Psychiatry, University of Münster, Münster, Germany

7 Center for Systems Neuroscience (ZSN), Hanover, Germany

*Corresponding author. Tel: +49 89 4400 53275; Fax: +49 89 4400 55853; E-mail: michael.wehr@med.uni-muenchen.de

**Corresponding author. Tel: +49 89 4400 55891; Fax: +49 89 4400 55853; E-mail: moritz.rossner@med.uni-muenchen.de

†These authors contributed equally to this work

hyperphosphorylated in postmortem brains from SZ patients (Hahn *et al*, 2006), suggesting that NRG1-ERBB4 hyperstimulation might represent a component of SZ pathophysiology.

In agreement, transgenic mice with increased *Nrg1* expression display SZ-relevant behavioral deficits, including hyperactivity, impaired sensorimotor gating, decreased social interaction, and reduced cognitive functions (Deakin *et al*, 2009, 2012; Kato *et al*, 2010). In particular, transgenic mice with neuronal overexpression of the membrane-bound cysteine-rich-domain (CRD) type III isoform of *Nrg1* (*Nrg1*-tg) display chronic ErbB4 hyperphosphorylation in the cortex, which is associated with a broad spectrum of SZ-relevant endophenotypes, including dysbalanced excitatory and inhibitory neurotransmission, altered spine growth, and impaired sensorimotor gating (Agarwal *et al*, 2014). Moreover, it has been shown recently that endophenotypes associated with elevated *Nrg1* expression are reversible in adult animals, which strongly supports the assumption that the NRG1/ERBB4 signaling system provides a valid target for pharmacological interventions (Yin *et al*, 2013; Luo *et al*, 2014). It thus appears plausible that compounds, which can re-balance the activity of the NRG1-ERBB4 signaling pathway, could represent candidates for the therapeutic treatment of schizophrenia beyond positive symptoms.

In this study, we have first developed a co-culture assay system compatible with high-throughput-screening (HTS) utilizing the split TEV technology (Wehr *et al*, 2006, 2008). We then used this assay to screen a library of clinically approved drugs in a repurposing approach to uncover new potential target specificities (Wang & Zhang, 2013), which resulted in the identification and validation of spironolactone as an inhibitor of ERBB4. Finally, we can show that spironolactone decreases phosphorylation levels of ERBB4 *in vitro* and *in vivo* and leads to an altered balance of excitation/inhibition of cortical projection neurons. Chronic spironolactone treatment ameliorates hyperactivity and reverses sensorimotor gating and working memory deficits in *Nrg1*-tg mice. Thus, spironolactone alleviates novel aspects of SZ-relevant symptoms in this mouse model of increased NRG1-ERBB4 signaling.

Results

A split TEV-based co-culture assay to screen for modulators of NRG1-ERBB4 signaling

Screening for modulators of NRG1-ERBB4 signaling in cell culture requires an adequate setup reflecting endogenous signaling mechanisms. According to a current model, NRG1 ligands reside in presynaptic terminals of principle pyramidal neurons, whereas ERBB4 receptors are mainly expressed at the postsynaptic density of dendrites in inhibitory interneurons (Rico & Marín, 2011). Based on this ligand-receptor configuration, NRG1 mediates juxtacrine and paracrine signaling to ERBB4. We established a cellular HTS-compatible co-culture assay, in which NRG1 was expressed in the signal-sending cell population A, whereas ERBB4 was expressed in the signal-receiving cell population B (Fig 1A). Initially, we used the full-length NRG1 type I β 1a isoform that undergoes proteolytic cleavage resulting in the release of the extracellular domain, which contains the biologically active EGF-like domain (EGFId), into the extracellular space (Hu *et al*, 2006; Willem *et al*, 2006). Therefore, NRG1 type I β 1a can elicit juxtacrine (non-cleaved form) and paracrine (cleaved

form) stimuli. To screen for approved small compounds that could modulate NRG1-ERBB4 signaling, we combined this co-culture assay with the split TEV protein-protein interaction technique to monitor ERBB4 activation through induced PI3K adaptor recruitment by the human ERBB4-JMa-Cyt1 variant (Fig 1A).

The functionality and robustness of the co-culture assay was investigated by co-plating increasing numbers of PC12 cells carrying a stably integrated mouse *Nrg1 type I β 1a* expression cassette (Nrg1 cells, Fig EV1A for stable *Nrg1* expression) with ERBB4-PIK3R1-expressing PC12 cells (split TEV assay cells). Co-culture conditions were verified using two PC12 cell populations expressing either EYFP or ECFP (Fig EV1B). A dose-response analysis showed that the assay reached a plateau of activation when 10,000 *Nrg1*-expressing cells were co-plated with 40,000 split TEV assay cells, with half-maximal activation at 5,000 cells (Fig 1B). Calculation of the *Z'* factor, a measure of HTS applicability and quality (Zhang *et al*, 1999), resulted in a value of 0.5 indicating a large separation band at screening conditions. Importantly, addition of the soluble EGFId resulted in a twofold increase of ERBB4 activation compared with *Nrg1* cells alone, implying that ERBB4 activation in the co-culture assay can be decreased and increased by potential NRG1-ERBB4 inhibitors and activators, respectively (Fig 1C). In addition, dose-response assays using ERBB4-PIK3R1 split TEV assay cells only and soluble EGFId as stimulus (single-culture assay) showed stable and reproducible dose-responses that also qualified for HTS, with *Z'* factors between 0.56 and 0.68 for three independent assays (Fig EV1C). The specificity of the NRG1-ERBB4 co-culture assay was validated in dose-response assays using established ERBB4 inhibitors, such as lapatinib (IC₅₀ value at 2.61 μ M, co-culture assay, Fig 1D; 0.45 μ M, single-culture assay, Fig EV1D) and CI-1033 (IC₅₀ value at 0.01 μ M, co-culture assay, Fig EV1E; 0.004 μ M, single-culture assay, Fig EV1F). Taken together, these data indicate that the split TEV-based co-culture assay provides a robust platform to screen for modulators of NRG1-ERBB4 signaling.

Screening the NIH clinical compound collection recovers spironolactone as ERBB4 receptor antagonist

We used the split TEV-based NRG1-ERBB4-PIK3R1 co-culture assay to screen two sets of the NIH Clinical Collection (NIH-NCC) containing 727 FDA-approved drugs in total (Fig 2A). From this screen, we selected a primary hit list of candidates that were at least three standard deviations away from the mean (Fig 2B for NIH-NCC set 1; Fig EV2A for NIH-NCC set 2; Dataset EV1). These candidates were then subjected to individual re-screening to eliminate off-target effects, such as toxicity and interference with assay tools, and 18 substances met these criteria and were selected for the final hit list (Appendix Fig S1 for a flowchart of all screening and validation steps; see Appendix Table S1 for final hit list). Spironolactone, a mineralocorticoid receptor (MR) antagonist formerly used as a diuretic and to treat high blood pressure (Gaddam *et al*, 2010), was recovered as top antagonist candidate (Fig 2B). In a dose-response co-culture assay using *Nrg1 type I β 1a*, spironolactone displayed an IC₅₀ value of 1.0 μ M, and marginal toxic effects at higher concentrations, as indicated by reduced *Renilla* luciferase readings (Fig 2C). ERBB4-specific effects were confirmed by dose-response control assays, which showed absence of spironolactone effects on assay components (Fig EV2B and C).

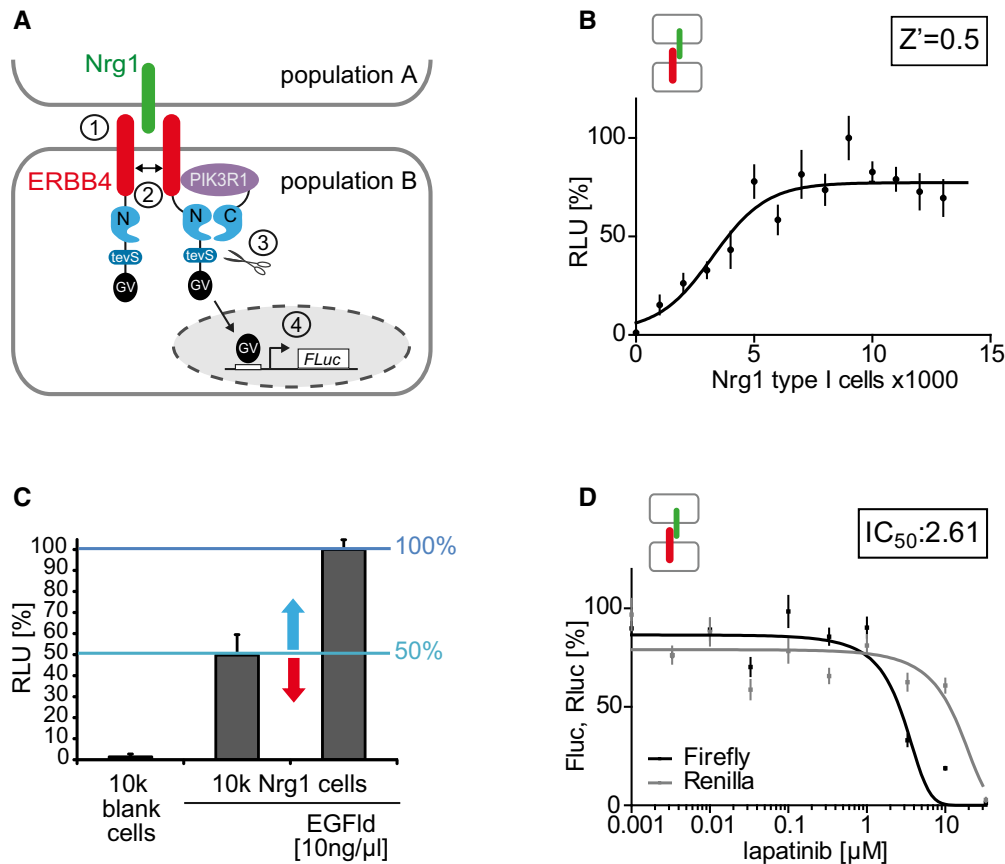


Figure 1. A co-culture assay based on the split TEV technique for monitoring NRG1-ERBB4 signaling activity.

- A** The ERBB4-PIK3R1 split TEV assay monitors NRG1-ERBB4 signaling in PC12 cells. The Nrg1 ligand (green) is stably expressed in the signal-sending cell population A. The signal-receiving cell population B (or split TEV assay cells) is transfected with plasmids encoding the assay components ERBB4 (red) fused to NTEV-tevS-GV (ERBB4-NTEV-tevS-GV), the adapter molecule PIK3R1 (purple, the regulatory subunit alpha of the PI3K) fused to CTEV (PIK3R1-CTEV), and a UAS-driven firefly luciferase reporter (Fluc). Upon Nrg1 binding to the extracellular domain of ERBB4 (1), ERBB4-NTEV-tevS-GV dimerizes and cross-phosphorylates itself (2). PIK3R1-CTEV binds to the phosphorylated ERBB4 receptor leading to the functional reconstitution of TEV protease activity and the concomitant release of the artificial co-transcriptional activator Gal4-VP16 (GV) through proteolytic cleavage at a TEV protease cleavage site (tevS) (3). In turn, released GV translocates to the nucleus and binds to UAS sequences (open box) to activate the transcription of a firefly reporter gene (4).
- B** Dose-response assay using increasing numbers of Nrg1 type I β 1a-expressing PC12 cells. For each 96-well, 40,000 split TEV assay cells were co-plated with increasing numbers of Nrg1-expressing cells and incubated for 24 h. Half-maximal activation is reached at 5,000 Nrg1-expressing cells. The Z' factor is 0.5 indicating a large separation band for this assay.
- C** Adding 10 ng/ml EGFlD resulted in a twofold activation. Per 96-well, 40,000 split TEV assay cells were co-plated with empty PC12 cells (no Nrg1 expression), 10,000 Nrg1-expressing cells, and 10,000 Nrg1-expressing cells plus 10 ng/ml EGFlD. Arrows indicate measuring window of activation (blue arrow) and inhibition (red arrow) relative to baseline activity.
- D** Lapatinib antagonizes ERBB4-PIK3R1 signaling in a dose-dependent manner. Per 96-well, 40,000 split TEV assay cells were incubated with increasing amounts of lapatinib, followed by co-plating 10,000 Nrg1 type I β 1a-expressing cells. The inset depicts the IC_{50} value in μ M.

Data information: After compound/stimulus addition, each assay was incubated for 24 h. RLU, relative luciferase units; Fluc, firefly luciferase activity (black line); Rluc, *Renilla* luciferase activity (gray line); $n = 6$; data are shown as mean, and error bars represent SEM.

Importantly, spironolactone also inhibited ERBB4 activity (IC_{50} value of 1.1 μ M) in a co-culture assay using the membrane-bound CRD containing type III isoform of Nrg1, the major NRG1 isoform in the brain, which is implicated in juxtacrine signaling (Fig 2D). Thus, spironolactone modulates ERBB4 activity downstream from both paracrine and juxtacrine NRG1 signaling. Further, spironolactone acts at a proximal step of ERBB4 receptor activation upstream of tyrosine phosphorylation and adapter recruitment as ERBB4 dimerization stimulated by EGFlD was efficiently inhibited (IC_{50} value of 1.1 μ M) in a single-culture assay (Fig 2E). Finally, we used an ERBB4 variant that lacks the

intracellular domain, and thus is signaling incompetent, but expresses at the cell cortex and dimerizes upon EGFlD stimulation (Fig EV3A and B). Notably, spironolactone inhibits dimerization of full-length ERBB4, but not of C-terminally truncated ERBB4 (Fig EV3C).

Spironolactone but not its metabolic products antagonizes the ERBB4/PIK3R1 assay

Spironolactone also inhibited ERBB4 signaling activity in an ERBB4-PIK3R1 single-culture assay, albeit with a slightly increased IC_{50}

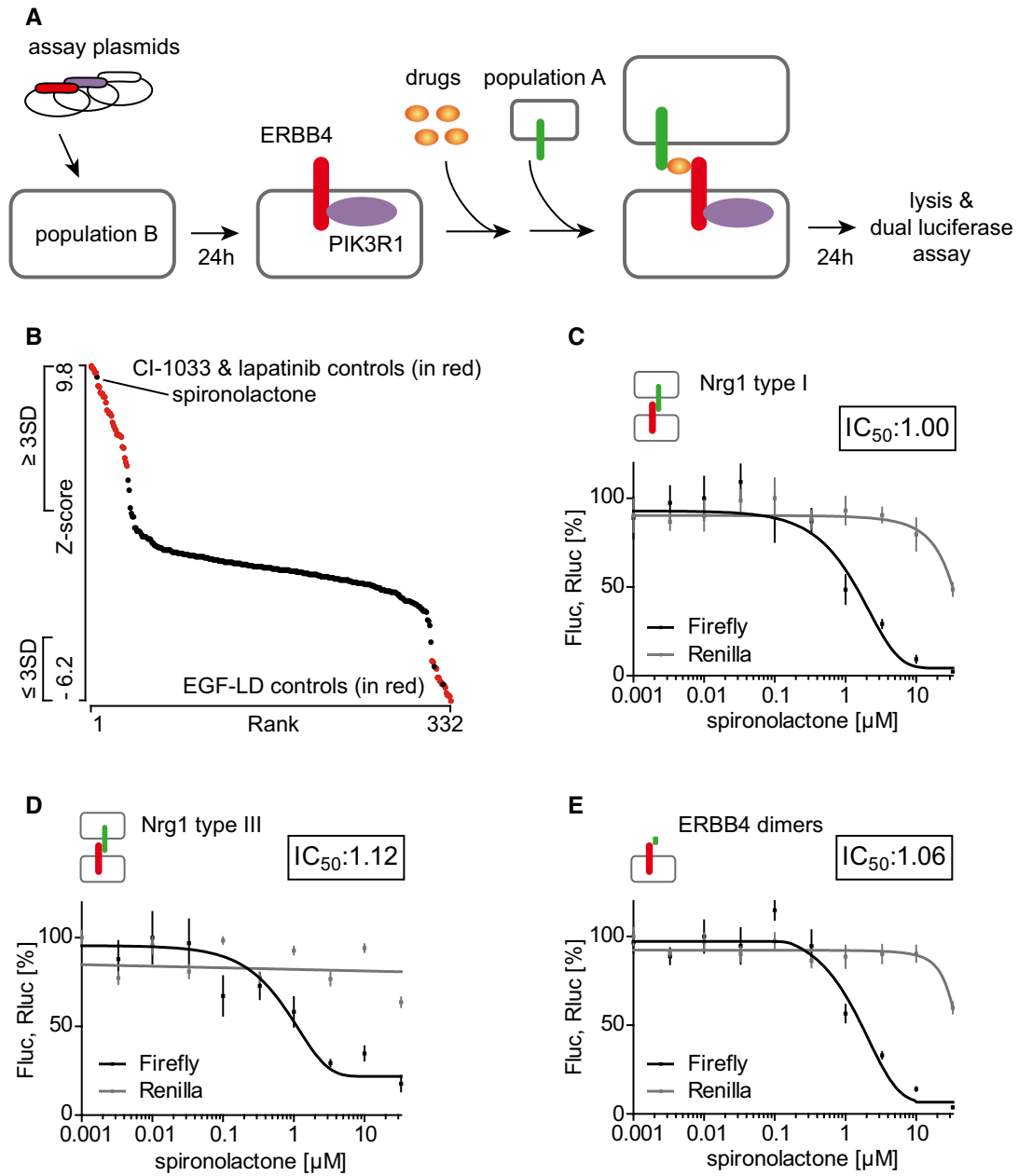


Figure 2. Spironolactone is the primary candidate recovered from the co-culture screen.

A Flow chart of the compound screen. PC12 cells (population A) were transfected in solution with the split TEV assay plasmids ERBB4-NTEV-tevS-GV and PIK3R1-CTEV and incubated for 2 h before seeded onto 96-well plates. Population A cells were allowed to express the plasmids for 24 h. Compounds were added in a concentration of 10 μM, followed by seeding the Nrg1-expressing PC12 cells (population B) half an hour later. After 24 h of compound incubation, cells were lysed and subjected to a dual luciferase assay. The screening data were analyzed using the cellHTS2 package in R Bioconductor.

B Graphic visualization of the primary screen data of the NIH-NCC library set 1. All counts (320 compounds and 64 controls) from the Nrg1-ERBB4-PIK3R1 split TEV compound screen were plotted against the Z-score using the Mondrian program, with pathway activators displaying high values and inhibitors low values. For the secondary analysis, we selected all candidates that were at least three standard deviations away from the mean. EGFld-positive and lapatinib/CI-1033-negative controls are shown in red.

C, D Spironolactone antagonizes Nrg1-ERBB4-PIK3R1 signaling. In dose–response assays using ERBB4-NTEV-tevS-GV and PIK3R1-CTEV plasmids transfected into PC12 cells, spironolactone was administered at increasing concentrations before seeding (C) Nrg1 type I- or (D) Nrg1 type III-expressing PC12 cells.

E Spironolactone inhibits ERBB4 receptor dimerization. Dose-dependent dimerization of the ERBB4 receptor was analyzed using a split TEV assay encompassing ERBB4-NTEV-tevS-GV and ERBB4-CTEV plasmids transfected into PC12 cells. 10 ng/ml EGFld was applied as Nrg1 stimulus.

Data information: Fluc, firefly luciferase activity (black lines); Rluc, *Renilla* luciferase activity (gray lines, indicating toxicity levels); $n = 6$; data are shown as mean, and error bars represent SEM. The insets depict IC_{50} values in μM.

value of 2.8 μM (Fig 3A). We used the assay to identify molecular structures in spironolactone (Fig 3A) required for the inhibition of ERBB receptor activation in this assay and examined structurally highly related compounds, such as the metabolites canrenone

(Fig 3B) and 7 α -thiomethyl-spironolactone (Fig 3C) as well as the second-generation MR antagonist eplerenone (Fig 3D). Canrenone lacks the thio-ketone group attached to the sterol core structure, whereas 7 α -thiomethyl-spironolactone lacks the ketone group only.

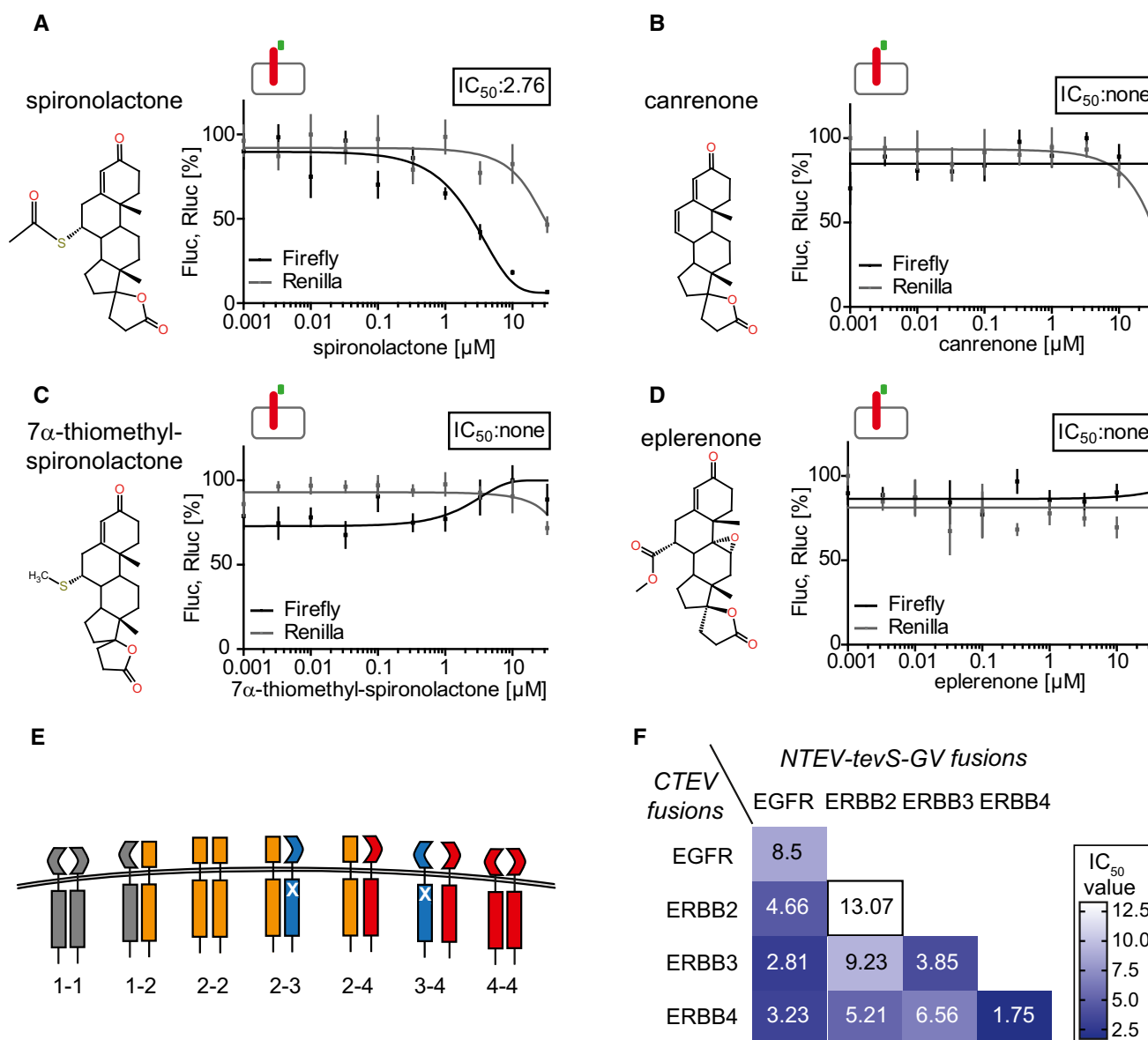


Figure 3. Multilevel profiling approach of spironolactone treatment assessing target specificities and adapter recruitment.

A Spironolactone, molecular structure shown on the left, inhibits ERBB4/PIK3R1 split TEV assay activity (black line), with an IC_{50} value of 2.76 μM .

B–D The spironolactone metabolites (B) canrenone and (C) 7 α -thiomethyl-spironolactone as well as the second-generation drug (D) eplerenone do not attenuate the ERBB4/PIK3R1 assay activity (black lines). Note that only spironolactone bears a thio-ketone group attached to the sterol core structure. All ERBB4/PIK3R1 assays were run in a single-culture assay mode using 10 ng/ml EGF1d as functional Nrg1 stimulus, and ERBB4-NTEV-tevS-GV and PIK3R1-CTEV plasmids were transfected into PC12 cells (indicated by icon).

E Schematic representation of the most critical ERBB dimers tested in spironolactone dose–response assays using the split TEV protein–protein interaction detection technique. Note that not all possible combinations are depicted.

F Heat map showing the IC_{50} values obtained from individual ERBB dimerization split TEV assays. All single dose–response assays can be found in Fig EV4; the combination ERBB4-ERBB4 is shown in Fig 2E.

Data information: Fluc, firefly luciferase activity (black lines, reporting ERBB4-PIK3R1 assay activity); Rluc, *Renilla* luciferase activity (gray lines, assessing viability); $n = 6$; data are shown as mean, and error bars represent SEM. The insets depict IC_{50} values in μM .

In eplerenone, the thio-ketone group is replaced by an acidic group, in addition to a minor modification at the sterol core structure. None of these compounds showed an inhibitory effect in the ERBB4-PIK3R1 single-culture assay (Fig 3B–D), suggesting that the thio-ketone group specific for spironolactone plays a role for its inhibitory function in this assay.

Spironolactone preferentially inhibits dimers containing ERBB4

Target specificity is a crucial aspect for the evaluation of pharmacological active compounds (Feng *et al*, 2009). As ERBB4 is a member of the ERBB family, we determined spironolactone's antagonistic effects on dimer formation of other ERBB receptors (Fig 3E). As indicated by IC₅₀ values obtained from dose–response assays (Figs 3F and EV4A–I), spironolactone preferentially inhibits formation of ERBB4 homodimers (at 1.75 μM). Spironolactone antagonizes also other ERBB combinations, albeit with less efficacy, and efficiently inhibits EGFR homodimer formation when stimulated by EGF (at 1.74 μM) (Figs 3F and EV4J). Collectively, these data suggest that spironolactone acts as a pan-ERBB family inhibitor, which preferentially inhibits dimer formation involving EGFR or ERBB4. In adult cortical tissues of mice, however, EGFR is not detectably expressed (Appendix Fig S2), suggesting that ERBB4 is the major target of the ERBB family for spironolactone in the brain.

Spironolactone reverts ERBB4 hyperphosphorylation

Dose–response assays indicated that spironolactone reduces the phosphorylation-dependent recruitment of PIK3R1 by activated ERBB4 (Figs 2C and 3A), prompting us to examine the phosphorylation levels reverted by spironolactone biochemically. EGFR treatment of human T-47D cells that endogenously express *ERBB4* induced hyperphosphorylation at Tyr1056 and Tyr1284 of ERBB4. Addition of lapatinib completely reverted Tyr1056 and Tyr1284 phosphorylation, whereas treatment with spironolactone reduced phosphorylation to intermediate levels (Fig 4A and B). Likewise, spironolactone antagonized EGFR-mediated hyperphosphorylation of transfected human ERBB4 in PC12 cells that were used in the screen (Fig EV3D). To translate our findings into a potential therapeutic rationale for SZ, we utilized a transgenic mouse model, in which *Nrg1 type III* is overexpressed under the control of the neuronal Thy1.2 promoter (referred to as *Nrg1-tg*) and causes hyperphosphorylation of ERBB4 receptors in the prefrontal cortex (Velanac *et al*, 2012). We tested whether phospho-ERBB4 levels were also regulated by chronic spironolactone treatment in *Nrg1-tg* mice and injected the drug for 21 consecutive days before sacrificing the mice for biochemical analysis (Fig 4C). In lysates from mouse prefrontal cortex, phospho-ErbB4 levels were efficiently visualized using the p-ERBB4-Y1284 antibody (Fig 4D and E). Notably, addition of spironolactone resulted in a robust reduction of NRG1-induced ERBB4 hyperphosphorylation. Downstream signaling effects, as assessed by pERK and pAKT, were neither modulated by Nrg1 overexpression, nor by spironolactone treatment. Next, we tested whether LIM kinase 1 (LIMK1) displays regulated phosphorylation levels upon spironolactone treatment. LIMK1 is a non-receptor protein serine/threonine kinase implicated in cytoskeleton dynamics and the regulation of synaptic spine morphology and function (Meng *et al*, 2002, 2004) and has been associated with

NRG1 signaling (Yin *et al*, 2013). Notably, phospho-Limk1 levels were slightly upregulated in wt and markedly upregulated in spironolactone-treated *Nrg1-tg* mice, suggesting that LIMK1 activity integrates, at least in part, spironolactone's inhibitory effect (Fig 4D and E). Taken together, these results indicate that spironolactone serves as an inhibitor of NRG1-mediated ERBB4 signaling.

Since NRG1-ERBB4 signaling has been shown to modulate inhibitory neurotransmission (Yin *et al*, 2013; Agarwal *et al*, 2014; Mei & Nave, 2014), we tested the impact of spironolactone treatment on synaptic transmission in acute slices prepared from prefrontal cortex. When we measured spontaneous inhibitory postsynaptic currents (sIPSCs) at layer II/III pyramidal neurons, canrenone (10 μM) showed no significant effect on sIPSC frequencies and amplitudes (Fig 4F). In contrast, administration of spironolactone (10 μM) caused an increase of sIPSC frequency ($n = 12$; $P < 0.05$) and amplitude ($n = 12$, $P < 0.05$) shortly after bath application (Fig 4G). Next, evoked IPSCs were measured in pyramidal neurons in layer II/III of prefrontal cortex after stimulating in layer I. To distinguish between MR and ERBB4-mediated effects by spironolactone, these experiments were performed in the presence of canrenone (10 μM), which is a more potent MR antagonist relative to spironolactone. Under these conditions, spironolactone (5 μM) significantly increased the eIPSC amplitude (Fig 4H), a finding also increased by the pan-ERBB family inhibitor compound lapatinib as control (5 μM) (Fig 4I). Together, these findings are consistent with the hypothesis that spironolactone modulates GABAergic neurotransmission via ERBB4.

Chronic spironolactone treatment ameliorates SZ-relevant behavioral endophenotypes in *Nrg1-tg* mice

Nrg1-tg mice exhibit SZ-relevant behavioral abnormalities, including deficits in prepulse inhibition (PPI) (Agarwal *et al*, 2014), an operational measure of sensorimotor gating. In a pilot experiment, we performed a two-arm study, in which *Nrg1-tg* and wt mice were tested for PPI before and after chronic spironolactone treatment as above (Fig EV5A). Before treatment, *Nrg1-tg* mice displayed PPI deficits (Fig EV5B), in line with our previous findings (Agarwal *et al*, 2014). Spironolactone treatment significantly improved PPI in *Nrg1-tg* mice (Fig EV5C), but had no effect in wt controls, suggesting that spironolactone modulates behavioral deficits of enhanced NRG1-ERBB4 signaling (Fig EV5D).

Based on these results, we performed a four-arm study, in which an independent cohort of *Nrg1-tg* and wt mice was tested following spironolactone or vehicle treatment (Fig 5A). In this study, we assessed a battery of behavioral domains with relevance for SZ, such as motor activity, curiosity, light–dark preference, working memory, motivation, PPI, fear memory, and pain sensitivity.

Vehicle-treated *Nrg1-tg* mice covered longer distances in the open-field arena than vehicle-treated wt controls (Fig 5B and C). This locomotor hyperactivity, however, was reverted by spironolactone (Fig 5B and D). Further, *Nrg1-tg* mice showed, increased anxiety, paralleled by higher frequency of defecation and urination during the open-field test (Fig EV5E–G), supporting previous observations (Agarwal *et al*, 2014). When testing for light–dark preference, spironolactone-treated *Nrg1-tg* spent more time in the light compartment. This suggests an anxiolytic rather than a sedative effect of spironolactone (Fig 5E), as *Nrg1-tg* animals and wt controls

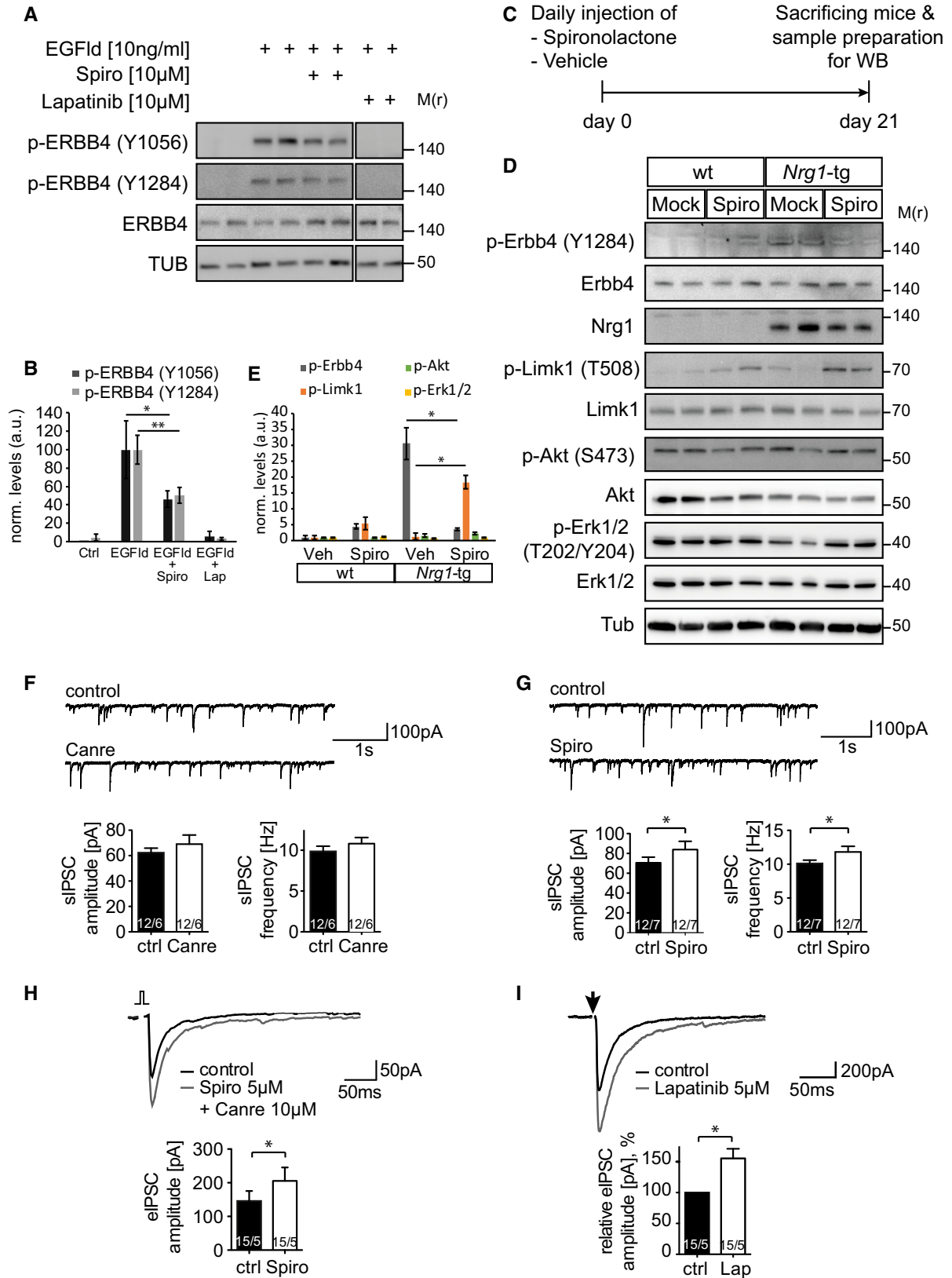


Figure 4.

Figure 4. Spironolactone antagonizes ERBB4 phosphorylation both in *in vitro* and *in vivo*.

- A Spironolactone reduces ERBB4 levels. T-47D cells were stimulated with 10 ng/ml EGFid, 10 μ M lapatinib and 10 μ M spironolactone for 5 min as indicated. Cell lysates were probed for ERBB4 phosphorylation levels at Tyr1056 and Tyr1284.
- B Quantification of band intensities for phospho-ERBB4 levels ($n = 4$ per condition) shown in (A) using ImageJ. Phosphorylation levels are normalized to protein levels of ERBB4. Data are shown as mean, and error bars represent SD; t -test, with $*P = 0.0356$ for p-ERBB4 (Y1056), and $**P = 0.0079$ for p-ERBB4 (Y1284).
- C Experimental design for Western blot analysis shown in (D) and (E). *Nrg1*-tg and wt animals were treated daily with spironolactone (50 mg/kg, s.c.) or vehicle ($n = 2$ per genotype and per treatment) for 21 days.
- D Spironolactone reduces phospho-ErbB4 levels in *Nrg1*-tg mice. Mice were treated with spironolactone for 21 days and sacrificed for Western blot analysis. Lysates were probed with indicated antibodies.
- E Quantification of band intensities for phospho-ErbB4 and phospho-Limk1 levels ($n = 2$ per condition) shown in (D) using ImageJ. Phosphorylation levels are normalized to protein levels of ErbB4 and Limk1. Data are shown as mean, and error bars represent SD; t -test, with $*P = 0.0330$ for p-ErbB4, and $*P = 0.0201$ for p-Limk1.
- F Canrenone (applied as 10 μ M) showed no effects on frequencies and amplitudes of sIPSCs in pyramidal neurons of the prefrontal cortex (PFC). Representative traces of sIPSCs (upper) and a histogram of mean sIPSC (lower) are shown for both before and after addition of canrenone.
- G Spironolactone (applied as 10 μ M) significantly increases frequencies ($n = 12$; $*P = 0.0454$) and amplitudes ($n = 12$, $*P = 0.0478$) of sIPSCs in pyramidal neurons of PFC. Representative traces of sIPSCs (upper) and a histogram of mean sIPSC (lower) are shown for both before and after addition of spironolactone.
- H Spironolactone increases amplitudes of evoked IPSCs in pyramidal neurons of PFC ($n = 15$, $*P = 0.0286$). Spironolactone (5 μ M) was applied in the presence of canrenone (10 μ M).
- I Lapatinib increases amplitudes of evoked IPSCs in pyramidal neurons of PFC ($n = 15$, $*P = 0.0124$). Lapatinib was applied at 5 μ M. Arrow indicates an evoked IPSC stimulus.

Data information: For (H, I), sample recording (upper) and a histogram of averaged eIPSC (lower) is shown for both before and after drug application. For (F–I), the numbers displayed inside the histogram bars indicate the number of recorded slices/number of animals. Data are shown as mean, and error bars represent SD (for B, E) and SEM (for F–I); paired t -test, with $*P \leq 0.05$; Spiro, spironolactone; Canre, canrenone; Lap, lapatinib. Source data are available online for this figure.

displayed a similar transition activity in the light–dark test (Fig EV5H). In contrast, *Nrg1*-tg mice showed an increased activity in the tail suspension test (Fig EV5I). Working memory was assessed in the Y-maze test. *Nrg1*-tg mice performed significantly less alterations than wt controls, suggesting an impaired working memory performance in transgenics (Fig 5F). Notably, spironolactone treatment rescued these deficits (Fig 5F), without influencing the activity in the Y-maze (Fig EV5J). However, the number of choices was higher in transgenics, supporting their hyperactivity phenotype observed in the open-field test (Fig 5B and C).

In the contextual fear memory test, spironolactone-treated *Nrg1*-tg mice displayed a non-significant reduction in freezing (Fig EV5K), which was paralleled by significantly decreased levels of pain sensitivity as assessed in the hot plate test (Fig EV5L). Cue memory testing revealed neither genotype nor treatment-dependent alterations (Fig EV5K). Moreover, spironolactone treatment significantly enhanced PPI in *Nrg1*-tg (Fig 5G), but not in wt mice (Fig EV5M), replicating the data obtained from the pilot experiment (Fig EV5D).

As *Nrg1* is a critical regulator for brain development, we aimed to exclude age-related consequences on the behavioral effects observed using a covariate analysis, which links age with test performance. To do this, we grouped mice into juvenile (8–11 weeks) and adult (12–16 weeks) categories, and ANCOVA with the covariate age did not reveal an effect on the genotype-dependent treatment response (Appendix Fig S3).

Taken together, chronic spironolactone treatment alleviates hyperactivity, PPI and working memory deficits in *Nrg1*-tg mice, findings that are paralleled by a reduction in ErbB4 hyperphosphorylation levels in these mice.

Discussion

To obtain repurposed drugs for schizophrenia, we have developed a co-culture assay system mimicking several proximal aspects of

NRG1-ERBB4 signaling (Citri & Yarden, 2006; Mei & Xiong, 2008). Its successful application in a repurposing screen with clinical substances resulted in the identification of the MR antagonist spironolactone as a potent ERBB4 inhibitor. The efficacy of spironolactone as novel inhibitor of NRG1-ERBB4 signaling was validated in heterologous cells with an endogenous expression of human ERBB4 and *in vivo* using transgenic mice, which model NRG1 overexpression and ERBB4 hyperphosphorylation linked to several endophenotypes with relevance for SZ (Agarwal *et al.*, 2014). We thus provide a pharmacological proof-of-principle for targeting NRG1-ERBB4 signaling in the context of SZ and exploited the opportunity to repurpose a clinical compound, a strategy that was strongly demanded in the last years for mental diseases (Insel, 2012). In addition, a recent study suggested to fast track all SZ susceptibility genes, which encode potential targets for approved drugs, for repurposing (Lencz & Malhotra, 2015). Therefore, our multilevel approach targeting NRG1-ERBB4 signaling that identified a hidden mode-of-action of spironolactone antagonizing ERBB4 activity strongly supports this approach. As spironolactone is a clinically safe and available substance, it immediately qualifies for therapeutic intervention trials. Finally, the co-culture assay is qualified for high-throughput conditions under industry quality standards and will allow the exploratory screen of large exploratory compound libraries.

Spironolactone inhibited the association between ERBB4 and PIK3R1 in the split TEV-based co-culture assay, with an IC_{50} value at approximately 1 μ M. Our data suggest that spironolactone also targets other ERBB family members, however, with a preference for ERBB4. Our biochemical analysis suggests that spironolactone shows an intermediate efficacy of ERBB4 inhibition. Notably, fine tuning of excitation and inhibition between excitatory projection neurons expressing NRG1 and inhibitory parvalbumin-positive interneurons expressing ERBB4 is thought to be a critical determinant of endophenotypes observed in gain- and loss-of-function mouse models (Chen *et al.*, 2010; Yin *et al.*, 2013; Agarwal *et al.*, 2014). Therefore, moderate changes in NRG1/ERBB4 activity may be desired to achieve rebalanced signaling levels under pathological

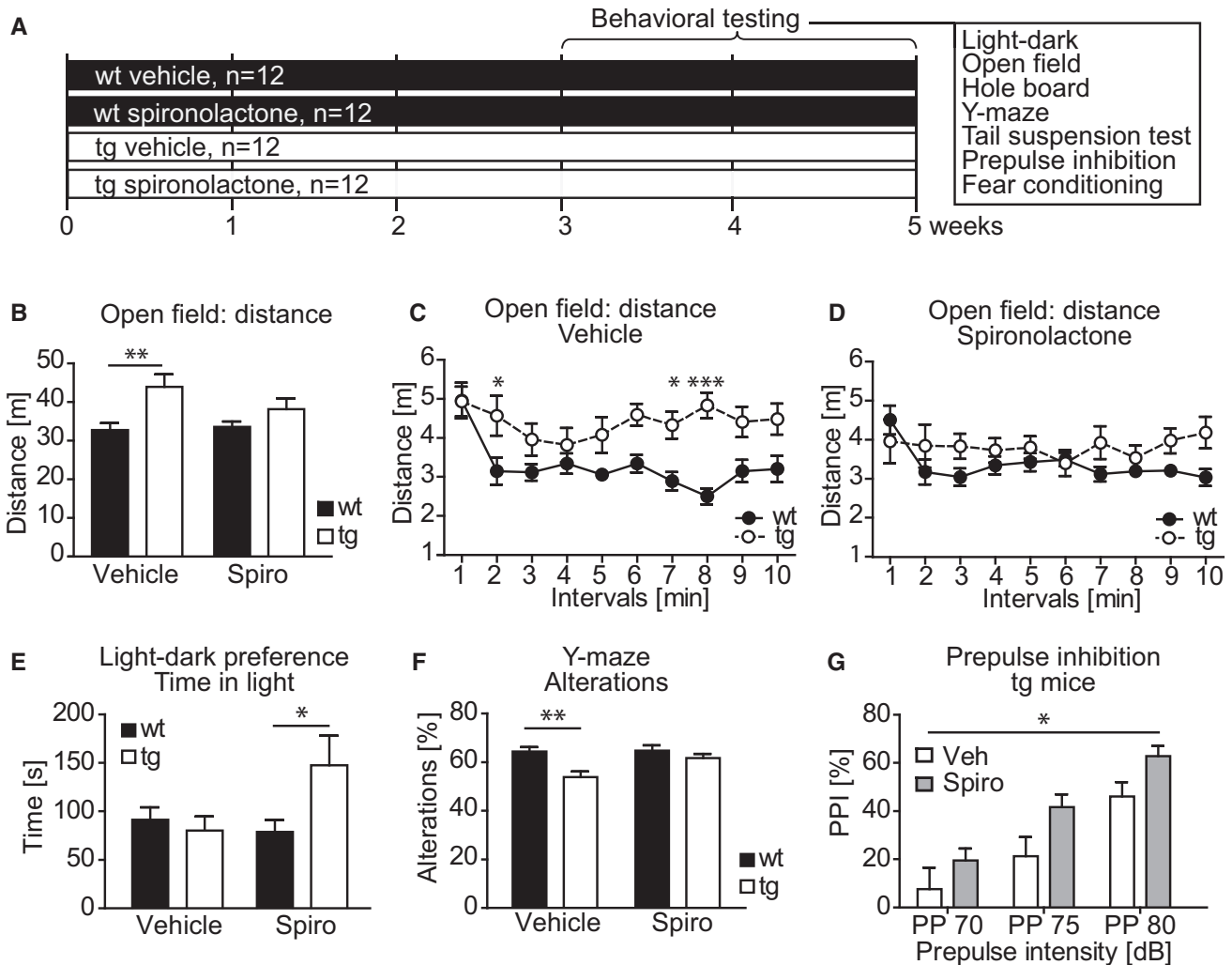


Figure 5. Chronic spironolactone treatment ameliorates deficits of behavioral endophenotypes in *Nrg1*-tg mice.

A Experimental design. *Nrg1*-tg and wt animals were treated daily with spironolactone (50 mg/kg, s.c.) or vehicle ($n = 12$ per genotype and per treatment) for 3 weeks, followed by behavioral phenotyping using the tests as indicated. Spironolactone or vehicle treatment was continued throughout the phenotyping phase.

B *Nrg1*-tg mice travelled longer distances in the open-field arena (effect of genotype $F_{1,44} = 10.53$; $P = 0.0022$; two-way ANOVA). Bonferroni *post hoc* analysis revealed a significant genotype-dependent difference between vehicle-treated groups (** $P = 0.0044$) but not in spironolactone-treated groups ($P = 0.3783$). Genotype differences were abolished upon spironolactone treatment.

C When vehicle-treated animals were analyzed in 1-min intervals, transgenic mice showed an increased activity throughout the entire test (effect of genotype $F_{1,22} = 9.27$; $P = 0.0060$; two-way ANOVA), most prominent in intervals 2, 7, and 8 (* $P = 0.0427$, * $P = 0.0385$, and *** $P = 0.000036$, respectively, Bonferroni *post hoc* test).

D There was no significant difference between the genotypes when treated with spironolactone (effect of genotype $F_{1,22} = 2.19$; $P = 0.1535$; two-way ANOVA). However, the interaction of genotype and treatment was significant ($F_{9,198} = 1.94$; $P = 0.0481$; two-way ANOVA).

E *Nrg1*-tg mice treated with spironolactone spent more time in the light compartment during the light–dark test (interaction gene \times treatment $F_{1,41} = 4.90$; $P = 0.0324$; two-way ANOVA, and * $P = 0.0219$, Bonferroni *post hoc* test).

F In the Y-maze test, transgenic mice performed less alterations (effect of genotype $F_{1,44} = 11.50$; $P = 0.0015$; two-way ANOVA). The Bonferroni test confirmed this phenotype in vehicle-treated groups (** $P = 0.0011$), but not in spironolactone-treated animals ($P = 0.5950$). Spironolactone treatment had a significant effect on the number of alterations ($F_{1,44} = 4.12$; $P = 0.0484$; two-way ANOVA).

G Spironolactone treatment significantly enhanced PPI in *Nrg1*-tg mice (effect of treatment $F_{1,21} = 5.07$; * $P = 0.0325$; two-way repeated-measures ANOVA).

Data information: Data are shown as mean, and error bars represent SEM. Spiro, spironolactone; Veh, vehicle. $n = 12$ per genotype and treatment with an exception of (E) (*Nrg1*-tg vehicle, $n = 11$; *Nrg1*-tg Spiro, $n = 10$; wt vehicle, $n = 12$; wt Spiro, $n = 12$) and (G) (*Nrg1*-tg vehicle, $n = 11$; *Nrg1*-tg Spiro, $n = 12$).

conditions. We found that the chronic administration of spironolactone to *Nrg1*-tg mice reverted Erbb4 hyperphosphorylation and largely rescued hyperactivity (considered as a surrogate marker for

positive symptoms in SZ), PPI deficits and working memory impairments. Importantly, behavior in wild-type mice remained largely unaffected by chronic spironolactone treatment. Spironolactone, but

not canrenone, enhanced inhibitory neurotransmission when applied acutely to cortical slices of wild-type mice, suggesting an ERBB4-mediated mechanism. Likewise, the ERBB4 kinase inhibitor lapatinib caused similarly increased IPSCs within the same experimental model. Increased amplitudes of mIPSCs have also been observed in conditional *Nrg1* loss-of-function mutants, most likely as a consequence of reduced activity of ERBB4 in inhibitory neurons (Agarwal *et al*, 2014). In conditional ERBB4 mutants, however, mIPSC frequencies were reduced in the hippocampus (Fazzari *et al*, 2010). A recent study reports that NRG2, a close relative of NRG1, is expressed in inhibitory interneurons and activates ERBB4 cell-autonomously, causing a downregulation of NMDA receptor activity in these cells (Vullhorst *et al*, 2015). In such a scenario, inhibition of ERBB4 activity may indeed increase IPSCs, a hypothesis fitting to our observations, for both spironolactone and lapatinib control treatments. Overall, these findings indicate that altered NRG1/ERBB4 signaling modulates inhibitory signaling, although different adaptations may prevail in different brain regions and genetic models as well as pharmacological treatments.

Our biochemical analysis implicates LIMK1 signaling, but not ERK1/2 nor AKT1 as potential downstream effectors of spironolactone treatment in *Nrg1*-tg mice. As a non-receptor protein serine/threonine kinase, LIMK regulates synaptic spine morphology and function by modulating cytoskeleton dynamics (Meng *et al*, 2002, 2004; Bennett, 2011). Further, LIMK1 has been linked to NRG1 signaling and SZ-relevant endophenotypes in a *Nrg1*-tg mouse model (Yin *et al*, 2013). We show that phospho-LIMK1 levels were upregulated in *Nrg1*-tg mice treated with spironolactone suggesting that LIMK1 activity may possibly integrate spironolactone's inhibitory effect by promoting spine enlargement, and thus synapse formation, through controlling actin cytoskeleton dynamics. *Nrg1*-tg animals display subtle structural changes related to spine morphology, that is, the number of bifurcated spines is increased (Agarwal *et al*, 2014). Therefore, it might be possible that spironolactone treatment reverts this structural endophenotype. Nonetheless, the increased levels of p-LIMK1 rather favor a mechanism compensating for the structural changes in *Nrg1*-tg mice, which may underlie network disturbances in these animals, by stimulating structural plasticity via increased LIMK1 activity. To further explore the mode-of-action of spironolactone in the future, its impact on structural plasticity should be addressed in additional studies.

Spironolactone has been developed as MR antagonist and was clinically applied for decades as a potent and safe diuretic (Ogden *et al*, 1961). As brain-expressed corticoid receptors are implicated in modulating the stress response, spironolactone treatment has been tested in the context of depression and was shown to increase motivation and curiosity in mice (Wu *et al*, 2012). Moreover, anxiety was partially improved in a small group of patients suffering from bipolar disorder (Jurueña *et al*, 2009) in good agreement with our finding that spironolactone affects anxiety-related behavior in *Nrg1*-tg mice. Acute spironolactone administration to healthy human volunteers, however, reduced memory retrieval (Zhou *et al*, 2011; Rimmele *et al*, 2013) and reportedly impaired recent fear memory formation in mice (Zhou *et al*, 2011). Upon chronic administration of spironolactone, however, we could not observe any detrimental effects on cognitive performance in fear and working memory tests in wild-type mice. However, spironolactone-treated *Nrg1*-tg mice displayed a slightly reduced level of fear memory, which may be

partially dependent on anxiolytic actions of spironolactone or decreased pain sensitivity in transgenic mice. Nonetheless, working memory deficits of *Nrg1*-tg mice were rescued upon spironolactone treatment.

Structure-function analysis using spironolactone metabolites and second-generation analogues revealed that the intact structure of spironolactone is paramount for inhibiting ERBB4 signaling activity. We speculate that other structural modifications of spironolactone may improve its selectivity for ERBB4 binding and concomitant inhibition. Spironolactone may therefore also serve as a template for a lead optimization process, which could produce a new molecular entity with improved characteristics to inhibit ERBB4 signaling and avoiding potentially adverse effects on the MR. Nonetheless, given our observations and the safety profile of spironolactone, a clinical study might be warranted to assess the chronic effects of spironolactone treatment in SZ patients.

Materials and Methods

Plasmids

Gateway recombination cloning (Life Technologies) was applied for generating plasmids. Each ORF cloned was PCR-amplified using the Pwo proofreading DNA polymerase (Roche) and BP-recombined into the pDONR/Zeo plasmid (Life Technologies) to yield an entry vector, which was control-digested using BsrGI to release the insert, and sequence-verified. The following human ORFs were cloned using cDNA image clones ordered from Source BioScience: ERBB4 transcript variant JM-a/CYT-1 (Accession: BC112199), PIK3R1 (BC094795), GRB2 transcript variant 1 (BC000631), SHC1 transcript variant 2 (BC014158), STAT5A (BC027036), and SRC transcription variant 1 (BC051270). For EGFR, ERBB2, and ERBB3, entry vectors were obtained from the human CCSB kinase collection available from Addgene (Johannessen *et al*, 2010). Entry vectors were LR-recombined into split TEV destination vectors [either pcDNA_attR1-ORF-attR2-NTEV-tevS-GV-2xHA_DEST or pTag4C_attR1-ORF-attR2-CTEV-2xHA_DEST, plasmids were described in detail before (Wehr *et al*, 2006)] to yield expression vectors, which were control-digested using BsrGI. The plasmids for *Nrg1* type I β 1a and rat *Nrg1* type III β 1a have been described before (Wehr *et al*, 2006).

The oligonucleotides used for cloning are shown in the Appendix Table S2.

Cell culture

PC12 Tet-Off cells (Clontech, 631134, termed PC12 cells for simplicity) and their derivatives stably expressing *Nrg1* were cultured in low glucose DMEM medium (1 g/l, Lonza) supplemented with 10% FCS, 5% HS, 50 μ g penicillin, 50 μ g streptomycin and GlutaMAX (Life Technologies) at 37°C, and 5% CO₂. T-47D cells (ATCC:HTB-133) were grown RPMI-1640 (Life Technologies) supplemented with 0.2 units/ml bovine insulin (Sigma), 10% FCS, 50 μ g penicillin, 50 μ g streptomycin and GlutaMAX (all Life Technologies) at 37°C, and 5% CO₂. PC12 cells were grown on poly-L-lysine-coated surfaces for both maintenance and experiments; T-47D cells were only grown on poly-L-lysine-coated surfaces for experiments. Cell lines were negative for mycoplasma contamination.

Generation of PC12 cells stably expressing Nrg1

1 Mio PC12 cells were either transfected with 10 µg of a Nrg1 type I β1a plasmid or Nrg1 type III β1a plasmid using Lipofectamine 2000. Following an initial expression of 24 h, 400 µg/ml G418 was applied to select stable clones as each Nrg1 plasmid harbors a neomycin resistance gene for selection in mammalian cells. After 2 weeks of culturing, visible PC12 cell clones were transferred into a single well of a 24-well plate. Following to a recovery and expansion phase, stable Nrg1 expression was validated in a split TEV-based ERBB4-PIK3R1 co-culture assay. Positive clones were also verified by Western blot analysis.

Protein lysates and Western blotting

PC12 cells were transfected with indicated plasmids using Lipofectamine 2000 (Life Technologies). After 24 h of expression, cells were treated as indicated and lysed in a 1% Triton-X lysis buffer (50 mM Tris [pH 7.5], 150 mM NaCl, 1% Triton X-100, 1 mM EGTA) supplemented with 10 mM NaF, 1 mM Na₂VO₄, 1 mM ZnCl₂, 4.5 mM Na₄P₂O₇, as phosphatase inhibitors, and the complete protease inhibitor cocktail (Roche). Lysates from T-47D cells were analyzed for endogenous proteins only. For the analysis of cytosolic proteins, cell extracts were spun for 10 min at 4°C at 17,000 g.

For the biochemical analysis of spironolactone-treated mice (for a precise description of the injection paradigm, see subheading “Mouse behavior analysis”, “Spironolactone treatment”), vehicle control or spironolactone was subcutaneously injected daily for 21 days into age-matched (11–13 weeks) male mice prior to preparation of the mouse prefrontal cortex (*n* = 2 per genotype and treatment). For the generation of lysates, the isolated tissue was immediately placed into cooled (4°C) sucrose buffer (320 mM sucrose, 10 mM Tris-HCl, 1 mM NaHCO₃, 1 mM MgCl₂, supplemented with 10 mM NaF, 1 mM Na₂VO₄, 1 mM ZnCl₂, 4.5 mM Na₄P₂O₇ as phosphatase inhibitors, and the complete protease inhibitor cocktail (Roche)), homogenized using an ultra-turrax (IKA GmbH, Staufen, Germany), sonicated (3 pulses for 10 s), and denatured for 10 min at 70°C in LDS sample buffer.

Protein gels were run using the Mini-PROTEAN Tetra Electrophoresis System (Bio-Rad), and gels were blotted using the Mini-PROTEAN Tetra Electrophoresis System (Bio-Rad). Detection of proteins was performed by Western blot analysis using chemiluminescence (Western Lightning[®] Plus-ECL, PerkinElmer). Western blots were probed with antibodies at dilutions as shown in the Appendix Table S3. Each blot was replicated two times. Western blots were densitometrically quantified using ImageJ following the protocol openly accessible at lukemiller.org (<http://lukemiller.org/index.php/2010/11/analyzing-gels-and-western-blots-with-image-j/>).

Immunofluorescence staining of PC12 cells

1 Mio PC12 cells were plated per well onto poly-L-lysine (PLL)-coated coverslips in a 6-well plate at day 1. At day 2, cells were transfected with ERBB4-NTEV-tevS-GV or ERBB4_1-685-NTEV-tevS-GV. At day 3, cells were gently washed twice by adding and removing 1× TBS (50 µl per coverslip), fixed in cold 4% PFA for 10 min,

washed twice with 1× TBS, and permeabilized in TBS/0.1% Triton X-100 for 5 min. Then, cells were washed again three times in 1× TBS and blocked in blocking buffer (3% BSA, 0.1% Triton X-100 in 1× TBS) for 1 h at room temperature. Primary antibodies diluted in blocking buffer and cells were incubated for 1 h at room temperature. Following three washes in TBS, cells were incubated with a secondary antibody (Alexa 594 anti-rat, 1:500, Abcam, ab150160) diluted in blocking buffer for 1 h at room temperature. Coverslips were washed three times in 1× PBS, once quickly dipped into ddH₂O to remove traces of salt, mounted on microscope slides, and sealed with ProLong Gold Antifade Mountant with Dapi (ThermoFisher Scientific, P36935). Slides were stored at 4°C before imaged on a Zeiss Observer Z.1 microscope.

Compound screening and validation

Cell-based split TEV assay to monitor ERBB4 activity

The split TEV method is based on the functional complementation of two previously inactive TEV protease fragments denoted NTEV and CTEV fused to interacting proteins. It has been shown to robustly and sensitively quantify protein–protein interactions and receptor activities, as proven before for the ERBB4 receptor and the regulatory adapter subunits of the PI3K, PIK3R1, and PIK3R2 (Wehr et al, 2006, 2008). Recently, the split TEV method was also successfully applied to genomewide RNAi screening in *Drosophila* cell culture, supporting its applicability to high-throughput applications (Wehr et al, 2013).

For our HTS-compatible split TEV assay approach, human full-length ERBB4-Cyt1 was fused to the NTEV fragment, a TEV protease cleavage site (tevS) and the artificial co-transcriptional activator Gal4-VP16 (ERBB4-NTEV-tevS-GV); human PIK3R1 was fused to the CTEV fragment (PIK3R1-CTEV) (Fig 1A). Upon ERBB4 activation, PIK3R1 is recruited to the receptor resulting in a reconstituted protease activity that cleaves off GV. In turn, released GV translocates to the nucleus and binds to upstream activating sequences (UAS) to activate the transcription of a firefly luciferase reporter gene (Fig 1A). A constitutively expressed *Renilla* luciferase driven under the control of the human thymidine kinase (TK) promoter was used as control to address off-target effects related to toxicity.

Compound library

For small molecule screening, the NIH-NCC Clinical Collection library (sets NCC-003 and NCC-201) was used containing 727 small molecules that are FDA-approved and have a history in clinical applications (www.nihclinicalcollection.com). A Hamilton Labstar robot connected to 37 and 4°C incubators for cell incubation and compound storage and application (Cytomat automated incubator, ThermoScientific) and to a luciferase reader (Berthold Technologies) was used to automatically perform the screening. Batch 1 (compounds 1–320) was run in quadruplets, batch 2 (compounds 321–727) in triplicates. Each batch was screened three times.

Transfection of cells

To equally transfect large amounts of cells, PC12 cells were transfected with the split TEV assay components in solution. For one 96-well plate, 4 × 10⁶ PC12 cells were harvested and diluted in 5 ml assay medium (phenol red-free DMEM (low glucose, Life

Technologies), 10% FCS, 5% HS, no antibiotics). The split TEV assay plasmids (2 μ g pcDNA3_ERBB4-NTEV-tevS-GV-2xHA, 2 μ g pTag4C_PIK3R1-CTEV-2xHA, 2 μ g p5xUAS_firefly luciferase, 2 μ g pTK_Renilla luciferase, and 0.5 μ g pECFP-C1 for examining transfection efficiency) were diluted in 2.5 ml Opti-MEM (Life Technologies) and vortexed. In parallel, 20 μ l of the transfection reagent Lipofectamine 2000 was diluted in 2.5 ml Opti-MEM and vortexed. Both Opti-MEM aliquots were mixed, vortexed, and incubated for 20 min at room temperature, followed by carefully mixing the DNA/Lipofectamine/Opti-MEM solution with the PC12 cells and incubating the cell suspension at 37°C and 5% CO₂ for 2 h without shaking.

Plating the cells

For plating of one 96-well plate, 10 ml suspension, containing the 4×10^6 in solution-transfected cells, was placed in the bubble paddle reservoir of the Hamilton Cellstar robot. 100 μ l was seeded per 96-well using the 96-tip pipetting head. The homogeneity of the cell suspension was guaranteed over time by mild stirring using the paddling device inside the reservoir. For five plates each, 50 ml of additional cell suspension was used to allow for losses of inaccessible volume. After seeding, plates were transferred and stored in the Cytomat device at 37°C and 5% CO₂.

Addition of compounds

The cells were allowed to express the plasmids for 24 h before compounds were added. Proper expression and transfection efficiency were verified by ECFP expression on a clear control plate. The compounds were applied in a final concentration of 10 μ M using DMSO as diluent. Sixteen positions per 96-well plate (i.e., columns A and H) were reserved for controls; in detail, four wells each were taken for positive controls (stimulated with 10 ng/ml EGFld (Reprokine, RKQ02297) in DMSO, 96-well positions A1 to D1), baseline controls (DMSO only, 96-well positions E1 to H1), negative controls I (100 nM CI-1033 (Canertinib dihydrochloride, Axon, 1433) in DMSO, 96-well positions A12-D12), and negative controls II (10 μ M lapatinib (Lapatinib ditosylate, Axon, 1395) in DMSO, 96-well positions E12 to H12). Thirty minutes later, 10,000 Nrg1-expressing PC12 cells in 100 μ l assay medium were seeded on top. 24 h after addition of the compounds, the cells were lysed using 40 μ l Passive Lysis buffer (Promega) and subjected to a Dual Luciferase Assay (Promega) according to the manufacturer's instructions. The data were analyzed in R Bioconductor using the package cellHTS2 (<http://www.bioconductor.org/packages/devel/bioc/html/cellHTS2.html>), assessed using the z-score, and visualized using the program Mondrian (<http://stats.math.uni-augsb.de/mondrian/>).

Dose-response luciferase assays for validation

Individually re-screened candidates were validated using a dose-response assay. PC12 cells were batch-transfected as described in the section "Transfection of cells", manually plated, and incubated for 24 h at 37°C and 5% CO₂. Candidate small molecules were prepared in a series of dilutions using DMSO as diluent and ranging from 0.0001 to 100 μ M at final concentrations, thus covering at least five orders of magnitude. Candidate dilutions were added, followed by the addition of 10,000 Nrg1-expressing cells in 100 μ l volume 30 min later. Cells were lysed in 40 μ l Passive Lysis Buffer and

analyzed in a Dual Luciferase Assay. Data were analyzed in Excel and GraphPad Prism. For single-culture assays that used EGFld as stimulus, 100 μ l assay medium containing EGFld (f.c. 10 ng/ml) was administered. The following candidates were analyzed in dose-response assays: spironolactone (Sigma-Aldrich, S3378), eplerenone (Sigma-Aldrich, E6657), canrenone (Santa Cruz Biotechnology, sc-205616), 7 α -thiomethyl-spironolactone (Santa Cruz Biotechnology, sc-207187). Dose-response assays were run in six replicates per concentration and repeated at least two times. Data are shown as mean, and error bars represent SEM.

Electrophysiology

300- μ m-thick transverse slices comprising the medial prefrontal cortex (mPFC) area were prepared from 7- to 8-week-old C57Bl/6 mice as described previously (Teng *et al*, 2013; Agarwal *et al*, 2014). All recordings were performed in cortical layer V projection neurons. The bath solution consisted of oxygenated artificial cerebrospinal fluid (ACSF) containing NaCl 126 mM, KCl 3 mM, NaH₂PO₄ 1.25 mM, MgSO₄ 1 mM, NaHCO₃ 26 mM, CaCl₂ 2 mM, glucose 10 mM, and the pH 7.2 adjusted with NaOH. Spontaneous GABAergic inhibitory postsynaptic currents (sIPSC) and evoked GABAergic inhibitory postsynaptic currents (eIPSC) were recorded at a holding potential of -70 mV in the presence of 6-cyano-7-nitroquinoxaline-2,3-dione (CNQX, 10 μ M) and DL-2-amino-5-phosphonovaleric acid (D-APV, 50 μ M). Glass pipettes were filled with the solution containing: KCl 140 mM, MgCl₂ 2 mM, CaCl₂ 1 mM, Na₂GTP 0.5 mM, Na₂ATP 4 mM, EGTA 10 mM, HEPES 10 mM. Patches with a series resistance of > 25 M Ω , a membrane resistance of < 0.8 G Ω , or leak currents of > 150 pA were excluded. Biphasic rectangular electric pulses (10 ms, 100–300 μ A) were applied to layer I of the prelimbic area of mPFC through another glass pipette filled with ACSF. Synaptic currents were acquired at 20 kHz and filtered at 6 kHz, with a Digidata 1440 ADC-converter coupled to a Multiclamp 700B amplifier (Molecular Devices, USA). Data acquisition was performed using pClamp10 software (Molecular Devices). MiniAnalysis 6.0.9 (Synaptosoft Inc., Decatur, USA) and pClamp10.1 were used for amplitude and frequency analysis of sIPSCs and eIPSCs, respectively. Paired Student's *t*-test was used for statistical analysis.

Mouse behavior analysis

For behavioral testing, age-matched male mice (8–16 weeks) on C57Bl/6 background that constitutively overexpress the 2xHA-tagged Nrg1 type III β 1a isoform (Nrg1-tg) under the control of the mouse Thy1.2 promoter (Velanac *et al*, 2012) and their wild-type (wt) littermates as controls were used. Animals were group-housed in the same ventilated sound-attenuated rooms under a 12-h light/12-h dark schedule (lights on at 8:00 am) at an ambient temperature of 21°C with food and water available *ad libitum*. One week prior to experiments, mice were separated into single cages and habituated to the experimental rooms. To minimize the influence of the circadian rhythm on drug actions, the treatment groups were analyzed at balanced time points during the light phase. The investigators for behavioral tests were blind to genotypes and/or spironolactone administration. All animal experiments were conducted in accordance with NIH principles of laboratory animal care and were

approved by the Government of Lower Saxony, Germany, in accordance with the German Animal Protection Law.

Spironolactone treatment

50 mg of Spironolactone (Sigma-Aldrich) was initially dissolved in DMSO and suspended in 10 ml of 0.9% NaCl, 1% DMSO, and 0.002% Tween[®]20. Spironolactone (5 mg/ml) and a vehicle control (0.9% NaCl, 1% DMSO, and 0.002% Tween[®]20) were subcutaneously injected with a 50 mg/kg dose daily (e.g., corresponding to 0.3 ml injection volume of a mouse with 30 g weight) for 3 weeks prior to behavioral testing ($n = 12$ per genotype and per treatment). Treatment was continued throughout the behavioral analysis period. To avoid injection-induced stress prior to behavioral testing, mice were injected in the afternoon, after the entire cohort has completed the behavioral paradigm.

Calculation of spironolactone dosage

The calculated daily dosage of 50 mg/kg/day spironolactone for mice is based on the following assumptions. Patients are routinely treated with 400 mg/day spironolactone (Aldactone 100, Riemser Pharma; spironolactone 100, Ratiopharm). Dosages of 50 to 100 mg/day were administered to patients in long-term treatments (Jurueña *et al*, 2009). The dosage of 400 mg/80 kg patient body weight per day is equal to 5 mg/kg/day. Human doses are converted to mouse doses using the body surface area normalization method, which integrates various aspects of biological parameters including basal metabolism, blood volume, caloric expenditure, and oxygen utilization (Reagan-Shaw *et al*, 2008). For the calculation of the mouse dose (mg/kg), the human dose (mg/kg) is multiplied by the human K_m /mouse K_m , where the human $K_m = 37$ and the mouse $K_m = 3$. Therefore, mice should be treated with a 12-fold higher dose. The chosen dosage of 50 mg/kg/day is slightly below the calculated maximum dose of 61.7 mg/kg/day [(400 mg/80 kg) * (37/3)/day]. The IC_{50} of spironolactone is > 1,000 mg/kg/day. Spironolactone is FDA-approved, used in patients for decades, and shows no major side effect in treated mice.

Behavioral tests applied for mouse behavior analysis

Open field and hole board Spontaneous locomotor activity was verified in the open-field test using a Plexiglas box (45 × 45 × 55 cm). The same test arena was modified with a floor insert containing 16 symmetrically allocated holes for the hole board test. During a 10-min testing session, mouse behavior was monitored by infrared sensors and recorded by the ActiMot software (TSE, Bad Homburg, Germany). Levels of urination (scored in events) and defecation (scored as feci in events) were determined manually during the open-field test.

Light–dark preference The light–dark preference test was conducted in a plastic chamber divided into two compartments of same size, with one having black and the second one having transparent Plexiglas walls. A door-like opening in the center of the separating wall allowed transitions between both compartments. For testing, each mouse was placed into the light compartment facing away from the door and left undisturbed. The latency to enter the dark compartment, the time spent in the dark compartment, and the number of crossings between the compartments were monitored

for 5 min using the AnyMaze software. Mice that did not enter the dark compartment within 10 min were excluded from the experiment. After each session, the chambers were cleaned with 70% ethanol.

Y-maze The assessment of working memory was performed using an in-house made Y-shaped runway. Animals were placed individually into the Y-maze facing the wall and allowed to explore the maze for 10 min. The experiment was video recorded. The number of arm choices (as a measure of activity) and the percent of alterations (choices of a “novel” arm, i.e., when animals chose a different arm as before is regarded as a measure of working memory) were scored and analyzed. To avoid any olfactory cues, the apparatus was cleaned with 70% ethanol between animals.

Tail suspension test Mice were manually suspended upside down for 6 min by attaching them to a fixed rod using an adhesive tape positioned at the tip of the tail. The escape motivation of a mouse was measured as the time spent active, video recorded, and scored offline.

Prepulse inhibition (PPI) The startle response was measured using a two test cabinet (SR-LAB, San Diego Instruments) using a protocol as described in Brzózka *et al* (2010).

Fear conditioning Fear memory assessment that is measured by freezing behavior was performed using the Ugo Basile Fear Conditioning System (Varese, Italy). For conditioning, mice were placed into the animal box (furnished with a stainless shock grid floor and striped black-white walls) and positioned into an isolation cubicle equipped with a lamp, a loudspeaker and infrared camera. For conditioning, striped black-white walls were inserted into the animal box. The conditioning and fear memory assessment were performed as described in Brzózka *et al* (2010).

Hot plate Pain sensitivity was measured in the hot plate test. Animals were placed onto a metal plate preheated to 52°C. The latency to the first reaction (hind paw licking or jumping) was scored manually. Immediately after the first response, mice were placed onto another metal plate (not heated) to allow cooling their paws.

Statistical analysis

Statistical significance was determined using Microsoft Excel, IBM SPSS Statistics v22 and GraphPad Prism 5.0 software. Data are presented as means ± SD or SEM as indicated ($n \geq 3$, for luciferase assays $n = 6$). For behavioral experiments, Student's *t*-tests were used for comparing two data samples. If the experimental setup required a paired data analysis, paired Student's *t*-test or paired Wilcoxon signed ranks test was used for comparing two normally or not-normally distributed data samples, respectively. Two-way ANOVA with Bonferroni *post hoc* test was used for the analysis of three or more samples. Two-way ANCOVA was used for the age-corrected analyses of open-field, Y-maze and light–dark preference tests. Repeated-measures ANOVA was used to analyze the effects of treatment in the PPI analyses. The robustness of cell-based assays was assessed using the Z' factor. Data from screening were analyzed

The paper explained**Problem**

NRG1-ERBB4 signaling is a schizophrenia risk pathway in humans and altered signaling activity causes schizophrenia-relevant endophenotypes in transgenic mouse models. To date, no treatment options are available targeting this pathway in schizophrenic patients.

Results

Here, we have developed a NRG1-ERBB4 pathway-selective screening assay based on the split TEV technology to monitor activities of FDA-approved drugs for repurposing. The anti-mineralocorticoid spironolactone was identified as top candidate from the screen to antagonize ERBB4 receptor activity. Spironolactone's effect was biochemically validated both *in vitro* and *in vivo*, and it was found to improve schizophrenia-relevant behavioral deficits in a *Nrg1* transgenic mouse model.

Impact

We provide preclinical evidence for an approved drug that may immediately qualify for a clinical study in schizophrenic patients.

using the cellHTS2 package available for R and evaluated using the z-score.

Expanded View for this article is available online.

Acknowledgements

We thank Elena Ciirdaeva, Nadia Gabellini, Monika Rübekell, and Barbara Meisel for excellent technical support. M.C.W. was supported by the Deutsche Forschungsgemeinschaft (WE 5683/1-1). M.J.R. was supported by the Deutsche Forschungsgemeinschaft (Klinische Forschergruppe (KFO) 241: RO 4076/1-1 and PsyCourse: RO 4076/5-1). W.Z. was supported by the IZKF of the University of Münster Medical School (Zha3-005-14) and by the Deutsche Forschungsgemeinschaft (SFB TRR58 to W.Z.).

Author contributions

Designed, performed, and analyzed the compound screen: MCW, WH, SPW, MJR; performed luciferase and biochemical validation experiments: MCW, WH, JPW, AH; performed immunocytochemistry: MCW, MCS-B; performed electrophysiological experiments: MK, MZ; designed behavioral analysis: MMB; performed and analyzed behavioral experiments: MMB, WH, TU, SP, MCW, MJR; supervised students and provided essential reagents: K-AN, PF, WZ, MHS; conceived the study and wrote the manuscript: MCW, MJR.

Conflict of interest

Systasy Bioscience GmbH holds the patent for the split TEV technique (termed splitSENSOR technology at Systasy Bioscience GmbH). M.C. Wehr, S.P. Wichert, and M.J. Rossner are co-founders and shareholders of Systasy Bioscience GmbH, Munich, Germany.

References

Agarwal A, Zhang M, Trembak-Duff I, Unterbarnscheidt T, Radyushkin K, Dibaj P, Martins de Souza D, Boretius S, Brzózka MM, Steffens H *et al* (2014) Dysregulated expression of neuregulin-1 by cortical pyramidal neurons disrupts synaptic plasticity. *Cell Rep* 8: 1130–1145

- Bennett MR (2011) Schizophrenia: susceptibility genes, dendritic-spine pathology and gray matter loss. *Prog Neurobiol* 95: 275–300
- Brzózka MM, Radyushkin K, Wichert SP, Ehrenreich H, Rossner MJ (2010) Cognitive and sensorimotor gating impairments in transgenic mice overexpressing the schizophrenia susceptibility gene *Tcf4* in the brain. *Biol Psychiatry* 68: 33–40
- Chen Y-J, Zhang M, Yin D-M, Wen L, Ting A, Wang P, Lu Y-S, Zhu X-H, Li S-J, Wu C-Y *et al* (2010) ErbB4 in parvalbumin-positive interneurons is critical for neuregulin 1 regulation of long-term potentiation. *Proc Natl Acad Sci USA* 107: 21818–21823
- Citri A, Yarden Y (2006) EGF-ERBB signalling: towards the systems level. *Nat Rev Mol Cell Biol* 7: 505–516
- Deakin IH, Law AJ, Oliver PL, Schwab MH, Nave KA, Harrison PJ, Bannerman DM (2009) Behavioural characterization of neuregulin 1 type I overexpressing transgenic mice. *NeuroReport* 20: 1523–1528
- Deakin IH, Nissen W, Law AJ, Lane T, Kanso R, Schwab MH, Nave K-A, Lamsa KP, Paulsen O, Bannerman DM *et al* (2012) Transgenic overexpression of the type I isoform of neuregulin 1 affects working memory and hippocampal oscillations but not long-term potentiation. *Cereb Cortex* 22: 1520–1529
- Fazzari P, Paternain AV, Valiente M, Pla R, Luján R, Lloyd K, Lerma J, Marín O, Rico B (2010) Control of cortical GABA circuitry development by *Nrg1* and *ErbB4* signalling. *Nature* 464: 1376–1380
- Feng Y, Mitchison TJ, Bender A, Young DW, Tallarico JA (2009) Multi-parameter phenotypic profiling: using cellular effects to characterize small-molecule compounds. *Nat Rev Drug Discov* 8: 567–578
- Gaddam K, Pimenta E, Thomas SJ, Cofield SS, Oparil S, Harding SM, Calhoun DA (2010) Spironolactone reduces severity of obstructive sleep apnoea in patients with resistant hypertension: a preliminary report. *J Hum Hypertens* 24: 532–537
- Goff DC, Hill M, Barch D (2011) The treatment of cognitive impairment in schizophrenia. *Pharmacol Biochem Behav* 99: 245–253
- Hahn C-G, Wang H-Y, Cho D-S, Talbot K, Gur RE, Berrettini WH, Bakshi K, Kamins J, Borgmann-Winter KE, Siegel SJ *et al* (2006) Altered neuregulin 1-erbB4 signaling contributes to NMDA α receptor hypofunction in schizophrenia. *Nat Med* 12: 824–828
- Harrison PJ, Law AJ (2006) Neuregulin 1 and schizophrenia: genetics, gene expression, and neurobiology. *Biol Psychiatry* 60: 132–140
- Hashimoto R, Straub RE, Weickert CS, Hyde TM, Kleinman JE, Weinberger DR (2004) Expression analysis of neuregulin-1 in the dorsolateral prefrontal cortex in schizophrenia. *Mol Psychiatry* 9: 299–307
- Hu X, Hicks CW, He W, Wong P, Macklin WB, Trapp BD, Yan R (2006) *Bace1* modulates myelination in the central and peripheral nervous system. *Nat Neurosci* 9: 1520–1525
- Insel TR (2010) Rethinking schizophrenia. *Nature* 468: 187–193
- Insel TR (2012) Next-generation treatments for mental disorders. *Sci Transl Med* 4: 155 ps19
- Johannessen CM, Boehm JS, Kim SY, Thomas SR, Wardwell L, Johnson LA, Emery CM, Stransky N, Cogdill AP, Barretina J *et al* (2010) COT drives resistance to RAF inhibition through MAP kinase pathway reactivation. *Nature* 468: 968–972
- Juruena MF, Gama CS, Berk M, Belmonte-de-Abreu PS (2009) Improved stress response in bipolar affective disorder with adjunctive spironolactone (mineralocorticoid receptor antagonist): case series. *J Psychopharmacol* 23: 985–987
- Kato T, Kasai A, Mizuno M, Fengyi L, Shintani N, Maeda S, Yokoyama M, Ozaki M, Nawa H (2010) Phenotypic characterization of transgenic mice overexpressing neuregulin-1. *PLoS One* 5: e14185

- Law AJ, Lipska BK, Weickert CS, Hyde TM, Straub RE, Hashimoto R, Harrison PJ, Kleinman JE, Weinberger DR (2006) Neuregulin 1 transcripts are differentially expressed in schizophrenia and regulated by 5' SNPs associated with the disease. *Proc Natl Acad Sci USA* 103: 6747–6752
- Law AJ, Kleinman JE, Weinberger DR, Weickert CS (2007) Disease-associated intronic variants in the ErbB4 gene are related to altered ErbB4 splice-variant expression in the brain in schizophrenia. *Hum Mol Genet* 16: 129–141
- Law AJ, Wang Y, Sei Y, O'Donnell P, Piantadosi P, Papaleo F, Straub RE, Huang W, Thomas CJ, Vakkalanka R et al (2012) Neuregulin 1-ErbB4-PI3K signaling in schizophrenia and phosphoinositide 3-kinase-p110 δ inhibition as a potential therapeutic strategy. *Proc Natl Acad Sci USA* 109: 12165–12170
- Lencz T, Malhotra AK (2015) Targeting the schizophrenia genome: a fast track strategy from GWAS to clinic. *Mol Psychiatry* 20: 820–826
- Li D, Collier DA, He L (2006) Meta-analysis shows strong positive association of the neuregulin 1 (NRG1) gene with schizophrenia. *Hum Mol Genet* 15: 1995–2002
- Luo X, He W, Hu X, Yan R (2014) Reversible overexpression of bace1-cleaved neuregulin-1 N-terminal fragment induces schizophrenia-like phenotypes in mice. *Biol Psychiatry* 76: 120–127
- Margraf J, Schneider S (2016) From neuroleptics to neuroscience and from Pavlov to psychotherapy: more than just the “emperor’s new treatments” for mental illnesses?. *EMBO Mol Med* 8: 1115–1117
- Mei L, Xiong W-C (2008) Neuregulin 1 in neural development, synaptic plasticity and schizophrenia. *Nat Rev Neurosci* 9: 437–452
- Mei L, Nave K-A (2014) Neuregulin-ERBB signaling in the nervous system and neuropsychiatric diseases. *Neuron* 83: 27–49
- Meng Y, Zhang Y, Tregoubov V, Janus C, Cruz L, Jackson M, Lu WY, MacDonald JF, Wang JY, Falls DL et al (2002) Abnormal spine morphology and enhanced LTP in LIMK-1 knockout mice. *Neuron* 35: 121–133
- Meng Y, Takahashi H, Meng J, Zhang Y, Lu G, Asrar S, Nakamura T, Jia Z (2004) Regulation of ADF/cofilin phosphorylation and synaptic function by LIM-kinase. *Neuropharmacology* 47: 746–754
- Nestler EJ, Hyman SE (2010) Animal models of neuropsychiatric disorders. *Nat Neurosci* 13: 1161–1169
- Nicodemus KK, Luna A, Vakkalanka R, Goldberg T, Egan M, Straub RE, Weinberger DR (2006) Further evidence for association between ErbB4 and schizophrenia and influence on cognitive intermediate phenotypes in healthy controls. *Mol Psychiatry* 11: 1062–1065
- Ogden DA, Scherr L, Spritz N, Rubin AL (1961) A comparison of the properties of chlorothiazide, spironolactone and a combination of both as diuretic agents. *N Engl J Med* 265: 358–362
- Reagan-Shaw S, Nihal M, Ahmad N (2008) Dose translation from animal to human studies revisited. *FASEB J* 22: 659–661
- Rico B, Marín O (2011) Neuregulin signaling, cortical circuitry development and schizophrenia. *Curr Opin Genet Dev* 21: 262–270
- Rimmele U, Besedovsky L, Lange T, Born J (2013) Blocking mineralocorticoid receptors impairs, blocking glucocorticoid receptors enhances memory retrieval in humans. *Neuropsychopharmacology* 38: 884–894
- Silberberg G, Darvasi A, Pinkas-Kramarski R, Navon R (2006) The involvement of ErbB4 with schizophrenia: association and expression studies. *Am J Med Genet B Neuropsychiatr Genet* 141B: 142–148
- Stefansson H, Sigurdsson E, Steinthorsdottir V, Bjornsdottir S, Sigmundsson T, Ghosh S, Brynjolfsson J, Gunnarsdottir S, Ivarsson O, Chou TT et al (2002) Neuregulin 1 and susceptibility to schizophrenia. *Am J Hum Genet* 71: 877–892
- Teng Z, Zhang M, Zhao M, Zhang W (2013) Glucocorticoid exerts its non-genomic effect on IPSC by activation of a phospholipase C-dependent pathway in prefrontal cortex of rats. *J Physiol* 591: 3341–3353
- Velanac V, Unterbarnscheidt T, Hinrichs W, Gummert MN, Fischer TM, Rossner MJ, Trimarco A, Brivio V, Taveggia C, Willem M et al (2012) Bace1 processing of NRG1 type III produces a myelin-inducing signal but is not essential for the stimulation of myelination. *Glia* 60: 203–217
- Vullhorst D, Mitchell RM, Keating C, Roychowdhury S, Karavanova I, Tao-Cheng J-H, Buonanno A (2015) A negative feedback loop controls NMDA receptor function in cortical interneurons via neuregulin 2/ErbB4 signalling. *Nat Commun* 6: 7222
- Wang Z-Y, Zhang H-Y (2013) Rational drug repositioning by medical genetics. *Nat Biotechnol* 31: 1080–1082
- Wehr MC, Laage R, Bolz U, Fischer TM, Grünewald S, Scheek S, Bach A, Nave K-A, Rossner MJ (2006) Monitoring regulated protein-protein interactions using split TEV. *Nat Methods* 3: 985–993
- Wehr MC, Reinecke L, Botvinnik A, Rossner MJ (2008) Analysis of transient phosphorylation-dependent protein-protein interactions in living mammalian cells using split-TEV. *BMC Biotechnol* 8: 55
- Wehr MC, Holder MV, Gailite I, Saunders RE, Maile TM, Ciirdeaeva E, Instrell R, Jiang M, Howell M, Rossner MJ et al (2013) Salt-inducible kinases regulate growth through the Hippo signalling pathway in *Drosophila*. *Nat Cell Biol* 15: 61–71
- Weickert CS, Tiwari Y, Schofield PR, Mowry BJ, Fullerton JM (2012) Schizophrenia-associated HapICE haplotype is associated with increased NRG1 type III expression and high nucleotide diversity. *Transl Psychiatry* 2: e104
- Willem M, Garratt AN, Novak B, Citron M, Kaufmann S, Rittger A, DeStrooper B, Saftig P, Birchmeier C, Haass C (2006) Control of peripheral nerve myelination by the beta-secretase BACE1. *Science* 314: 664–666
- Wu T-C, Chen H-T, Chang H-Y, Yang C-Y, Hsiao M-C, Cheng M-L, Chen J-C (2012) Mineralocorticoid receptor antagonist spironolactone prevents chronic corticosterone induced depression-like behavior. *Psychoneuroendocrinology* 38: 871–883
- Yin D-M, Chen Y-J, Lu Y-S, Bean JC, Sathyamurthy A, Shen C, Liu X, Lin TW, Smith CA, Xiong W-C et al (2013) Reversal of behavioral deficits and synaptic dysfunction in mice overexpressing neuregulin 1. *Neuron* 78: 644–657
- Zhang JH, Chung TD, Oldenburg KR (1999) A simple statistical parameter for use in evaluation and validation of high throughput screening assays. *J Biomol Screen* 4: 67–73
- Zhou M, Kindt M, Joëls M, Krugers HJ (2011) Blocking mineralocorticoid receptors prior to retrieval reduces contextual fear memory in mice. *PLoS One* 6: e26220



License: This is an open access article under the terms of the Creative Commons Attribution 4.0 License, which permits use, distribution and reproduction in any medium, provided the original work is properly cited.

Expanded View Figures

Figure EV1. A co-culture assay based on the split TEV technique to monitor NRG1-ERBB4 signaling activity.

- A PC12 cell lines stably expressing mouse Nrg1 type I β 1a and Nrg1 type III β 1a. PC12 cells were stably transfected with a plasmid encoding Nrg1 type I β 1a or type III β 1a, and Nrg1 expression was verified by Western blot analysis using an Nrg1 antibody that detects the β 1a C-terminus.
- B Co-culturing two populations of PC12 cells. Cell population A was transfected with a nuclear localized EYFP (EYFPnuc), and cell population B was transfected with ECFP. Following to an initial expression of 24 h, cells were mixed and imaged 24 h later. Scale bar, 100 μ m.
- C ERBB4-PIK3R1 dose-response assay using EGFld as stimulus. Three independent experiments using the ERBB4-PIK3R1/EGFld assay are shown. The EC₅₀ value for this assay is at 1 ng/ml EGFld. The inset depicts the Z' factors for each individual assay.
- D Lapatinib antagonizes ERBB4-PIK3R1 signaling in a dose-dependent manner. Per 96-well, 40,000 split TEV assay cells were incubated with increasing amounts of lapatinib, followed by a stimulation using 10 ng/ml EGFld.
- E, F CI-1033 antagonizes ERBB4-PIK3R1 signaling in a dose-dependent manner. Per 96-well, 40,000 split TEV assay cells were incubated with increasing amounts of CI-1033, followed by either co-plating 10,000 Nrg1-expressing cells (E) or stimulation with 10 ng/ml EGFld (F).

Data information: Fluc, firefly luciferase activity (black lines); Rluc, *Renilla* luciferase activity (gray lines, indicating toxicity levels). Data are shown as mean, and error bars represent SEM, $n = 6$. The insets depict IC₅₀ values in μ M.

Source data are available online for this figure.

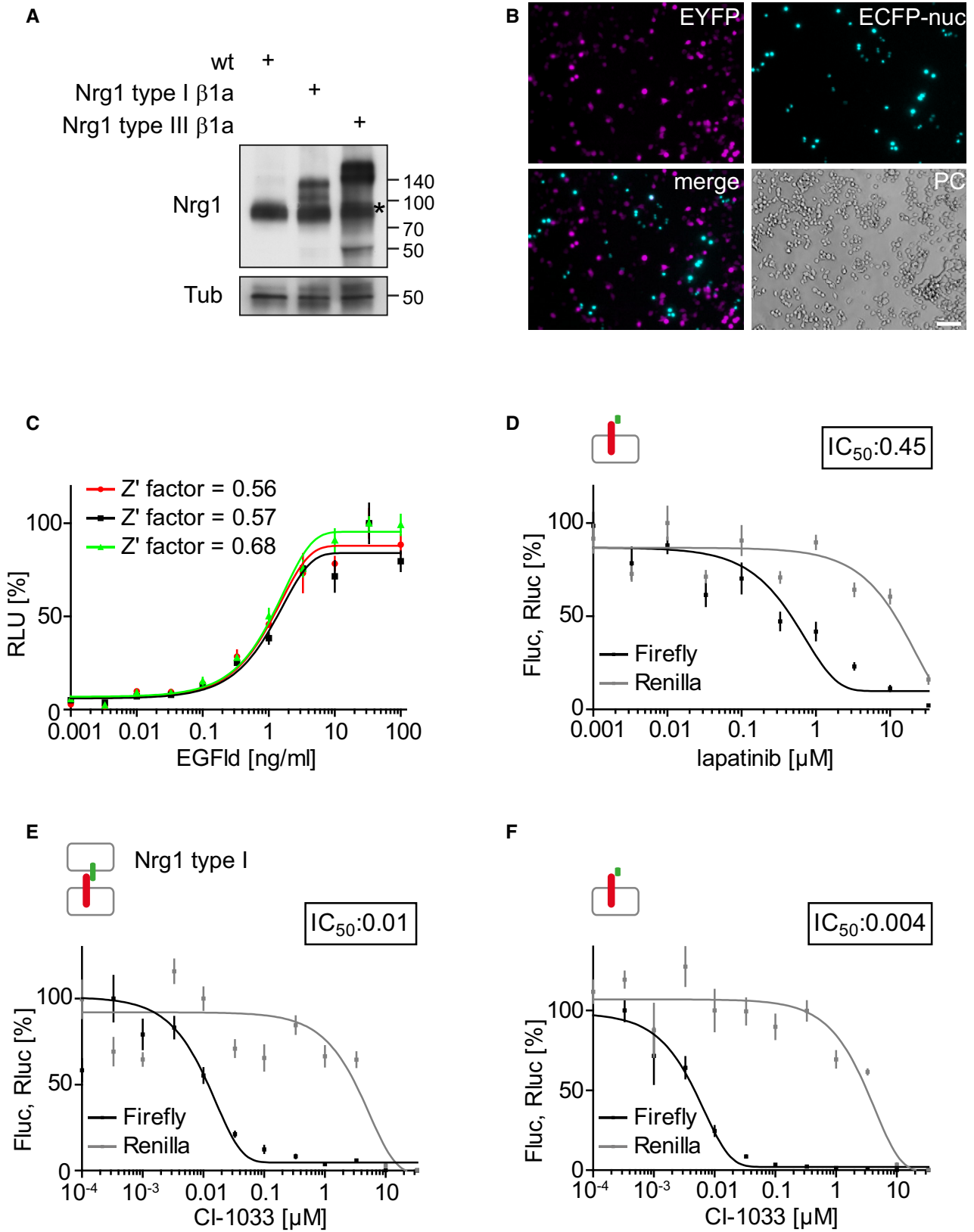


Figure EV1.

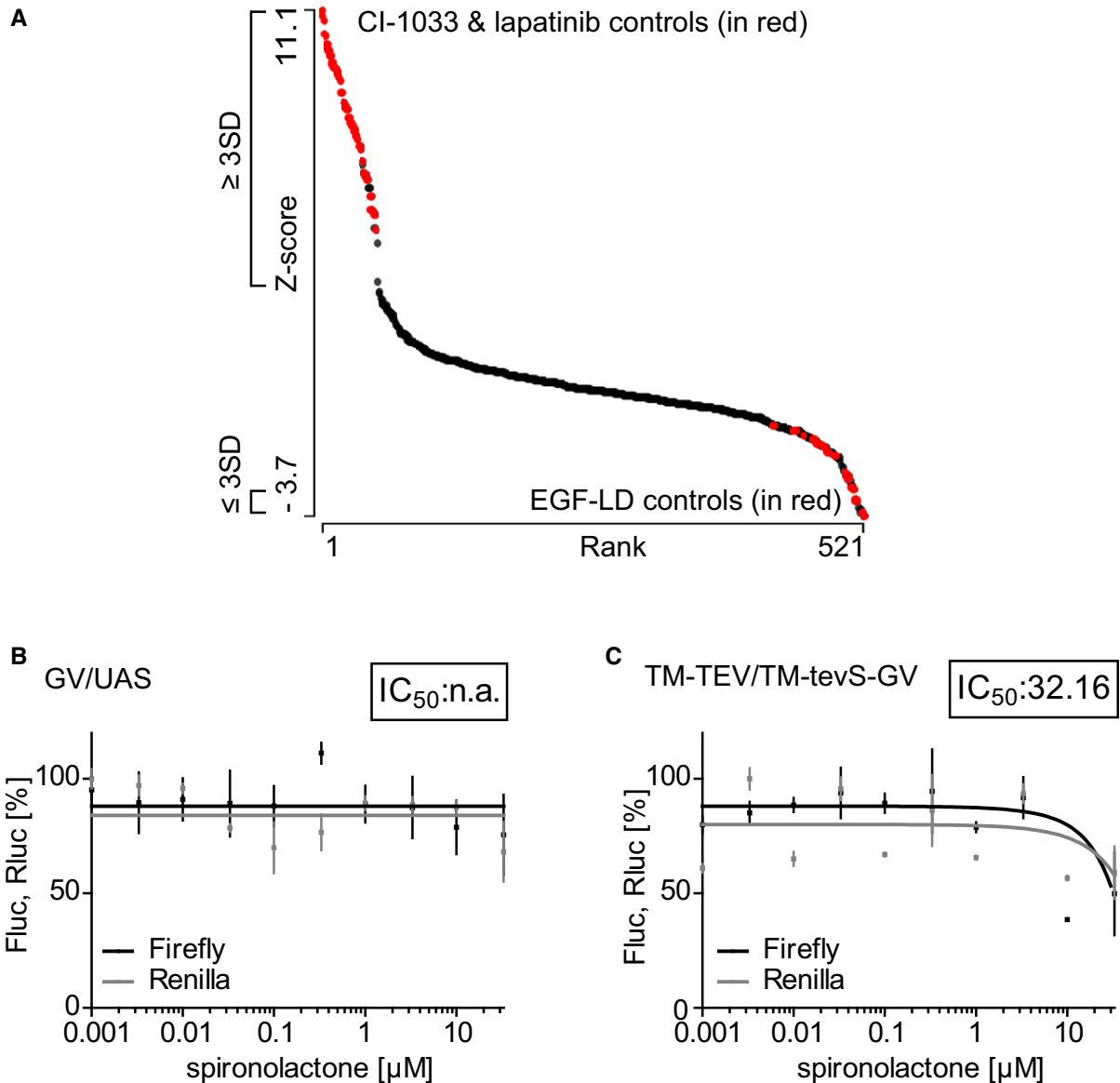


Figure EV2. Spironolactone is the top candidate recovered from the co-culture screen.

A Graphic visualization of the primary screen data of the NIH-NCC library, set 2. All counts (407 compounds and 96 controls) from the Nrg1-ERBB4-PIK3R1 split TEV compound screen were plotted against the z-score using Mondrian, with pathway activators displaying high values and inhibitors low values. For the secondary analysis, we selected all candidates that were at least three standard deviations away from the mean. EGFlD-positive and lapatinib/CI-1033-negative controls are shown in red.

B, C Spironolactone does not affect activities of control assays. Neither the activity of the GAL4/UAS system (**B**) nor the activity of the TEV protease (**C**) was affected in spironolactone dose-dependent assays. For the GAL4/UAS assay, GAL4-VP16 (GV) and 10 \times UAS firefly luciferase (10 \times UAS-Fluc) plasmids were transfected into PC12 cells. For TEV protease activity assays, a transmembrane-localized TEV protease (TM-TEV) was expressed in PC12 cells with a transmembrane-localized and TEV-cleavable GV (TM-tevS-GV) and the 10 \times UAS-Fluc reporter. 10 ng/ μ l EGFlD was applied as Nrg1 stimulus. In both control assays, the assay activity (firefly luciferase, black lines) was similar to the toxicity levels (gray lines). Data are shown as mean, and error bars represent SEM, $n = 6$. The insets depict IC₅₀ values in μ M.

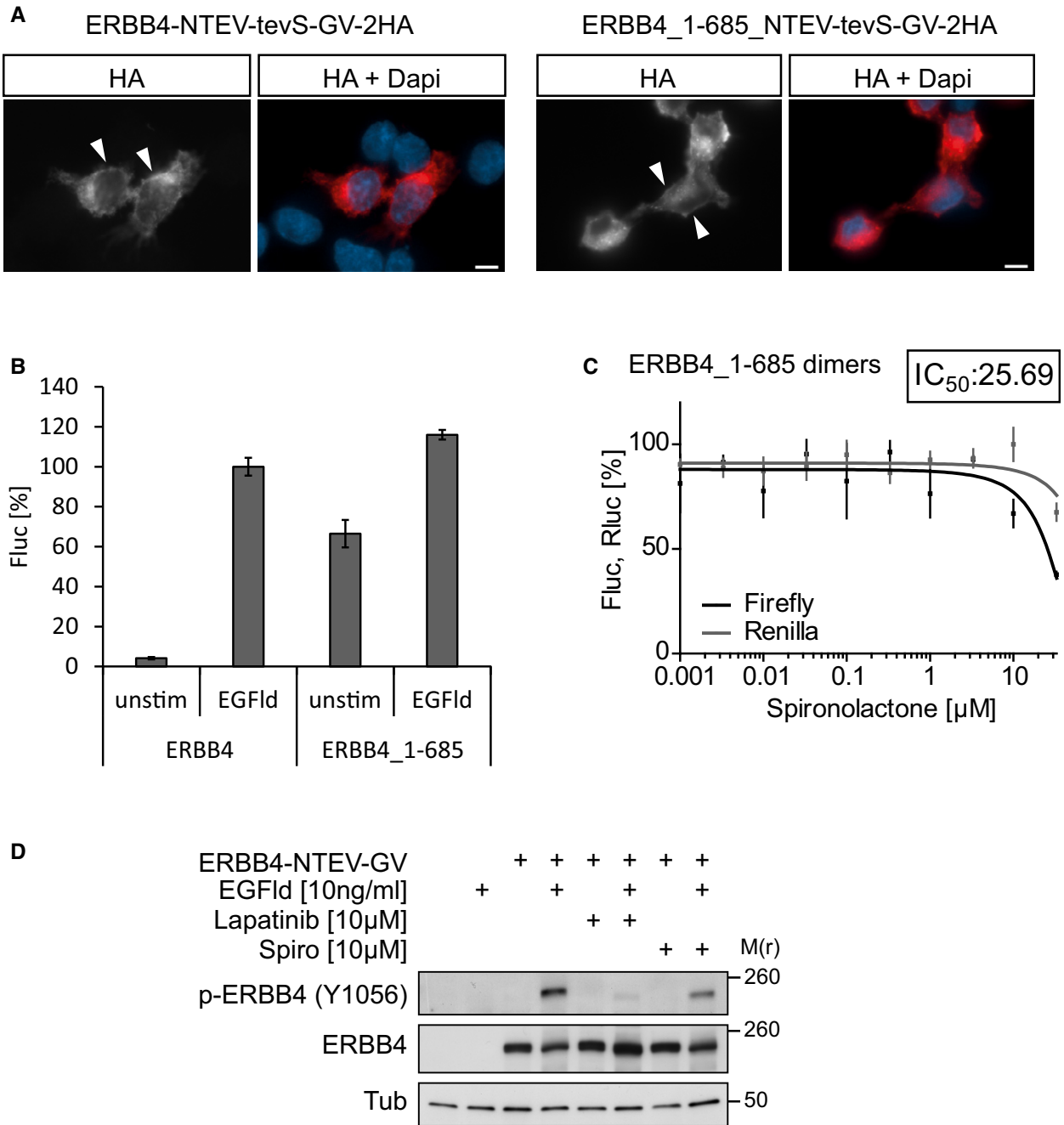


Figure EV3.

Figure EV3. Truncated ERBB4 dimers are not inhibited by spironolactone.

- A Full-length and truncated ERBB4 split TEV fusions localize to the cell membrane. PC12 cells were transfected with a full-length human ERBB4 split TEV fusion (ERBB4-NTEV-tevS-GV-2HA) (left panels) or a truncated human ERBB4 split TEV fusion (ERBB4_1–685_NTEV-tevS-GV-2HA) that covers residues 1–685 and contains the transmembrane domain but lacks the intracellular domain (right panels). Cells were allowed to express the fusion proteins for 24 h, fixed, and stained for the double HA (2HA) tag. Arrowheads indicate expression of full-length and truncated ERBB4 at the membrane. Scale bars, 5 μ m.
- B Both full-length and truncated ERBB4 dimerize in split TEV assays when stimulated with extracellular EGFlid. PC12 cells were transfected with split TEV pairs of ERBB4-NTEV-tevS-GV/-CTEV and ERBB4_1–685_NTEV-tevS-GV/-CTEV, starved overnight, stimulated with EGFlid (10 ng/ml) or mock-stimulated (unstim), incubated for 20 h, lysed, and subjected to a luciferase assay. Fluc, firefly luciferase activity.
- C Spironolactone-mediated inhibition of the ERBB4 dimerization requires the intracellular domain. Truncated ERBB4 receptor molecules (amino acids 1–685) were fused to N- and CTEV moieties, transfected into PC12 cells and assayed in a spironolactone dose-dependent assay in the presence of 10 ng/ml EGFlid using the split TEV technique. Spironolactone had no inhibitory effect, as the assay activity (Fluc, firefly luciferase, black line) was comparable to the toxicity levels (Rluc, *Renilla* luciferase, gray line). The inset depicts the IC₅₀ value in μ M.
- D Spironolactone reduces ERBB4 levels. PC12 cells were transfected with the split TEV assay plasmid ERBB4-NTEV-tevS-GV (where indicated), stimulated with 10 ng/ml EGFlid, 10 μ M lapatinib, and 10 μ M spironolactone for 1 h as indicated. Cell lysates were probed for ERBB4 phosphorylation levels at Tyr1056. Note that spironolactone reduces but not abolishes the phosphorylation levels.

Data information: Data are shown as mean, and error bars represent SEM, $n = 6$.
Source data are available online for this figure.

Figure EV4. Collection of ERBB dimer dose–response assays assessing the target specificity of spironolactone treatment.

- A–J Fluc, firefly luciferase activity reporting ERBB dimer assay activity (black lines) using the split TEV assay technique; Rluc, *Renilla* luciferase activity (gray lines) assessing viability. EGFlid (10 ng/ml) was applied as stimulus unless stated otherwise. Data are shown as mean, and error bars represent SEM, $n = 6$. The insets depict IC₅₀ values in μ M. The following combinations were tested (X-NTEV-tevS-GV with Y-CTEV): (A) ERBB1 (EGFR)/ERBB1, (B) ERBB1/ERBB2, (C) ERBB1/ERBB3, (D) ERBB1/ERBB4, (E) ERBB2/ERBB2, (F) ERBB2/ERBB3, (G) ERBB2/ERBB4, (H) ERBB3/ERBB3, (I) ERBB3/ERBB4, (J) EGFR/EGFR with 100 ng/ml EGF as stimulus.

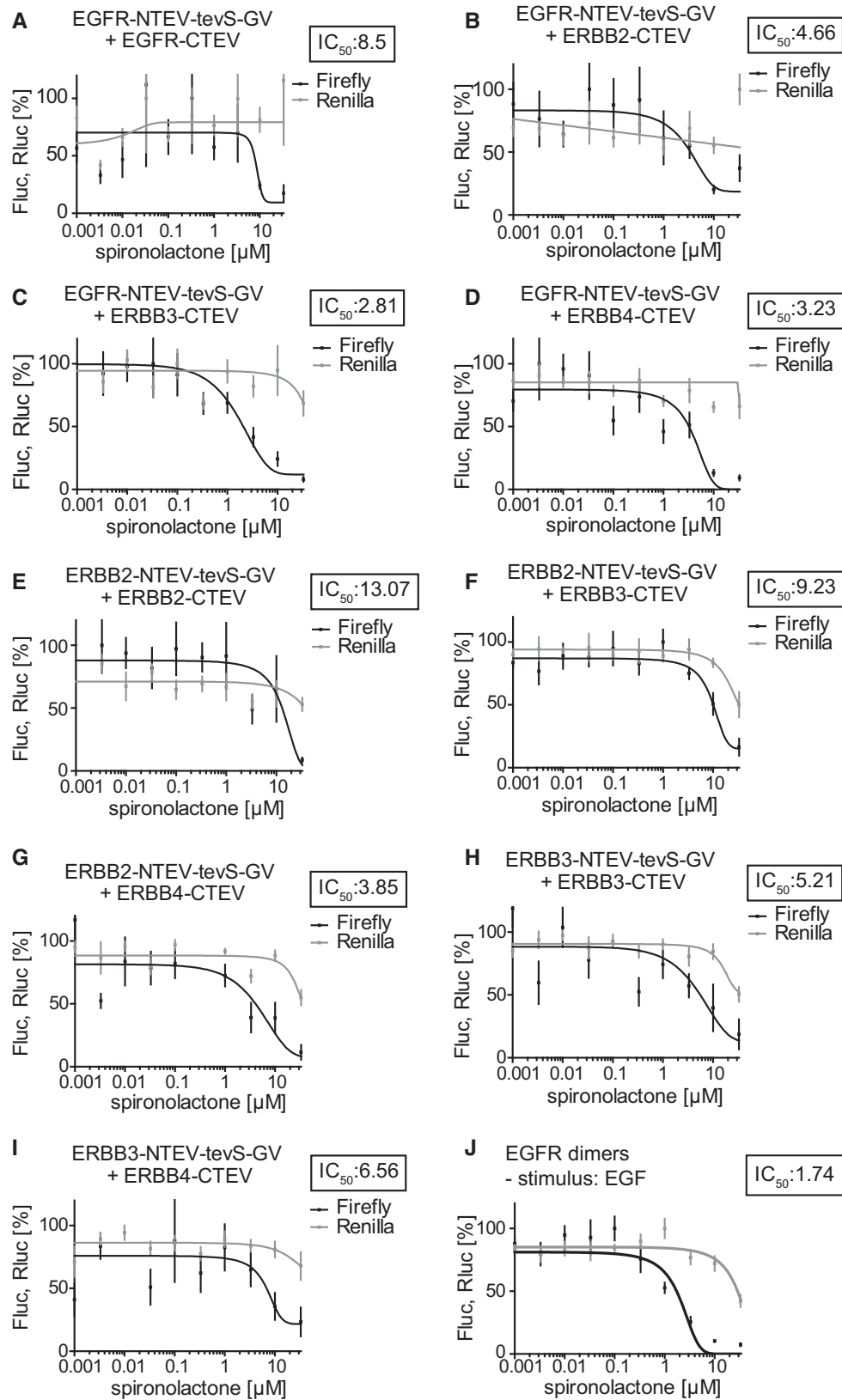


Figure EV4.

Figure EV5. Behavioral analysis of *Nrg1*-tg and wt mice upon spironolactone treatment.

- A Experimental design to test PPI deficits in *Nrg1*-tg mice. *Nrg1*-tg mice and wt controls were tested in the PPI test 1 day prior to chronic spironolactone treatment. One day after the last injection, transgenic and control mice were submitted to the PPI paradigm.
- B Naïve *Nrg1*-tg displayed strong PPI deficits prior to chronic spironolactone treatment (effect of genotype $F_{1,33} = 25.74$; $P < 0.0001$, two-way ANOVA, and Bonferroni *post hoc* test: $***P < 0.0001$, $***P = 0.0002$, $***P = 0.0003$ for prepulse intensities 70, 75 and 80 dB, respectively).
- C Chronic treatment with spironolactone improved PPI in transgenic animals (effect of treatment $F_{1,20} = 9.63$; $P = 0.0056$, two-way ANOVA), with the most prominent effect when a prepulse of 70 dB was presented ($**P = 0.0060$, Bonferroni test; 75 and 80 dB were $P = 0.3067$ and $P = 0.1077$, respectively, Bonferroni test).
- D Spironolactone treatment did not influence PPI in wt controls (effect of treatment $F_{1,26} = 0.14$; $P = 0.7096$, two-way ANOVA).
- E *Nrg1*-tg mice spent less time in the center of the open-field arena (effect of genotype $F_{1,44} = 6.69$; $P = 0.0131$, two-way ANOVA). Spironolactone treatment did not influence this parameter ($F_{1,44} = 0.12$; $P = 0.7290$, two-way ANOVA).
- F In the open-field test, *Nrg1*-tg mice showed increased defecation (effect of genotype $F_{1,44} = 10.35$; $P = 0.0024$, two-way ANOVA), which was significant in vehicle-treated animals ($*P = 0.0310$; Bonferroni test), but not in spironolactone-treated animals ($P = 0.0967$). There was no effect of treatment observed ($F_{1,44} = 0.65$; $P = 0.4256$, two-way ANOVA).
- G Transgenic animals displayed more frequent urination than wt controls (effect of genotype $F_{1,44} = 14.14$; $P = 0.0005$, two-way ANOVA) in both vehicle and spironolactone-treated animals ($*P = 0.0451$ for vehicle-treated and $*P = 0.0100$ for spironolactone-treated groups, Bonferroni test), without effect of treatment ($F_{1,44} = 0.17$; $P = 0.6781$, two-way ANOVA).
- H In the light–dark preference test, transgenic mice performed similar number of transitions between light and dark compartment when compared to wt controls (effect of genotype $F_{1,41} = 0.05$; $P = 0.8227$, two-way ANOVA).
- I In the tail suspension test, transgenic mice were more active than wt controls. The effect was independent of treatment (effect of genotype $F_{1,44} = 35.16$; $P < 0.0001$, two-way ANOVA). The Bonferroni test showed a significant difference between genotypes both in vehicle and spironolactone-treated groups ($***P < 0.0001$ and $**P = 0.0067$, respectively).
- J *Nrg1*-tg animals displayed an increased activity in the Y-maze test as they performed more arm choices (effect of genotype $F_{1,44} = 14.56$; $P = 0.0004$, two-way ANOVA), with $*P = 0.0301$ in vehicle-treated and $*P = 0.0127$ in spironolactone-treated groups (Bonferroni test). There was no effect of treatment ($F_{1,44} = 0.39$; $P = 0.5367$, two-way ANOVA).
- K Naïve *Nrg1*-tg mice did not display impairments in the fear conditioning test. However, transgenic animals treated with spironolactone showed a tendency toward lower freezing rate during contextual memory test ($P = 0.0885$; Mann–Whitney test). A two-way ANOVA yielded a substantial, but not significant, interaction in the contextual memory test ($F_{1,44} = 3.56$; $P = 0.0657$); but neither an effect of genotype ($F_{1,44} = 0.96$; $P = 0.3315$) nor of treatment ($F_{1,44} = 1.16$; $P = 0.2880$) was detected. Naïve *Nrg1*-tg showed an increased freezing rate during baseline recordings prior to the cue test ($^{##}P = 0.0351$, Mann–Whitney test); this difference between the genotypes was not observed in groups treated with spironolactone.
- L In the hot plate test, *Nrg1*-tg mice showed an increased latency to the first reaction (effect of genotype $F_{1,44} = 12.47$; $P = 0.0010$; two-way ANOVA), which was most prominent in the group treated with spironolactone ($**P = 0.0024$, Bonferroni test) but not in vehicle-treated groups ($P = 0.2662$, Bonferroni test).
- M Spironolactone treatment did not influence PPI in wt mice (effect of treatment $F_{1,22} = 0.00$; $P = 0.9461$, two-way ANOVA).

Data information: Data are shown as mean, and error bars represent SEM; n.s., not significant; Spiro, spironolactone; pre-Spiro, data collected before spironolactone treatment. $n = 12$ per genotype and treatment with an exception in (F): *Nrg1*-tg vehicle, $n = 11$; *Nrg1*-tg Spiro, $n = 10$; wt vehicle, $n = 12$; wt Spiro, $n = 12$.

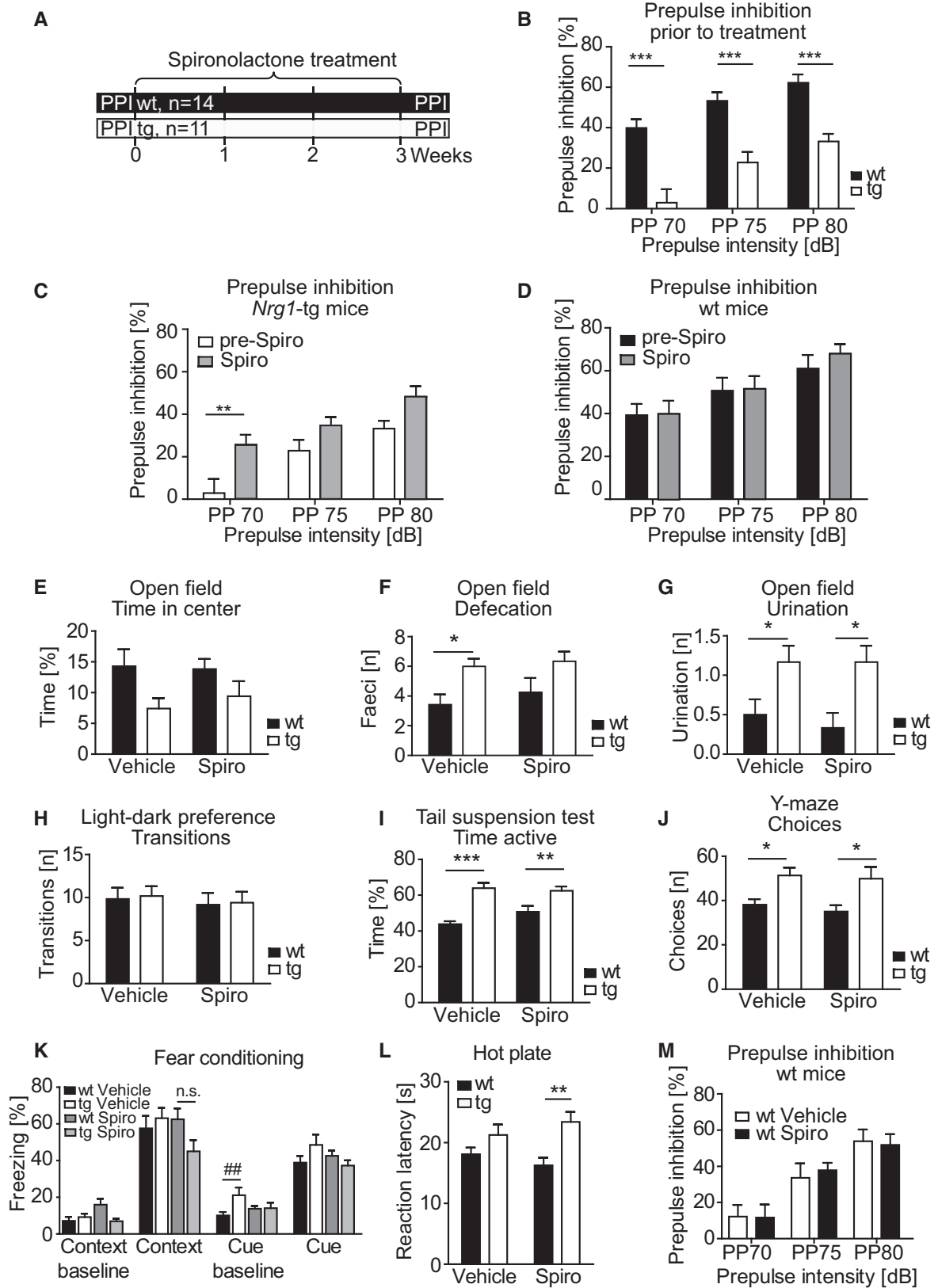


Figure EV5.

Appendix

Michael C. Wehr, Wilko Hinrichs, Magdalena M. Brzózka, Tilmann Unterbarnscheidt, Alexander Herholt, Jan P. Wintgens, Sergi Papiol, M. Clara Soto-Bernardini, Mykola Kravchenko, Mingyue Zhang, Klaus-Armin Nave, Sven P. Wichert, Peter Falkai, Weiqi Zhang, Markus H. Schwab & Moritz J. Rossner

Spirolactone is an Antagonist of NRG1-ERBB4 Signaling and Schizophrenia-Relevant Endophenotypes in Mice

Table of content

Appendix Fig S1. Summary of the validation strategy for drug repurposing performed on the NRG1-ERBB4-PI3K schizophrenia risk pathway.

Appendix Fig S2. Protein expression analysis reveals strong Erbb4, but no detectable Egfr expression in the adult mouse brain.

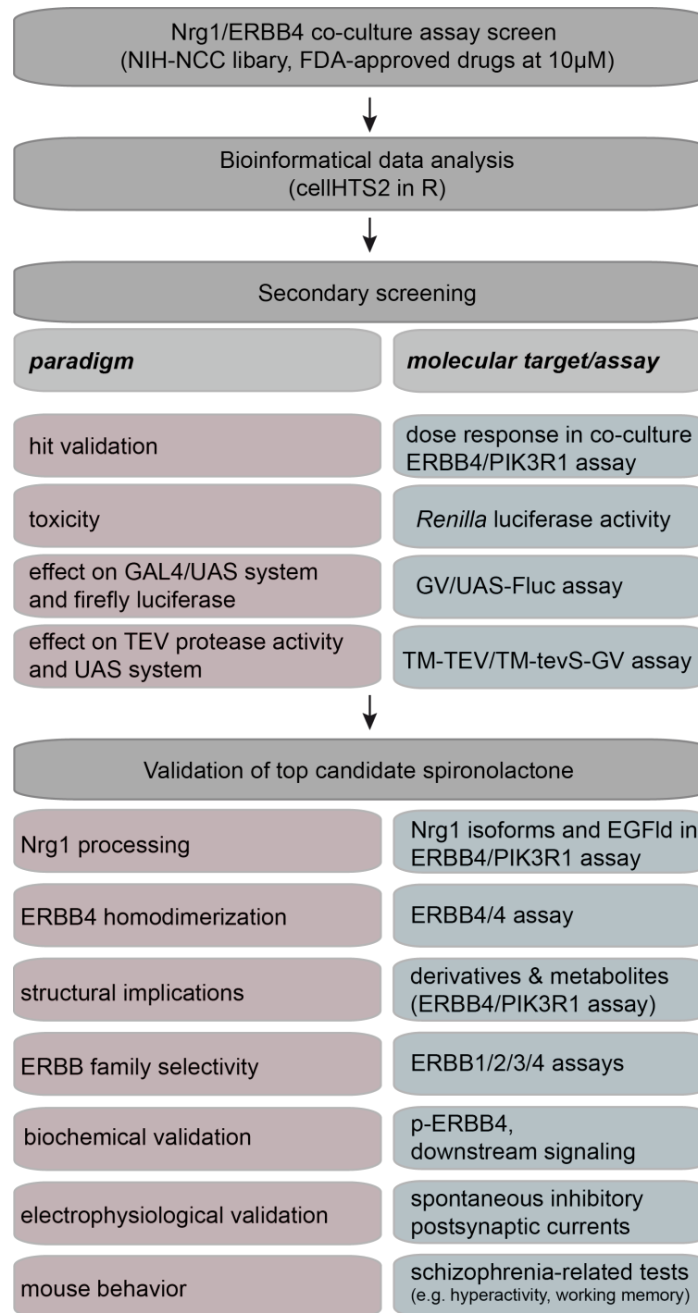
Appendix Fig S3. Covariate analysis revealed no significant effect of age on the treatment response.

Appendix Table S1. Final hit list of approved drugs.

Appendix Table S2. Oligonucleotides used for cloning.

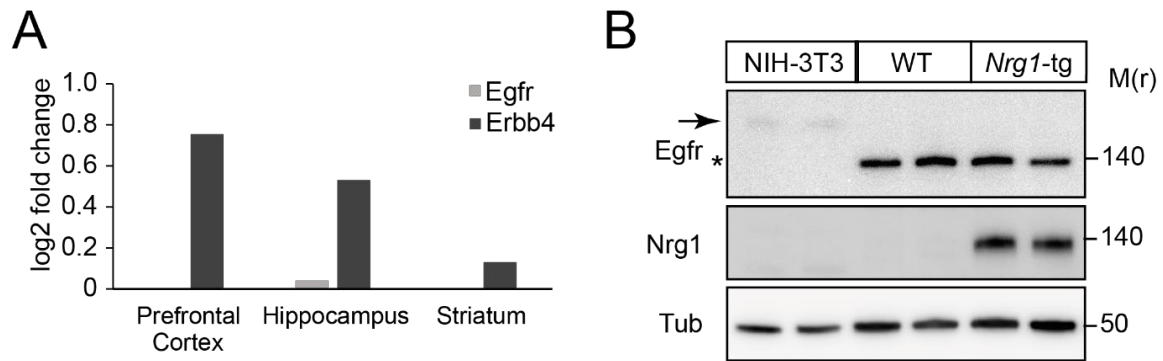
Appendix Table S3. List of antibodies used.

Appendix Supplementary Reference.



Appendix Fig S1. Summary of the validation strategy for drug repurposing performed on the NRG1-ERBB4-PI3K schizophrenia risk pathway.

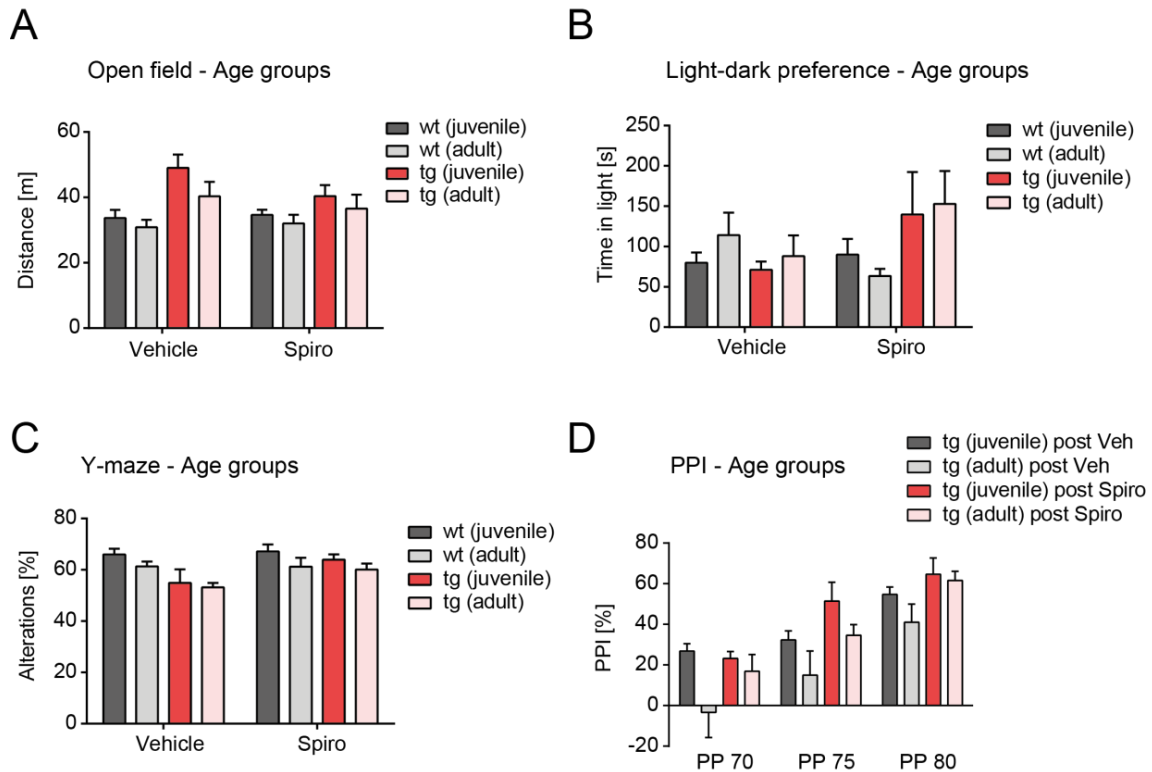
To identify small molecule modulators of NRG1-ERBB4 signaling in the context of drug repurposing and schizophrenia, the NIH-NCC compound collection was subjected to a cell-based co-culture assay screening approach using the split TEV technique as readout. Hits recovered from the screen were analyzed using the computational method cellHTS2 and validated using a consecutive analysis of various individual assays as depicted. The paradigm tested is shown on the left, the molecular target assessed or assay applied on the right.



Appendix Fig S2. Protein expression analysis reveals strong Erbb4, but no detectable Egfr expression in the adult mouse brain.

(A) Erbb4 protein expression is increased in prefrontal cortex, hippocampus and striatum. Expression data is normalized to overall protein expression and values are log₂-transformed, positive values are plotted. Data is extracted from <http://www.mousebrainproteome.com/> (Sharma *et al*, 2015).

(B) Egfr is not expressed in prefrontal cortex of adult WT and *Nrg1*-tg mice. Lysates from NIH-3T3 cells (fibroblast-derived mouse cell line with low Egfr expression) and prefrontal cortex (both WT and *Nrg1*-tg mice, P60) were subjected to Western Blotting and probed for indicated antibodies. Arrow indicates band representing Egfr; asterisk indicates an unspecific band.



Appendix Fig S3. Covariate analysis revealed no significant effect of age on the treatment response.

(A) Two-way ANCOVA considering age groups (juvenile/adult) as covariate did not report a significant genotype x treatment interaction ($F_{(1,43)}=2.174$; $p=0.148$). Related to Fig 5B. There were no overall differences between juvenile and adult mice within each experimental condition (all t-tests $p \geq 0.199$).

(B) Two-way ANCOVA considering age groups (juvenile/adult) as covariate reported a significant genotype x treatment interaction ($F_{(1,40)}=4.838$; $p=0.034$). Related to Fig 5E. Absence of statistically significant age-related effects on the light-dark preference test. There were no overall differences between juvenile and adult mice within each experimental condition (all t-tests $p \geq 0.221$).

(C) Two-way ANCOVA considering age groups (juvenile/adult) as covariate reported a suggestive genotype x treatment interaction ($F_{(1,43)}=3.528$; $p=0.067$). Related to Fig 5F. There were no overall differences between juvenile and adult mice within each experimental condition (all t-tests $p \geq 0.209$).

(D) Pairwise analyses revealed also for PPI no significant differences between juvenile and adult mice within each experimental condition (all t-tests $p \geq 0.107$). Related to Fig 5G.

Data are shown as mean, error bars represent SEM. *, $p < 0.05$; Spiro, spironolactone; Veh, vehicle; juvenile mice were defined as 8-11 weeks old, adult mice were defined as 12-16 weeks old.

For (A) and (C), juvenile *Nrg1*-tg vehicle, n=5, adult *Nrg1*-tg vehicle, n=7; juvenile *Nrg1*-tg Spiro, n=5; adult *Nrg1*-tg Spiro, n=7; juvenile wt Vehicle, n=8; adult wt vehicle, n=4; juvenile wt Spiro, n=7; adult wt Spiro, n=5.

For (B), juvenile *Nrg1*-tg vehicle, n=5, adult *Nrg1*-tg vehicle, n=6; juvenile *Nrg1*-tg Spiro, n=4; adult *Nrg1*-tg Spiro, n=6; juvenile wt Vehicle, n=8; adult wt vehicle, n=4; juvenile wt Spiro, n=7; adult wt Spiro, n=5;

For (D), juvenile *Nrg1*-tg vehicle, n=4, adult *Nrg1*-tg vehicle, n=7; juvenile *Nrg1*-tg Spiro, n=5; adult *Nrg1*-tg Spiro, n=7.

Appendix Table S1. Final hit list of approved drugs.

Rank	Z-score	NCC_Sample_ID	Pubchem_CID	Compound_name, synonyms
1	9.25	SAM002264648	5833	Spironolactone
2	7.97	SAM001246651	60699	Topotecan HCl
3	6.59	SAM001246973	2690	CGS 15943
4	6.52	SAM002264631	4828	Pindolol
5	5.88	SAM001246964	23581797	3'-Deoxyadenosine
6	5.88	SAM001246573	23581791	Vardenafil citrate
7	4.7	SAM001246669	2161	Amlexanox
8	4.3	SAM002699899	5362129	Ramipril
9	4.26	SAM001246548	3749	Irbesartan
10	3.82	SAM002589959	3003	Betamethasone
11	3.13	SAM001246805	11693521	Telithromycin
12	3	SAM002548951	1349907	Methimazole
13	-3.6	SAM001246679	3793	Itraconazole
14	-3.5	SAM001246526	20279	2-Chloro-2'-deoxyadenosine
15	-3.45	SAM002264605	65327	Norpramin
16	-3.45	SAM001246775	2378	Bifonazole
17	-4.63	SAM002548959	4030	Mebendazole
18	-5.48	SAM002589939	2082	Albendazole

The final hit list contains candidates that score at least 3 standard deviations (measured as z-score) from the mean. Screening data for all compounds can be found the accompanying file Dataset EV1.

Appendix Table S2. Oligonucleotides used for cloning.

Oligonucleotide name	Sequence
GRB2_B1-Kozak	GGGG <u>CAAGTTTGTACAAAAAAGCAGG</u> CTCCACCATGGAAGCCATCGCCAAATATGACTTC
GRB2_B2	GGGG <u>ACCACTTTGTACAAGAAAGCTGGG</u> TCGACGTTCCGGTTCACGGGG
PIK3R1_B1-Kozak	GGGG <u>CAAGTTTGTACAAAAAAGCAGG</u> CTCCACCATGAGTGCTGAGGGGTACCAGTAC
PIK3R1_B2	GGGG <u>ACCACTTTGTACAAGAAAGCTGGG</u> TCTCGCCTCTGCTGTGCATATACTGG
SHC1_B1-Kozak	GGGG <u>CAAGTTTGTACAAAAAAGCAGG</u> CTCCACCATGGATCTCCTGCCCCCAAG
SHC1_B2	GGGG <u>ACCACTTTGTACAAGAAAGCTGGG</u> TCCAGTTCCGCTCCACAGGTTGC
SRC_B1-Kozak	GGGG <u>CAAGTTTGTACAAAAAAGCAGG</u> CTCCACCATGGGTAGCAACAAGAGCAAGCCC
SRC_B2	GGGG <u>ACCACTTTGTACAAGAAAGCTGGG</u> TCGAGGTTCTCCCCGGGCTGG
STAT5A_B1-Kozak	GGGG <u>CAAGTTTGTACAAAAAAGCAGG</u> CTCCACCATGGCGGGCTGGATCCAGG
STAT5A_B2	GGGG <u>ACCACTTTGTACAAGAAAGCTGGG</u> TCTGAGAGGGAGCCTCTGGCAG
ERBB4_B1-Kozak	GGGG <u>CAAGTTTGTACAAAAAAGCAGG</u> CTCTACCATGAAGCCGGCGACAGGACTTTGG
ERBB4_B2	GGGG <u>ACCACTTTGTACAAGAAAGCTGGG</u> TCCACCACAGTATTCCGGTGTCTGTAAG
ERBB4_1_685_B2	GGGG <u>ACCACTTTGTACAAGAAAGCTGGG</u> TCGGCTCTTTTCTTTTGTATGC

The oligonucleotides listed above were used for cloning of open reading frames (ORFs) using Gateway recombination cloning (attB1 and attB2 sites are underlined). The oligonucleotide names contain the HGNC nomenclature of human ORFs cloned.

Appendix Table S3. List of antibodies used.

Antibody	Species	Dilution	Experiment	Source	Catalog Number
Akt	rabbit	1:1000	WB	Cell Signaling Technology	9272
EGFR (A-10)	mouse	1:500	WB	Santa Cruz Biotechnology	sc-373746
ErbB4 (E200)	rabbit	1:1000	WB	Abcam	ab32375
HA (clone 3F10)	rat	1:500	ICC	Roche	11 867 423 001
LIMK1	rabbit	1:1000	WB	Cell Signaling Technology	3842
Neuregulin-1 α / β 1/2 (C-20)	rabbit	1:1000	WB	Santa Cruz Biotechnology	sc-348
p44/42 MAPK (Erk1/2) (137F5)	rabbit	1:2000	WB	Cell Signaling Technology	4695
Phospho-Akt (Ser473) (D9E)	rabbit	1:1000	WB	Cell Signaling Technology	4060
p-ErbB-4 (Tyr 1056)	rabbit	1:500	WB	Santa Cruz Biotechnology	sc-33040
Phospho-HER4/ErbB4 (Tyr1284) (21A9)	rabbit	1:500	WB	Cell Signaling Technology	4757S
Phospho-LIMK1 (Thr508)/LIMK2 (Thr505)	rabbit	1:500	WB	Cell Signaling Technology	3841
Phospho-p44/42 MAPK (Erk1/2) (Thr202/Tyr204) (D13.14.4E)	rabbit	1:2000	WB	Cell Signaling Technology	4370
Tubulin	mouse	1:2000	WB	Sigma	T 5168

WB, Western Blot; ICC, immunocytochemistry.

Appendix Supplementary Reference

Sharma K, Schmitt S, Bergner CG, Tyanova S, Kannaiyan N, Manrique-Hoyos N, Kongi K, Cantuti L, Hanisch U-K, Philips M-A, Rossner MJ, Mann M & Simons M (2015) Cell type- and brain region-resolved mouse brain proteome. *Nat. Neurosci.* **18** 1819–1831

Research Article II

Monitoring activities of receptor tyrosine kinases using a universal adapter in genetically encoded split TEV assays

Jan P. Wintgens¹, Sven P. Wichert^{1,2}, Luksa Popovic², Moritz J. Rossner¹, Michael C. Wehr^{1*}

(1) Department of Psychiatry and Psychotherapy, University Hospital, LMU Munich, Nussbaumstr. 7, 80336 Munich, Germany

(2) Systasy Bioscience GmbH, Adams-Lehmann-Str. 56, 80797 München, Germany

(*) Author for correspondence:

Dr. Michael C. Wehr, Michael.Wehr@med.uni-muenchen.de; phone: +49 (0) 89 4400 53275

ORIGINAL ARTICLE



Monitoring activities of receptor tyrosine kinases using a universal adapter in genetically encoded split TEV assays

Jan P. Wintgens^{1,2} · Sven P. Wichert^{1,2} · Luksa Popovic² · Moritz J. Rossner¹ · Michael C. Wehr^{1,2}

Received: 26 June 2018 / Accepted: 28 December 2018 / Published online: 8 January 2019
© The Author(s) 2019, corrected publication 2019

Abstract

Receptor tyrosine kinases (RTKs) play key roles in various aspects of cell biology, including cell-to-cell communication, proliferation and differentiation, survival, and tissue homeostasis, and have been implicated in various diseases including cancer and neurodevelopmental disorders. Ligand-activated RTKs recruit adapter proteins through a phosphotyrosine (p-Tyr) motif that is present on the RTK and a p-Tyr-binding domain, like the Src homology 2 (SH2) domain found in adapter proteins. Notably, numerous combinations of RTK/adapter combinations exist, making it challenging to compare receptor activities in standardised assays. In cell-based assays, a regulated adapter recruitment can be investigated using genetically encoded protein–protein interaction detection methods, such as the split TEV biosensor assay. Here, we applied the split TEV technique to robustly monitor the dynamic recruitment of both naturally occurring full-length adapters and artificial adapters, which are formed of clustered SH2 domains. The applicability of this approach was tested for RTKs from various subfamilies including the epidermal growth factor (ERBB) family, the insulin receptor (INSR) family, and the hepatocyte growth factor receptor (HGFR) family. Best signal-to-noise ratios of ligand-activated RTK receptor activation was obtained when clustered SH2 domains derived from GRB2 were used as adapters. The sensitivity and robustness of the RTK recruitment assays were validated in dose-dependent inhibition assays using the ERBB family-selective antagonists lapatinib and WZ4002. The RTK split TEV recruitment assays also qualify for high-throughput screening approaches, suggesting that the artificial adapter may be used as universal adapter in cell-based profiling assays within pharmacological intervention studies.

Keywords Cell-based assay · Receptor tyrosine kinases · TEV protease · Split TEV recruitment assay · Lapatinib

Abbreviations

EGF	Epidermal growth factor	IGF1R	Insulin growth factor 1 receptor
EGFld	EGF-like domain of NRG1	MET	Mesenchymal epithelial transition proto-oncogene, receptor tyrosine kinase
EGFR	Epidermal growth factor receptor	NRG1	Neuregulin 1
ERBB2	Erb-B2 receptor tyrosine kinase 2	PIK3R1	Phosphoinositide-3-kinase regulatory subunit 1
ERBB3	Erb-B2 receptor tyrosine kinase 3	RTK	Receptor tyrosine kinase
ERBB4	Erb-B2 receptor tyrosine kinase 4	SHC1	Src homology 2 domain-containing adaptor protein 1
GRB2	Growth factor receptor bound protein 2	SH2	Src homology 2
HTS	High-throughput screening	TEV	Tobacco etch virus

Electronic supplementary material The online version of this article (<https://doi.org/10.1007/s00018-018-03003-2>) contains supplementary material, which is available to authorized users.

✉ Michael C. Wehr
Michael.Wehr@med.uni-muenchen.de

¹ Department of Psychiatry and Psychotherapy, University Hospital, LMU Munich, Nussbaumstr. 7, 80336 Munich, Germany

² Systasy Bioscience GmbH, Adams-Lehmann-Str. 56, 80797 Munich, Germany

Introduction

Receptor tyrosine kinases (RTKs) are type I transmembrane protein receptors and respond, with few exceptions, to extracellular cues. RTK-mediated signalling regulates key processes of cell biology, including intercellular communication, proliferation and differentiation, cell survival and metabolism, cell migration, and cell cycle control [1, 2].

Further, RTK signalling is also implicated in central nervous system (CNS) and peripheral nervous system (PNS) development [3]. RTKs share a similar architecture, which consists of ligand-binding domains in the extracellular region, a single alpha-helix crossing the membrane and, in the cytoplasm, a juxtamembrane domain, a protein tyrosine kinase domain, and a carboxyl (C-) terminal regulatory region [2]. To date, 58 receptor tyrosine kinases in humans have been described, which can be divided into 20 subfamilies [2]. Together with the G protein-coupled receptors (GPCR), RTKs are the most important receptor class in human cells and represent the most relevant drug targets in the cell [4]. However, only 3% of marketed drugs target kinases as such, suggesting that the development of cell-based assays with broader applicability and robustness may contribute to better medicines.

Upon ligand stimulation, RTKs dimerise that causes a kinase domain-mediated phosphorylation of the cytoplasmic receptor tails in *trans*, followed by phosphorylation-dependent recruitment of adapter proteins. The ligand-induced binding between an RTK and an adapter is commonly mediated by phosphotyrosine (p-Tyr) motifs, which are present in the cytoplasmic tail of an RTK and serve as docking sites for adapter proteins containing phospho-binding modules, such as the Src homology 2 (SH2) domain or phosphotyrosine-binding (PTB) domain [5]. The SH2 domain is the largest class of p-Tyr recognition domains and comprises 120 different domains in 110 proteins [6]. The specificity of binding between a given SH2 domain and a p-Tyr docking site is mediated by the SH2 domain itself and the sequence of the p-Tyr motif, which is defined by the p-Tyr residue and its flanking residues [7].

One of the best studied RTK families is the Erb-b2 receptor tyrosine kinases (ERBB) family comprising the epidermal growth factor (EGFR, also known as HER1 in humans) and ERBB2, ERBB3, and ERBB4 (also known as HER2, HER3, and HER4 in humans). The ERBB family has been linked to the development of, amongst other tissues, skin, heart, CNS, and PNS, and is widely implicated in human diseases, such as cancer and neurodevelopmental disorders including schizophrenia [2, 3]. Upon ligand stimulation, ERBB receptors homo- or heterodimerise, depending on the cellular context. ERBB2, however, is the preferred dimerisation partner for the other ERBB receptors and does not respond to ligands [8, 9]. ERBB3 needs to heterodimerise to initiate downstream signalling, as the kinase domain lacks catalytic activity, and its preferred partner for heterodimerisation is ERBB2 [10]. The major ligand for EGFR is the epidermal growth factor (EGF), whereas ERBB3 and ERBB4 are predominantly activated by neuregulins (NRG1-4) [11]. NRG binding to the receptor is mediated by the EGF-like domain (EGF_{ld}), which on its own can stimulate ERBB3 and ERBB4 receptors [11].

The activity of ERBB receptors can be measured using genetically encoded bioassays, such as split TEV [12, 13]. This technique allows assessing dynamic protein–protein interactions in living cells and is based on the functional complementation of the tobacco etch virus (TEV) protease coupled to genetically encoded reporters, like the GAL4/UAS system combined with firefly luciferase (Fluc) as reporter gene readout. The assay system was, for example, applied to monitor phosphorylation-dependent interactions of ERBB4 with the adapters PIK3R1 (regulatory subunit of PI3K), SHC1, and GRB2, as well as the EGF_{ld}-induced homodimer formation of ERBB4 and the heterodimer formation of ERBB2 and ERBB3 [13–16].

In this work, we describe the application of split TEV-based RTK recruitment assays that provide a universal adapter recruitment strategy for robust and flexible cell-based assays applicable to dose–response profiling and high-throughput screening (HTS) assays. To do this, disease-relevant RTKs such as the complete ERBB family, the insulin growth factor 1 receptor (IGF1R), and mesenchymal epithelial transition proto-oncogene (MET, also known as c-MET or hepatocyte growth factor receptor) were selected and tested in split TEV dose–response assays for their assay performance, both using endogenous full-length adapters and artificial adapters consisting of clustered SH2 domains. The latter ones were designed to increase flexibility, robustness, and eventually lower the number of adapters needed for assaying various RTK activities, thus improving the comparability among the receptors tested. Notably, the artificial p-Tyr sensor based on the SH2 domain clustering derived from GRB2 displayed an improved signal-to-noise ratio in RTK recruitment assays. Furthermore, the p-Tyr sensor has been validated in dose–response assays using the ERBB family antagonists lapatinib and WZ4002, as well as the IGF1R inhibitor linsitinib and the MET antagonist foretinib. As expected, lapatinib and WZ4002 inhibited ERBB family assays. However, challenging IGF1R and MET split TEV recruitment assays with lapatinib did not have an effect, demonstrating the sensitivity of our approach. Taken together, we established robust split TEV recruitment assays to sensitively monitor RTK receptor activities in living cells using a universal adapter protein as recruitment sensor.

Materials and methods

Plasmids

ORFs were PCR-amplified using the Pwo proofreading DNA Polymerase (Roche) and BP-recombined into the pDONR/Zeo plasmid using Gateway recombination cloning (Life Technologies). Each entry vector was control digested using BsrGI, which releases the insert, and finally

verified by sequencing. LR recombination that was used to shuffle the ORFs from the entry vectors into the split TEV destination vectors (either pcDNA_attR1-ORF-attR2-NTEV-tcs-GV-2xHA_DEST or pcDNA3_attR1-ORF-attR2-CTEV-2xHA_DEST). The generation of the human ORFs for EGFR, ERBB2, ERBB3, ERBB4, SHC1, GRB2, and PIK3R1 has been described previously [16]. IGF1R and MET were obtained as pENTR plasmids from Harvard Plasmid ID (clone HsCD00040705) and Addgene (as part of the CCSB-Broad Human Kinase ORF Collection [17]), respectively. Concatenated ORFs of clustered SH2 domains that are flanked by attL1 and attL2 sites were synthesised by GenScript, USA. These sequences were provided in a pUC57 vector backbone harbouring a kanamycin resistance gene, allowing LR recombination cloning with destination vectors carrying an ampicillin resistance gene. DNA and protein sequences of clustered SH2 domains are provided in Fig. S1.

Cell culture

PC12 Tet-Off cells (Clontech, 631134, termed PC12 cells for simplicity) were maintained in DMEM medium (1 g/l glucose, Lonza) supplemented with 10% FCS, 5% horse serum (HS, Thermo Fisher Scientific), and 100 U/ml each of penicillin and streptomycin and 2 mM GlutaMAX. To starve PC12 cells, 2% FCS, 100 U/ml each of penicillin and streptomycin and 2 mM GlutaMAX, but no HS, were added to the DMEM medium (1 g/l glucose). PC12 cells were grown on poly-L-lysine (Sigma) coated surfaces for maintenance and experiments. A549 cells (ATCC, CCL-185) were cultured in DMEM medium (4.5 g/l glucose) supplemented with 10% FCS and 100 U/ml each of penicillin and streptomycin and 2 mM GlutaMAX. T-47D cells (ATCC, HTB-133) were cultured in RPMI 1640 medium supplemented with human insulin (f.c. 125 µg/l) (Sigma-Aldrich), 10% FCS, and 100 U/ml each of penicillin and streptomycin and 2 mM GlutaMAX. Cells were cultured at 37 °C and 5% CO₂.

Biochemistry

For assessing the phosphorylation levels of EGFR, A549 cells were starved overnight using 1% FCS, pre-incubated with increasing concentration of compounds [i.e. lapatinib (Selleckchem) or WZ4002 (Sigma-Aldrich)] at semi-logarithmic scale for 1 h, and stimulated with 30 ng/ml EGF (Sigma-Aldrich) for 5 min. Likewise, T-47D were starved overnight using 0.5% FCS, pre-incubated with increasing concentration of compounds (i.e. lapatinib or WZ4002) at semi-logarithmic scale for 1 h, and stimulated with 10 ng/ml EGF-like domain (Sigma-Aldrich) for 5 min. Split TEV expression plasmids were transfected into PC12 cells using Lipofectamine 2000 (Thermo Fisher Scientific) according to

the manufacturer's instructions. Cells were washed 1 × with PBS and lysed in a Triton-X lysis buffer (1% Triton-X100, 50 mM Tris pH7.5, 150 mM NaCl, 1 mM EGTA) containing the Complete Protease Inhibitor Cocktail (Roche) and PhosSTOP phosphatase inhibitor (Roche). Briefly, cells were lysed and kept on ice for 10 min, sonicated 3 × for 10 s at 4 °C, and denatured for 10 min at 70 °C. The Mini-PROTEAN Tetra Electrophoresis System and Trans-Blot Turbo Blotting System (both Bio-Rad) were used for running and blotting protein gels. Chemiluminescence detection of proteins by Western blot analysis was performed using the Western LightningPlus-ECL kit (PerkinElmer). HA-tagged proteins were visualised using an HA antibody (clone 3F10, dilution 1:250, No. 11 867 423 001, Roche). The ERBB2-V5 fusion was stained using a V5 antibody (clone D3H8Q, dilution 1:1000, Cell Signaling Technology). Phosphorylation levels of EGFR and ERBB4 were assayed using p-EGFR-Y1068 (clone D7A5, dilution 1:500, No. 3777, Cell Signaling Technology) and p-ERBB4-Y1284 antibodies (clone 21A9, dilution 1:500, No. 4757, Cell Signaling Technology). Total EGFR and ERBB4 protein levels were determined using an anti-EGFR antibody (clone A-10, dilution 1:1000, sc-373746, Santa Cruz Biotechnology) and an anti-ERBB4 antibody (clone E200, dilution 1:1000, ab32375, Abcam). Tubulin levels were determined using an anti-tubulin antibody (dilution 1:2000, No. T 5168, Sigma-Aldrich). For quantification, phosphorylation levels of p-EGFR relative to EGFR as well as p-ERBB4 relative to ERBB4 were calculated using the Lukemiller protocol (<http://lukemiller.org/index.php/2010/11/analyzing-gels-and-western-blots-with-image-j/>). Assays were run in triplicate.

Immunocytochemistry

On day 1, 1 Mio PC12 cells were plated on coverslips coated with poly-L-lysine (PLL) and placed in a six-well plate. On day 2, cells were transfected with EGFR-Glink-NTEV-tevS-GV-2HA, ERBB2-var1-V5, ERBB3-Glink-NTEV-tevS-GV-2HA, or ERBB4-JMa-CVT1-Glink-NTEV-tevS-GV-2HA using Lipofectamine 2000. On day 3, 50 µl of 1 × TBS was gently added per coverslip and removed twice to wash the cells, followed by fixation in 4% PFA diluted in 1 × TBS for 10 min, washed again once in 1 × TBS and then permeabilised in TBS/0.1% Triton X-100 for 5 min. Subsequently, cells were washed three times with 1 × TBS, then blocked in blocking buffer (3% BSA, 0.1% Triton X-100 in 1 × TBS) for 30 min at room temperature, and again washed three times with 1 × TBS. The HA antibody (Poly9023, BioLegend) and the V5 antibody (clone D3H8Q, Cell Signaling Technology), respectively, were diluted in blocking buffer (1:1000) and added to the cells and incubated overnight at 4 °C. After another three washing steps using 1 × TBS, the secondary antibody (Alexa 594 anti-rabbit, 1:500, Abcam,

ab150160) diluted in blocking buffer was added to the cells and incubated for 1 h at room temperature. Coverslips were washed three times in $1 \times$ TBS, dipped into ddH₂O to remove traces of salt, mounted on microscope slides, and sealed with ProLong Gold Antifade Mountant with Dapi (ThermoFisher Scientific, P36935). Slides were imaged on a Zeiss Observer Z.1 microscope.

Split TEV recruitment end-point assays

Split TEV recruitment assays were run in six replicates per condition in 96-well plates. 50,000 PC12 cells per well were seeded onto poly-L-lysine (PLL)-coated plates. The next day, cells were transfected with assay plasmids using Lipofectamine 2000. For transfection-based assays, no antibiotics were added to the medium. Per 96-well, a receptor-NTEV-tcs-GV fusion plasmid (10 ng), an adapter-CTEV fusion plasmid for either SHC1 (10 ng), SH2(SHC1) (10 ng), SH2(GRB2) (10 ng), SH2(mix) (10 ng), PIK3R1(50 ng), SH2(PIK3R1) (50 ng), or GRB2 (2.5 ng), and an Fluc reporter plasmid (10 ng, Fluc driven by 10x clustered upstream activating sequences coupled to a minimal CMV promoter, $10 \times$ UAS-minCMVp) were used. Additionally, 1 ng of a plasmid constitutively expressing an EYFP that is fused to nuclear localisation sequence (EYFPnuc) driven by a CMV promoter was transfected per 96-well to assess transfection efficiencies (EYFPnuc). In detail, assay plasmids were diluted in 30 μ l Opti-MEM (Thermo Fisher Scientific), vortexed, and mixed with 0.2 μ l Lipofectamine 2000 per well. The DNA/Lipofectamine/Opti-MEM mix was incubated for 20 min. The medium was removed from the wells and the DNA/Lipofectamine/Opti-MEM mix was added onto the cells. After 2 h of incubation, the maintenance medium without antibiotics was added to the Opti-MEM mix. On day 2, the maintenance medium was replaced by starvation medium. After 16–20 h (day 3), six wells per condition were stimulated with EGF (30 ng/ml, Sigma-Aldrich), EGF1d (10 ng/ml, Sigma-Aldrich), IGF1 (100 ng/ml, PeproTech), and HGF (100 ng/ml, Sigma-Aldrich), while six wells were left non-stimulated. 16 h later (day 4), the medium was removed, and cells were lysed using Passive Lysis Buffer (Promega) and luciferase activity was analysed using a dual luciferase assay (Promega) in a Mithras LB 940 Multimode Microplate Reader (Berthold Technologies). Significance for assays was calculated using an unpaired *t* test in GraphPad Prism 5. Error bars are calculated as standard error of the mean (SEM).

For split TEV recruitment assays in a dose–response format, the following amendments to the general protocol were made. For a dose–response assay, all cells on the plate were transfected with the same receptor-NTEV-tcs-GV and adapter-CTEV fusions, the Fluc reporter plasmid, 1 ng of a plasmid constitutively expressing *Renilla* luciferase driven

by a thymidine kinase promoter, and the EYFPnuc expressing plasmid. *Renilla* luciferase was used to assess toxic effects when applying compounds. For dose-dependent stimulation testing activation, six wells per condition were stimulated using increasing concentrations of an agonist at a semi-logarithmic scale. For assays testing inhibition, cells were treated with increasing concentrations of an antagonist at a semi-logarithmic scale, followed 1 h later by the addition of an agonist at a constant concentration. The following antagonists were used: lapatinib (Selleckchem), WZ4002 (Sigma-Aldrich), linsitinib (Selleckchem), and foretinib (Selleckchem). Dose–response data were analysed using the R-based ‘drc’ package, as described before [18, 19]. Error bars are calculated as standard error of the mean (SEM). For ease of presentation and intuition, we have transformed conventionally used IC₅₀ values into pIC₅₀ values [20]. These are calculated from IC₅₀ values using the formula $pIC_{50} = -\log_{10}(IC_{50})$, with units of molar for IC₅₀ and therefore log(molar) for pIC₅₀.

Live cell split TEV recruitment assay

To identify an optimal time point of lysis for split TEV recruitment assays, firefly luciferase expression was continuously monitored using a 32-channel luminometer (lumicycler 32 by ActiMetrics) for 69 h starting from the starvation phase. For one assay, 1,000,000 PC12 cells were seeded on a 3.5 cm dish suitable for the instrument. The next day, 100 ng of receptor-NTEV-tcs-GV, 100 ng of adapter-CTEV, and 100 ng of Fluc reporter plasmids were transfected using 3.5 μ l Lipofectamine 2000 and 1 ml Opti-MEM per dish. On day 2, cells were starved, and the cell culture medium was supplemented with 0.1% luciferin (Promega) to monitor firefly luciferase activity in a live cell setup. The dishes were wrapped with parafilm to avoid excess evaporation of medium and put into the luminometer, which was placed inside a cell culture incubator set to 37 °C and 5% CO₂. All assays were run using three replicates per condition.

Results

Design of concatenated SH2 domains as universal adapter for split TEV recruitment assays

Split TEV assays are based on a TEV protease split into two inactive fragments, an N-terminal NTEV moiety and a C-terminal CTEV moiety. When assessing receptor activities, like for RTKs, the receptor is fused to the NTEV moiety, a TEV cleavage site (tcs), and the artificial co-activator GAL4-VP16 (GV), forming an NTEV-tcs-GV tag. Adapters are fused to CTEV (Fig. 1a). To establish RTK split TEV recruitment assays that use a universal adapter

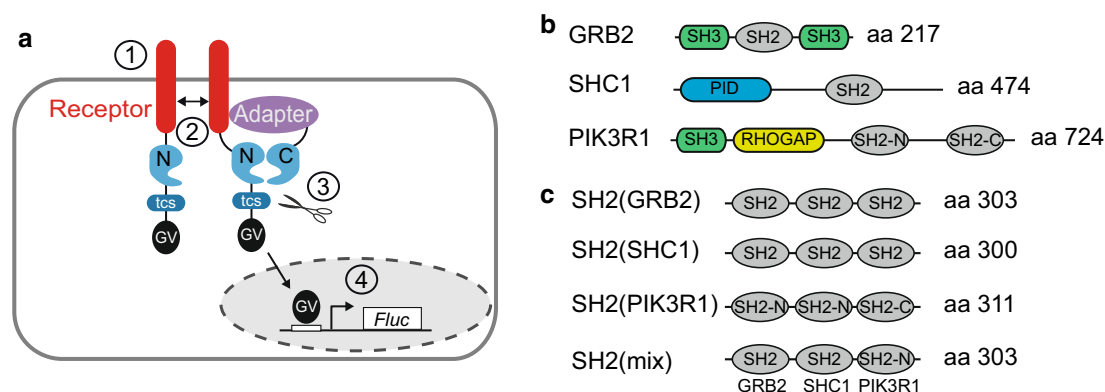


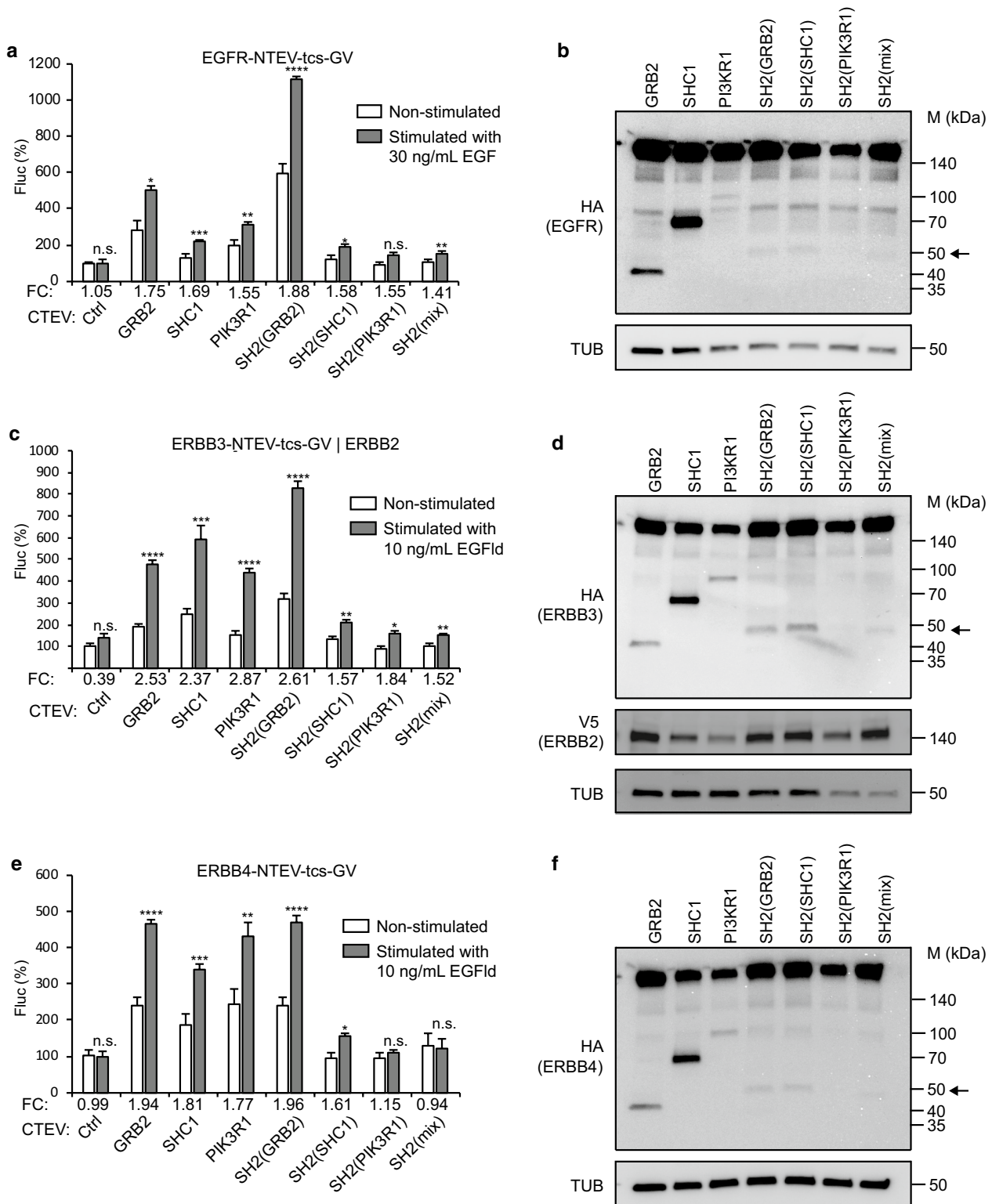
Fig. 1 Design of a versatile split TEV recruitment assay for receptor tyrosine kinases. **a** Scheme of the split TEV recruitment assay for receptor tyrosine kinases (RTKs). RTKs are fused to an NTEV moiety along with a TEV protease cleavage site (tcs) and an artificial co-transcriptional activator GAL4-VP16 (GV). Adapter proteins are fused to CTEV. Upon activation by a specific ligand (1), the RTK dimerises, is cross-phosphorylated by the kinase domains at Tyr residues, providing docking sites for adapter proteins that bind to phosphorylated tyrosines (2). The ligand-induced interaction between RTK and adapter causes the NTEV and CTEV moieties to form a reconstituted TEV protease (2). Reconstituted TEV protease cleaves

at tcs to release GV (3). Liberated GV migrates to the nucleus and initiates expression of firefly luciferase (Fluc) (4). **b** Domain organisation of full-length adapter proteins that are recruited by ERBB receptors. SH2 src homology 2 domain, SH3 src homology 3 domain, PID phosphotyrosine interaction domain, RHOGAP RhoGAP domain. Note that the adapter PIK3R1 contains two SH2 domains denoted as SH2-N (N-terminal) and SH2-C (C-terminal). **c** Domain organisation of the artificially concatenated SH2 domain phospho-adapters. For each clustered SH2 adapter, three single SH2 domains were fused. The SH2(mix) adapter contains an SH2 domain taken from each full-length adapter depicted in (b)

and are sensitive, robust, and likely reduce interference with cellular signalling as compared to native adapters, we designed artificial adapter proteins that only consist of clustered SH2 domains. The SH2 domain sequences were taken from the human adapter proteins GRB2, SHC1, and PIK3R1 (Fig. 1b). Notably, these adapters are known to interact with various RTK subfamilies, including the ERBB family [2], the INSR family [21], and the HGFR family [22]. For the ERBB family, we had previously developed split TEV recruitment assays using full-length PIK3R1, GRB2, and SHC1 as adapter proteins [14]. By contrast, each artificial adapter protein was constructed to contain three concatenated SH2 domains (Fig. 1c, Fig. S1). For artificial GRB2 and SHC1 adapters, the single SH2 domain present in the full protein was concatenated three times, termed SH2(GRB2) and SH2(SHC1). PIK3R1 contains two SH2 domains, an N-terminal SH2 domain (SH2-N), and a C-terminal SH2 domain (SH2-C). For the artificial adapter, two concatenated SH2-N domains were linked to a single SH2-C domain, termed SH2(PIK3R1). We also designed a chimeric protein adapter molecule containing one SH2 domain of each GRB2, SHC1, and the N-terminal SH2 domain of PIK3R1, termed SH2(mix). SH2 domains were separated via a flexible GS-linker formed of glycine, serine, and threonine residues (GGGGSTGGGG) to allow for optimal folding and flexibility of binding.

The concatenated SH2(GRB2) domain is a universal adapter for RTK split TEV recruitment assays

For RTK split TEV recruitment assays, receptors were fused to the NTEV moiety along with tcs and GV, yielding RTK-NTEV-tcs-GV fusion proteins. As receptors, we selected EGFR, ERBB3, and ERBB4 of the ERBB family, IGF1R of the INSR family and MET of the HGFR family. Adapter proteins were fused to the CTEV moiety. HTS-compatible split TEV recruitment assays are performed using an endpoint format (Fig. S2). Therefore, we first evaluated the optimal time point for this type of a split TEV assay. To do this, we monitored luciferase activity in a live cell split TEV recruitment assay using ERBB4 and PIK3R1, which has been used before in a compound screen [16]. ERBB4-NTEV-tcs-GV was transfected together with PIK3R1-CTEV and the Fluc reporter into PC12 cells, which were starved to reduce baseline activity, and thus enable proper stimulation by EGFLd. The best stimulation to baseline ratio was obtained 16 h after stimulation (Fig. S3). Hence, all RTK split TEV recruitment assays using an end-point format were performed accordingly. To obtain a most sensitive adapter for RTK split TEV recruitment assays, we compared the performance of established full-length adapters versus artificial domain adapters. First, we monitored the induced activity of EGFR, ERBB3 (as heterodimerisation with ERBB2),



and ERBB4 using the three full-length adapters GRB2, SHC1, and PIK3R1, as well as the SH2 domain adapters SH2(GRB2), SH2(SHC1), SH2(PIK3R1), and SH2(mix) in

PC12 cells (Fig. 2, Table S1). In these assays, EGFR activity was stimulated using EGF, whereas ERBB3 and ERBB4 activity was stimulated using EGFld. Notably, fold changes

◀**Fig. 2** Comparing adapter protein performance for split TEV recruitment assays to monitoring ERBB receptor activities. Split TEV recruitment assays for ERBB family receptors. EGFR (a), ERBB2/ERBB3 (c), and ERBB4 (e) activities were assessed in PC12 cells using EGF to stimulate EGFR, and EGF-like domain (EGF1d) to stimulate ERBB3 and ERBB4. For split TEV assays, the indicated receptor fusions were transfected together with indicated adapters that were fused to the CTEV moiety. Note that for the ERBB2/ERBB3 assay (c), ERBB2 is co-transfected to allow heterodimerisation and thus ERBB3 phosphorylation, which is required for the recruitment of adapters. Assays were stimulated for 16 h and analysed by a firefly luciferase assay. Non-stimulated samples are shown as open bars and stimulated ones as grey bars. *FC* fold change, *Ctrl* control (no adapter transfected). Results are shown as average of six samples, and error bars are shown as SEM. Significance was calculated using the unpaired *t* test, with ** $p \leq 0.01$; *** $p \leq 0.001$; **** $p \leq 0.0001$; *n.s.* not significant. Precise *p* values are provided in Table S1. Biochemical validation of the expression of ERBB receptors and adapters. Plasmids encoding EGFR (b), ERBB3 (d), and ERBB4 (f) (all tagged with NTEV-tcs-GV-2HA), ERBB2-V5 (d), and adapter proteins (all tagged with CTEV-2HA) were transiently transfected into PC12 cells, allowed to express for 16 h, and lysed. Lysates were subjected to Western blotting using the indicated antibodies. Calculated sizes of fusion proteins are provided in Table S1. Arrow indicates bands of artificial adapter fusions. Note that SH2(PIK3R1) is only very weakly expressed

using the SH2(GRB2) domain adapter scored highest for all ERBB receptor assays tested. Constitutive control *Renilla* luciferase readings remained stable for these assays (Fig. S4). In addition, various non-titrated amounts of transfected adapter plasmids that resulted in different expression lead to similar activation profiles of receptors, indicating that split TEV recruitment assays are robust and tolerate substantial differences in transfected adapter plasmids (Fig. S5). A live cell split TEV recruitment assay using ERBB4 and the SH2(GRB2) domain showed comparable kinetics to the ERBB4/PIK3R1 assay, indicating that the readout is stable over several hours (Fig. S3).

Then, we assessed whether RTK split TEV recruitment assays using full-length adapters and SH2 domain adapters can also be used to monitor the activity of RTKs that belong to other subfamilies. To do this, we selected IGF1R and MET that belong to INSR and HGFR families, respectively. Indeed, activation of IGF1R (using the ligand IGF1) and MET (using the ligand HGF) was robustly monitored using the SH2(GRB2) domain adapter, suggesting that the artificial adapter formed of three SH2(GRB2) domains serves as a universal adapter in split TEV recruitment assays (Fig. 3, Fig. S4). A Western blot analysis validates that the RTK-NTEV-tcs-GV fusion proteins for EGFR, ERBB3, ERBB4, IGF1R and MET (each harbouring an HA tag at the C-terminus) and all adapter-CTEV fusion proteins (each also harbouring an HA tag at the C-terminus) were correctly expressed at expected sizes in PC12 cells (Figs. 2b, d, f, 3b, d, Table S2). For the ERBB3 split TEV recruitment assay, a non-TEV-tagged, but V5-tagged ERBB2 was co-transfected

to enable ligand-induced phosphorylation of ERBB3, and successively, formation of p-Tyr docking sites (Fig. 2d). Using immunocytochemistry, the proper expression of the RTK-NTEV-tcs-GV fusions was corroborated, as all RTK fusion proteins were enriched at the cell surface in PC12 cells (Fig. S6).

Next, we validated the sensitivity of RTK split TEV recruitment assays using the SH2(GRB2) adapter in agonist dose–response assays using increasing concentrations of the respective agonists (Fig. 4, Fig. S7). For ERBB recruitment assays, the SH2(SHC1) and SH2(mix) adapters showed, compared to the SH2(GRB2) adapter, lower signal-to-noise ratios and reduced sensitivity in dose–response assays (Fig. 4a–c, Figs. S7, S8). Notably, agonist dose–response split TEV recruitment assays for both IGF1R and MET and applying the SH2(GRB2) adapter also resulted in robust dose-dependent increases of receptor activity (Fig. 4d, e, Fig. S7). Taken together, we identified the three times concatenated SH2 domain of GRB2, termed SH2(GRB2), as universal adapter for our set of selected RTK receptor split TEV recruitment assays.

The SH2(GRB2) universal adapter efficiently monitors lapatinib inhibition across all ERBB family receptors

Cell-based assays are frequently used to assess a compound's potential to inhibit the activity of a given receptor, such as for an RTK [23]. To measure the impact of inhibitory compounds on RTK targets using our split TEV recruitment assays, we challenged them with the well-characterised pan-ERBB family inhibitor lapatinib that is used in the clinic [24] and determined IC_{50} values for each assay (Fig. 5a–f, Figs. S9, S10). For a more intuitive comparison among assays, we transformed IC_{50} values into pIC_{50} values reflecting a logarithmic scale (see “Materials and methods” for details) (Fig. 5f, Table S3). When compared across ERBB receptor assays using both full-length and SH2 domain adapters, split TEV recruitment assays using the universal adapter SH2(GRB2) are most sensitive to lapatinib inhibition (Fig. 5f). The constitutive *Renilla* luciferase readout enabled us to discriminate between inhibitory and toxic effects, with the latter ones only occurring at 30 μ M lapatinib (Fig. S9). We found in our assays using the SH2(GRB2) adapter that lapatinib efficiently inhibits EGFR (IC_{50} : 305 nM, pIC_{50} : 6.52) and ERBB2/ERBB3 (IC_{50} : 72 nM, pIC_{50} : 7.14), and ERBB4 (IC_{50} : 166 nM, pIC_{50} : 6.78). However, lapatinib treatment did not inhibit IGF1R and MET activities (Fig. 5d, e, Fig. S9). In concordance with the literature, stimulated IGF1R and MET receptors were efficiently inhibited by linsitinib and foretinib, respectively (Fig. S9) [25, 26]. To further compare the sensitivity of our split TEV RTK recruitment assays with cellular assays that

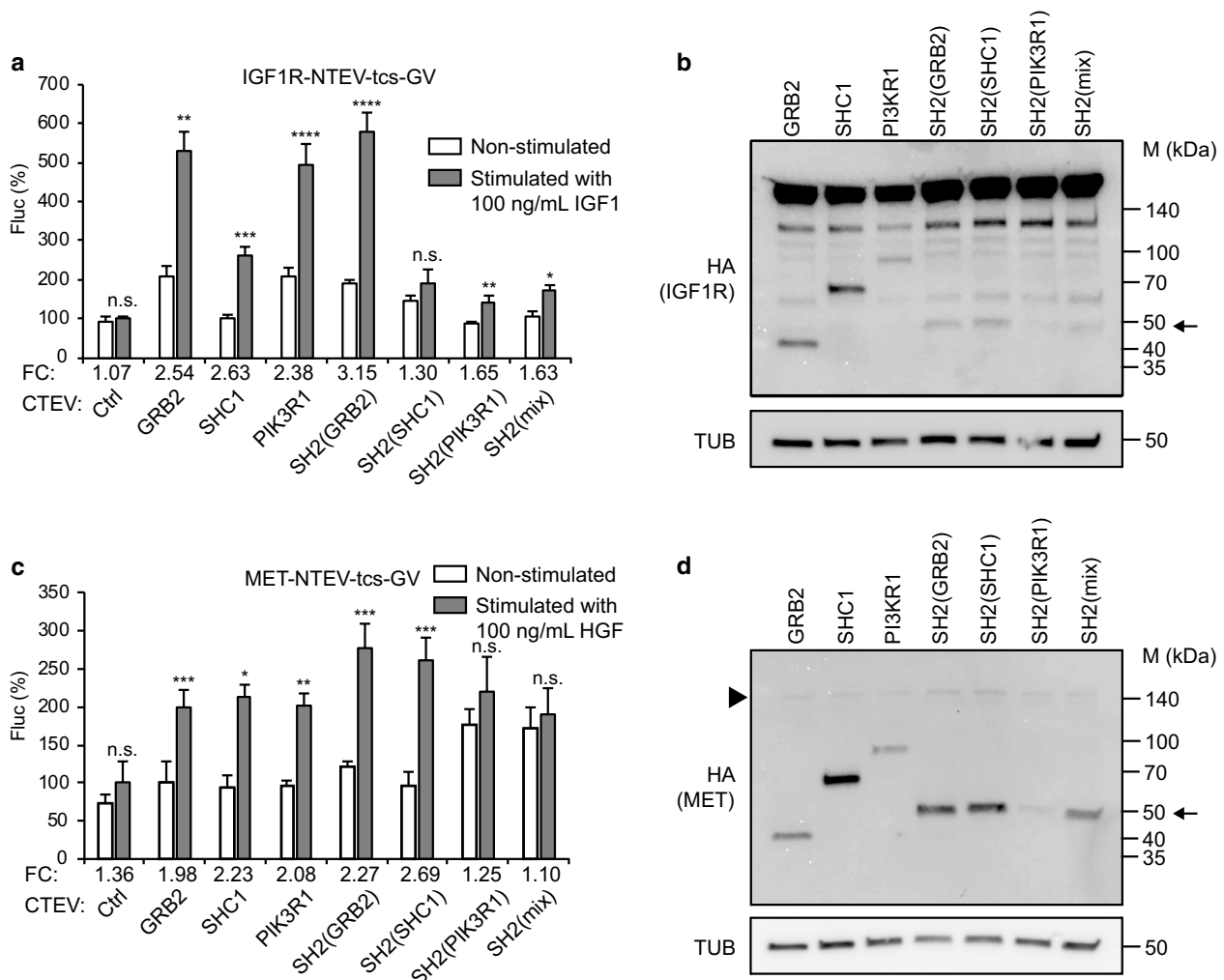


Fig. 3 Comparing adapter protein performance for split TEV recruitment assays to monitor IGF1R and MET receptor activities. **a**, **c** Split TEV recruitment assays for IGF1R and MET receptors. IGF1R (**a**) and MET (**c**) activities were assessed in PC12 cells using IGF1 to stimulate IGF1R, and HGF to stimulate MET. For split TEV assays, the indicated receptor fusions were transfected together with indicated adapters that were fused to the CTEV moiety. Assays were stimulated for 16 h and analysed by a firefly luciferase assay. Non-stimulated samples are shown as open bars and stimulated ones as grey bars. *FC* fold change, *Ctrl* control (no adapter transfected). Results are shown as average of six samples, error bars are shown as SEM. Significance was calculated using the unpaired *t* test, with

** $p \leq 0.01$; *** $p \leq 0.001$; **** $p \leq 0.0001$; *n.s.* not significant. Precise *p* values are provided in Table S1. **b**, **d** Biochemical validation of the expression of IGF1R and MET receptors and adapters. Plasmids encoding IGF1R (**b**), and MET (**d**) (all tagged with NTEV-tcs-GV-2HA) and adapter proteins (all tagged with CTEV-2HA) were transiently transfected into PC12 cells, allowed to express for 16 h, and lysed. Lysates were subjected to Western blotting using the indicated antibodies. Calculated sizes of fusion proteins are provided in Table S1. Arrow indicates bands of artificial adapter fusions. Note that SH2(PIK3R1) is only very weakly expressed. Arrowhead indicates band for MET, which is also very weakly expressed

use phospho-specific antibodies to monitor RTK activity, we explored the potency of EGFR and ERBB4 inhibition by lapatinib by assessing the phosphorylation levels of EGFR in A549 cells and of ERBB4 in T-47D cells. Both cell lines are of human origin and reasonably express EGFR and ERBB4, respectively. Dose-dependent addition of lapatinib led to an efficient inhibition of p-EGFR and p-ERBB4, as revealed by Western blotting (Fig. 5g–j, Fig. S11). Quantification of our Western blotting data indicate that EGFR and ERBB4 are

inhibited by lapatinib at similar concentrations in cellular assays when comparing antibody-based detection of phosphorylation levels and split TEV-based RTK recruitment assays. By contrast, a biochemical kinome profiling study reported that both EGFR (2.4 nM, kD) and ERBB2 (7 nM, kD) are more potently inhibited than ERBB4 (54 nM, kD) [27]. In support of our findings, data from published cellular assays, which use lysates as input for enzyme-linked immunosorbent assays (ELISA) and applied phospho-specific

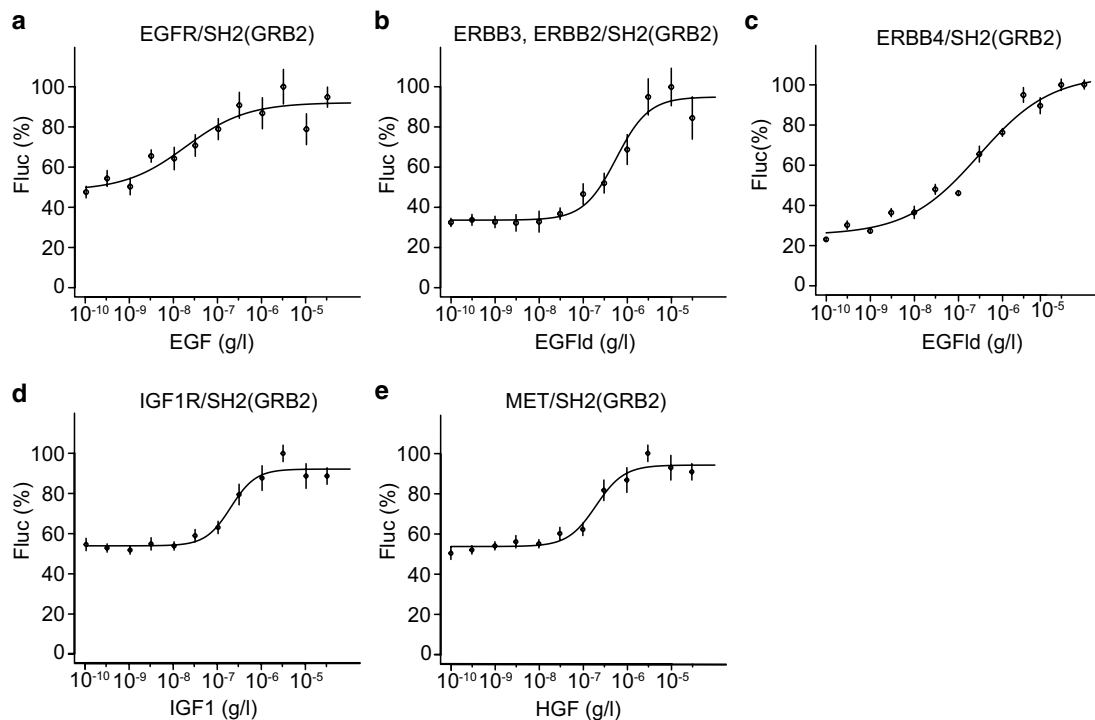


Fig. 4 The concatenated SH2(GRB2) domain fusion is a universal adapter to profile ERBB, IGF1R, and MET activities. Split TEV recruitment assays using increasing concentrations of agonists (EGF, EGFd, IGF1 and HGF shown below *x* axis) for the receptors EGFR (a), ERBB2/ERBB3 (b), ERBB4 (c), IGF1R (d), and MET (e). Each

receptor fusion (NTEV-tcs-GV tag for EGFR, ERBB3, ERBB4, IGF1R, MET; V5-tagged ERBB2) plasmid was co-transfected with the SH2(GRB2)-CTEV adapter plasmid into PC12 cells. Error bars are shown as SEM, with six replicates per condition

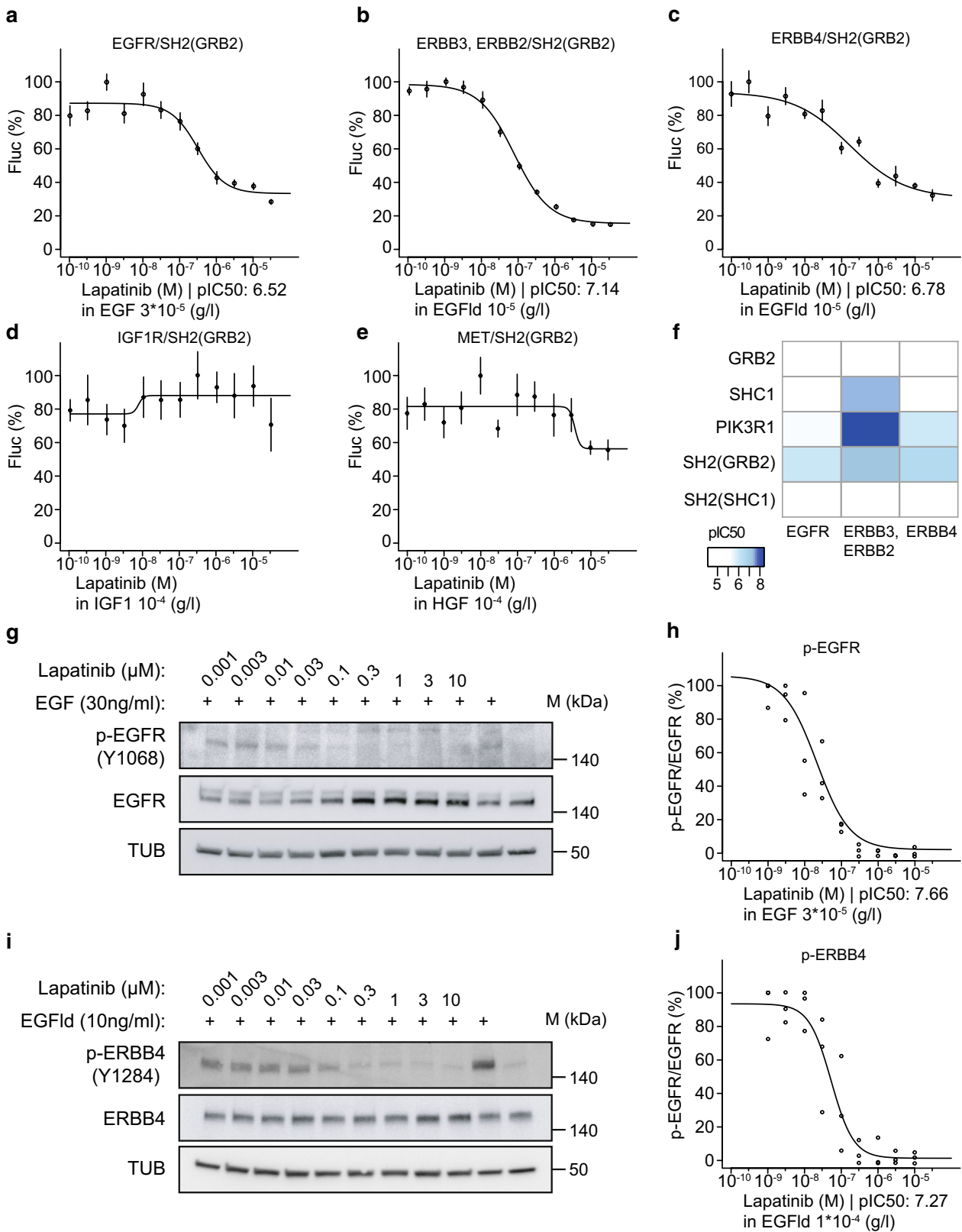
antibodies as sensor of receptor activity, reported a similar range of concentrations for IC_{50} values of EGFR and ERBB2 inhibition, suggesting that efficiencies may substantially vary between biochemical and cell-based assays (Table 1, Table S4) [24, 27–29]. Taken together, our own data obtained from the split TEV recruitment assays indicate that lapatinib efficiently inhibits ERBB receptors, with preferentially inhibiting ERBB2/ERBB3 (72 nM, IC_{50}) and ERBB4 (166 nM, IC_{50}) over EGFR (305 nM, IC_{50}).

To corroborate the use of our cell-based assays using the split TEV recruitment technique and the SH2(GRB2) adapter, we also tested the pan-ERBB inhibitor WZ4002 (Table 1, Table S5) [30, 31]. By performing antagonistic dose–response assays for WZ4002, we could confirm the usage of SH2(GRB2) as a universal adapter in ERBB split TEV recruitment assays. In split TEV assays, WZ4002 efficiently inhibited ERBB family receptors EGFR, ERBB3, and ERBB4 (Fig. 6a–c). Dose-dependent addition of WZ4002 to A549 and T-47D cells reduced phospho-levels of EGFR and ERBB4 to similar levels when compared to split TEV recruitment assays, as quantification of phospho-EGFR and phospho-ERBB4 indicates (Fig. 6d–g, Fig. S11). Further, we tested whether spironolactone exerts antagonistic effects on

ERBB family receptors as recently reported [16]. Spironolactone is a pan-ERBB inhibitor, displaying selectivity for ERBB4 over EGFR, as previously determined using a split TEV dimerisation assay. Spironolactone also inhibited ERBB activities using the universal SH2(GRB2) adapter in the split TEV recruitment assays, with some selectivity for ERBB4 over EGFR (Fig. S12). Further, the spironolactone metabolite canrenone did not exhibit any antagonistic effects on any ERBB assay, which is also consistent with our previous findings [16] (Fig. S12). In summary, these data suggest that the adapter SH2(GRB2) can be used in split TEV recruitment assays to monitor both agonist and antagonist actions targeting the RTK ERBB family in living cells.

Discussion

We describe a genetically encoded split TEV recruitment assay to monitor RTK activities using a universal adapter that consists of three concatenated SH2 domains, which bind to phosphorylated tyrosine residues. As examples for RTKs, we have selected the ERBB receptor family, IGF1R of the INSR family, and MET of the HGFR family. We tested



◀**Fig. 5** The universal SH2(GRB2) adapter displays the highest sensitivity to ERBB family inhibition by lapatinib. Split TEV recruitment assays monitoring the lapatinib-mediated inhibition of EGFR (a), ERBB2/ERBB3 (b), ERBB4 (c), IGF1R (d), and MET (e). Each receptor fusion (NTEV-tcs-GV tag for EGFR, ERBB3, ERBB4, IGF1R, MET; V5-tagged ERBB2) plasmid is co-transfected with the universal SH2(GRB2)-CTEV adapter plasmid into PC12 cells. Depicted are dose–response curves with a constant agonist stimulus (EGF, EGF1d, IGF1, and HGF) and increasing concentrations of lapatinib. Error bars are shown as SEM, with six replicates per condition. **f** Heatmap displaying pIC₅₀ values for lapatinib comparing assay performance of full-length and SH2(GRB2) domain concatenated CTEV adapters co-transfected with the ERBB family NTEV-tcs-GV fusions. Lapatinib reduces p-EGFR (Y1068) levels in A549 cells (**g**, **h**) and p-ERBB4 (Y1284) in T-47D cells (**i**, **j**). Cells were treated for 1 h with increasing concentrations of lapatinib and stimulated for 5 min with 30 ng/ml EGF (**g**) or 10 ng/ml EGF1d (**i**) where indicated. Lysates were subjected to Western blotting and probed with indicated antibodies. Quantification of p-EGFR/EGFR levels (**h**) as shown in (**g**) and p-ERBB4/ERBB4 levels (**j**) as shown in (**i**) are plotted as dose–response curves. For each concentration depicted, three data points from three different lysates were used for calculations (c.f. Fig. S11a, b)

full-length adapters GRB2, SHC1, and PIK3R1, as well as artificially constructed adapters consisting of concatenated SH2 domains of GRB2, SHC1, and PIK3R1 for efficient assay performance upon RTK receptor stimulation (Fig. 1). The adapter formed of three concatenated SH2 domains of GRB2, SH2(GRB2) displayed the best signal-to-noise ratio across all RTK biosensor assays tested (Figs. 2, 3), and the performance of this adapter was further validated in dose–response assays (Fig. 4). In addition, the SH2(GRB2) adapter was characterised in antagonist dose–response assays by applying the ERBB family inhibitors lapatinib, WZ4002, and spironolactone (Figs. 5, 6, Fig. S12).

SH2(GRB2) as a universal adapter for RTK activity measurement

For integrating cell-based assays into HTS, an appropriate signal-to-noise ratio is key to robustness [23, 32]. Therefore, the SH2(GRB2) adapter represents a universal approach towards HTS assays. In agreement, the SH2 domain of GRB2 was reported to bind all members of the ERBB family in a biochemical study using protein microarrays, supporting our findings of SH2(GRB2) as universal adapter [33]. The SH2 domain of GRB2 was also applied as p-Tyr sensor in living cells, where the SH2 domain was fused to the photoactivatable fluorescent protein tdEos to monitor EGFR activation [34]. Furthermore, full-length GRB2 has been shown to stronger bind to p-Tyr motifs present in EGFR and ERBB4 when compared to SHC1, suggesting that the SH2 domain of GRB2 is a better fit for a universal adapter in split TEV recruitment assays [35]. The general consensus sequence of the p-Tyr motifs that the SH2 domain of GRB2 binds to was initially described as pY-X-N [36]. However,

a more recent study expanded this view to a more general consensus sequence pY-[ϕ/Q]-[NQFDK], where ϕ stands for a hydrophobic residue [35], supporting the notion that the SH2 domain of GRB2 can bind to p-Tyr motifs with a rather flexible sequence. As the SH2 domain adapter only consists of SH2 domains and no other interaction modules are present in this adapter, this artificial adapter may solely function as a p-Tyr sensor [37]. Furthermore, the SH2(GRB2) adapter may be used for monitoring activities of other RTKs, such as the insulin growth factor receptor and tropomyosin receptor kinase families that also bind GRB2, potentially expanding the number of receptors [38, 39]. The split TEV recruitment assays presented are based on transient transfections and thus use overexpressed receptors and adapters. Therefore, we would like to emphasise that RTK split TEV recruitment assays were specifically designed to assay receptor activities in heterologous cells, and these assays may not be combined with analyses of downstream signalling [40]. As heterologous cells display abnormal activities of downstream signalling, events of cellular signalling should preferably be monitored in primary cell types. By contrast, activities of receptors may well be studied in heterologous cell lines, as studying receptor activities implicates the first step of a signalling cascade [23].

When RTKs become activated, the phosphorylation of intracellular tyrosine residues represents the first step upon ligand binding. Notably, different agonist ligands and varying concentrations thereof may cause diverse cellular outcomes, as for example described for EGFR ligands that differentially affect EGFR endocytosis and recycling [41]. Thus, it is of common interest to specify which of these tyrosine residues of an RTK are phosphorylated and act as docking sites for adapter proteins to initiate signalling [42]. Alternatively, phosphorylated docking sites may act additively to elicit a response by recruiting a defined set of adapters [43]. To understand which phospho-signature is generated by a given RTK, e.g. after agonist or antagonist treatment, full-length adapters as well as SH2 domain adapters may be used for profiling of biased adapter recruitment. In our split TEV recruitment assays, EGFR activation, for example, can be detected at very low EGF concentrations using the GRB2 full-length protein as adapter (Fig. S8). By contrast, when treating ERBB3 with the antagonist lapatinib, full-length PIK3R1 proved to be the most sensitive adapter protein to measure an inhibition (Fig. 5f, Fig. S10). The adapter SH2(GRB2) does not cover aspects of biased signalling per se, but can be used as universal adapter to study RTK activity profiles. Assessing differential binding properties may be important, as adapters have varying binding affinities to activated receptors and binding affinities depend on ligand concentrations [44]. Likewise, receptors can recruit distinct sets of adapter

Table 1 IC₅₀ and K_D values for ERBB receptor family inhibition by lapatinib and WZ4002 in cellular and biochemical assays

Name of compound	Compound ID (CID)	Target	PubChem assay ID (AID)	Type of assay	IC ₅₀ (nM)/K _D	pIC ₅₀	References
Lapatinib	208908	EGFR	474116	ELISA, cellular lysates	52	7.28	[28]
Lapatinib	208908	EGFR	517323	ELISA, cellular lysates	433	6.36	[29]
Lapatinib	208908	EGFR	n.a.	Split TEV, cell-based assay	305	6.52	This study
Lapatinib	208908	EGFR	624996	Biochemical	2.4	8.62	[27]
Lapatinib	208908	ERBB2	474117	ELISA, cellular lysates	100	7.00	[28]
Lapatinib	208908	ERBB2	517324	ELISA, cellular lysates	140	6.85	[29]
Lapatinib	208908	ERBB2/ERBB3	n.a.	Split TEV, cell-based assay	72	7.14	This study
Lapatinib	208908	ERBB2	624804	Biochemical	7	8.15	[27]
Lapatinib	208908	ERBB3	624851	Biochemical	5500	5.26	[27]
Lapatinib	208908	ERBB4	n.a.	Split TEV, cell-based assay	166	6.78	This study
Lapatinib	208908	ERBB4	624815	Biochemical	54	7.27	[27]
WZ4002	44607530	EGFR	770081	Western blotting, cellular lysates	1180	5.93	[30]
WZ4002	44607530	EGFR	n.a.	Split TEV, cell-based assay	4019	5.40	This study
WZ4002	44607530	EGFR	1204628	Biochemical	16	7.79	[55]
WZ4002	44607530	ERBB2/ERBB3	n.a.	Split TEV, cell-based assay	215	6.67	This study
WZ4002	44607530	ERBB2	1204629	Biochemical	0.42	9.37	[55]
WZ4002	44607530	ERBB3	1204629	Biochemical	0.42	9.37	[55]
WZ4002	44607530	ERBB4	n.a.	Split TEV, cell-based assay	1007	6.00	This study
WZ4002	44607530	ERBB4	1204629	Biochemical	0.42	9.37	[55]

ELISA and Western blotting data were retrieved from the PubChem database (<https://pubchem.ncbi.nlm.nih.gov>) and indicated references. Note that ELISA and Western blotting data from these sources were obtained using phospho-specific antibodies and cellular lysates. The full data set comprising both biochemical and cellular assays are shown in Table S4 (lapatinib) and Table S5 (WZ4002)

n.a. not applicable

proteins to initiate specific downstream signalling [45]. Thus, the SH2(GRB2) adapter may be used for a primary assessment of RTK activity in recruitment assays, followed by more specialised assays (e.g. using other adaptors in split TEV recruitment assays or cell-based assays using phospho-antibodies) to determine signalling fate.

In addition, usage of the universal adapter is not restricted to split TEV-based recruitment assays, but can be implemented into all genetically encoded recruitment assays that, for example, rely on the complementation of a reporter protein, the release of an artificial transcription factor, or both. For example, split green fluorescent protein (GFP) assays (and derivatives) [46, 47], split firefly luciferase [48], split ubiquitin [49], and full-TEV protease assays [50] may be applicable. Furthermore, the SH2(GRB2) adapter may also be used in fluorescence resonance energy transfer (FRET) and bioluminescence resonance energy transfer (BRET)-based assays [51, 52]. Taken together, the universal SH2(GRB2) adapter represents a p-Tyr biosensor to monitor RTK activities and may be used in various cell-based assays that are genetically encoded.

Lapatinib preferentially inhibits ERBB4 over EGFR in RTK/SH2 adapter recruitment assays

Lapatinib, an EGFR and ERBB2 receptor inhibitor, is used in the clinics, e.g. in combination therapies to treat cancers [53, 54]. It has been shown that lapatinib also inhibits ERBB3 and ERBB4 receptors in biochemical profiling studies [27]. Compared to data obtained from biochemical assays, IC₅₀ concentrations for lapatinib were substantially higher in cell-based assays [24, 27, 28] (Table 1, Table S4), suggesting that efficiencies of compounds in living cells cannot be precisely predicted from biochemical data. Thus, compounds should be efficiently tested in cell-based assays that best reflect the nature or the target or, in the case of a disease-linked phenotype, most faithfully replicate the disease state [23]. Furthermore, antagonistic preferences of a given target over related targets, a feature important for characterising selectivity of a compound, may vary between biochemical and cell-based assays, supporting the notion of applying the most appropriate test system possible.

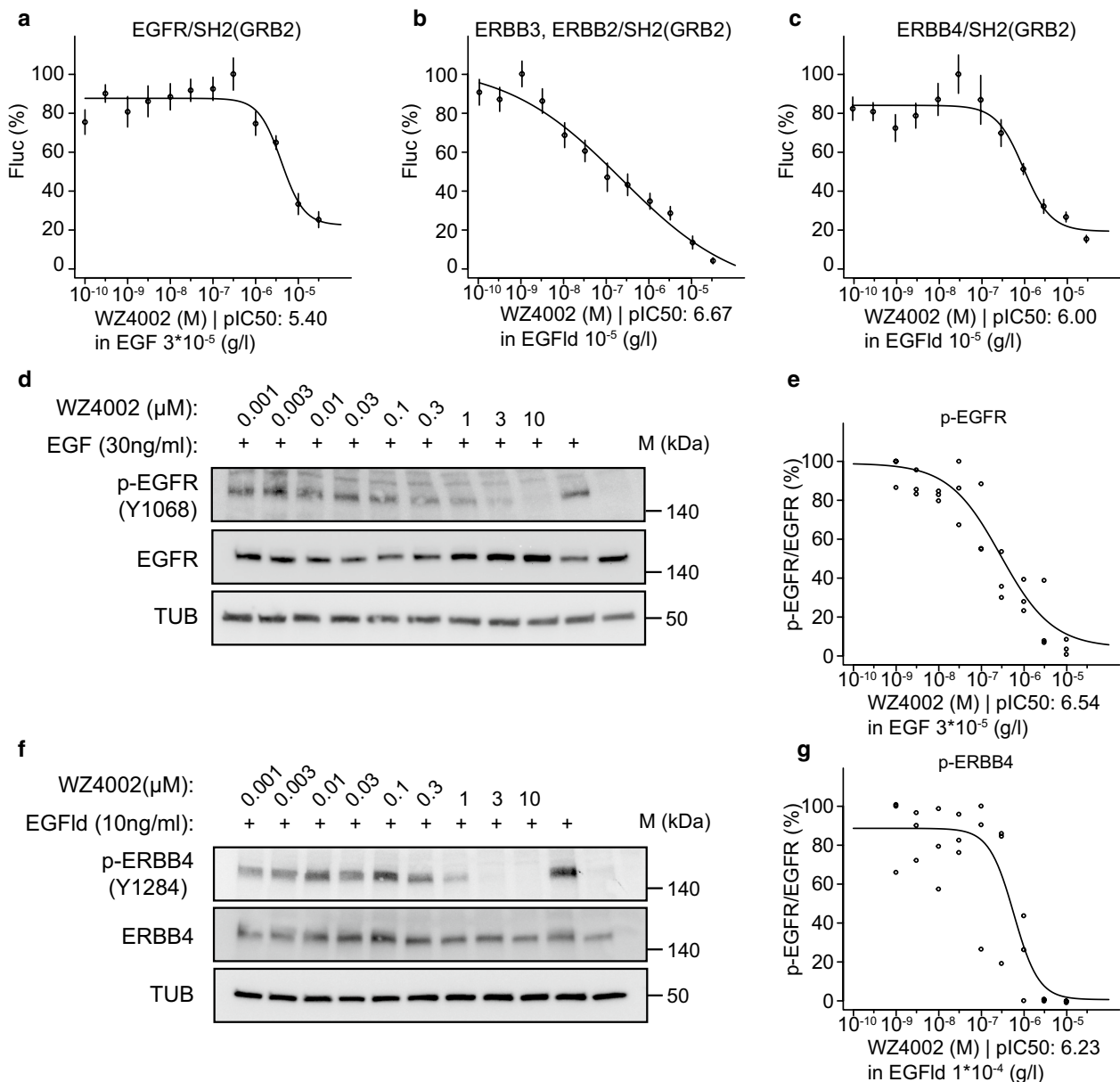


Fig. 6 The ERBB family antagonist WZ4002 inhibits split TEV recruitment assays using the universal SH2(GRB2) adapter. Split TEV recruitment assays monitoring the WZ4002-mediated inhibition of EGFR (a), ERBB2/ERBB3 (b), and ERBB4 (c). Each receptor fusion (NTEV-tcs-GV tag for EGFR, ERBB3, ERBB4; V5-tagged ERBB2) plasmid is co-transfected with the universal SH2(GRB2) CTEV adapter into PC12 cells. Depicted are dose-response curves with a constant stimulus (EGF, EGFlid) and increasing concentrations of lapatinib. Error bars are shown as SEM, with six replicates per condition. WZ4002 reduces p-EGFR (Y1068) levels in A549

cells (d, e) and p-ERBB4 (Y1284) in T-47D cells (f, g). Cells were treated for 1 h with increasing concentrations of WZ4002 and stimulated for 5 min with 30 ng/ml EGF (d) or 10 ng/ml EGFlid (f) where indicated. Lysates were subjected to Western blotting and probed with the indicated antibodies. Quantification of p-EGFR/EGFR levels (e) as shown in (d) and p-ERBB4/ERBB4 levels (g) as shown in (f) are plotted as dose-response curves. For each concentration depicted, three data points from three different lysates were used for calculations (c.f. Fig. S11c, d)

Profiling multiple RTK activities simultaneously using multiplexed cell-based assays

The abnormal activities of RTKs are linked to the

pathophysiology of various human diseases, such as cancers, diabetes, inflammation, angiogenesis, neurodegenerative diseases, and psychiatric disorders [2, 3]. Therefore, these associations have initiated the development of drugs that block or

attenuate aberrant activity of RTKs. However, many available drugs targeting RTKs lack selectivity, demonstrating the medical need for the development of better drugs. The need for more specific drugs is also reflected by the fact that only 3% of all marketed drugs target kinases including RTKs [4]. Cell-based profiling techniques that enable the simultaneous analysis of multiple targets and allow defining selectivity of a given compound will contribute to the development of better drugs [12]. For example, multiplexed cell-based assays that rely on complementation of a reporter, the release of an artificial transcription factor, and the use of barcoded RNA sequences as reporters can be applied to profile activities of disease-relevant targets, as we have recently shown for G protein-coupled receptors (GPCRs) [40]. Therefore, using the split TEV recruitment assay and integrating the universal SH2(GRB2) adapter may represent a promising approach to build a technology platform to assess RTK activities in early drug discovery to finally improve compound selectivity.

Acknowledgements We thank Barbara Meisel, Monika Rübkeil, Johanna Zach, and Nadia Gabellini for excellent technical support.

Author contributions Designed experiments and analysed data: JPW, MCW; performed experiments: JPW, LP; supported assay development with laboratory automation technology: SPW; provided essential reagents and promoted the study: MJR; wrote the manuscript: JPW, MCW; conceived and orchestrated the study: MCW.

Funding M.C.W. was supported by the Deutsche Forschungsgemeinschaft (WE 5683/1-1). Systasy Bioscience GmbH was a beneficiary of the PDZnet project that has received funding from the European Union's H2020 Framework Programme under the Marie Skłodowska-Curie Grant agreement no. 675341.

Compliance with ethical standards

Conflict of interest The authors declare competing financial interest.

Open Access This article is distributed under the terms of the Creative Commons Attribution 4.0 International License (<http://creativecommons.org/licenses/by/4.0/>), which permits unrestricted use, distribution, and reproduction in any medium, provided you give appropriate credit to the original author(s) and the source, provide a link to the Creative Commons license, and indicate if changes were made.

References

- Blume-Jensen P, Hunter T (2001) Oncogenic kinase signalling. *Nature* 411:355–365
- Lemmon MA, Schlessinger J (2010) Cell signaling by receptor tyrosine kinases. *Cell* 141:1117–1134. <https://doi.org/10.1016/j.cell.2010.06.011>
- Mei L, Nave K-A (2014) Neuregulin-ERBB signaling in the nervous system and neuropsychiatric diseases. *Neuron* 83:27–49. <https://doi.org/10.1016/j.neuron.2014.06.007>
- Santos R, Ursu O, Gaulton A et al (2017) A comprehensive map of molecular drug targets. *Nat Rev Drug Discov* 16:19–34. <https://doi.org/10.1038/nrd.2016.230>
- Yaffe MB (2002) Phosphotyrosine-binding domains in signal transduction. *Nat Rev Mol Cell Biol* 3:177–186. <https://doi.org/10.1038/nrm759>
- Liu BA, Jablonowski K, Raina M et al (2006) The human and mouse complement of SH2 domain proteins—establishing the boundaries of phosphotyrosine signaling. *Mol Cell* 22:851–868. <https://doi.org/10.1016/j.molcel.2006.06.001>
- Tinti M, Kierner L, Costa S et al (2013) The SH2 domain interaction landscape. *Cell Rep* 3:1293–1305. <https://doi.org/10.1016/j.celrep.2013.03.001>
- Klapper LN, Glathe S, Vaisman N et al (1999) The ErbB-2/HER2 oncoprotein of human carcinomas may function solely as a shared coreceptor for multiple stroma-derived growth factors. *Proc Natl Acad Sci* 96:4995–5000
- Kochupurakkal BS, Harari D, Di-Segni A et al (2005) Epigen, the last ligand of ErbB receptors, reveals intricate relationships between affinity and mitogenicity. *J Biol Chem* 280:8503–8512. <https://doi.org/10.1074/jbc.M413919200>
- Guy PM, Platko JV, Cantley LC et al (1994) Insect cell-expressed p180erbB3 possesses an impaired tyrosine kinase activity. *Proc Natl Acad Sci* 91:8132–8136
- Yarden Y, Sliwkowski MX (2001) Untangling the ErbB signalling network. *Nat Rev Mol Cell Biol* 2:127–137. <https://doi.org/10.1038/35052073>
- Wehr MC, Rossner MJ (2016) Split protein biosensor assays in molecular pharmacological studies. *Drug Discov Today* 21:415–429. <https://doi.org/10.1016/j.drudis.2015.11.004>
- Wehr MC, Laage R, Bolz U et al (2006) Monitoring regulated protein-protein interactions using split TEV. *Nat Methods* 3:985–993. <https://doi.org/10.1038/nmeth967>
- Wehr M, Reinecke L, Botvinnik A, Rossner M (2008) Analysis of transient phosphorylation-dependent protein-protein interactions in living mammalian cells using split-TEV. *BMC Biotechnol* 8:55. <https://doi.org/10.1186/1472-6750-8-55>
- Velanac V, Unterbarnscheidt T, Hinrichs W et al (2012) Bace1 processing of NRG1 type III produces a myelin-inducing signal but is not essential for the stimulation of myelination. *Glia* 60:203–217. <https://doi.org/10.1002/glia.21255>
- Wehr MC, Hinrichs W, Brzózka MM et al (2017) Spironolactone is an antagonist of NRG1-ERBB4 signaling and schizophrenia-relevant endophenotypes in mice. *EMBO Mol Med*. <https://doi.org/10.15252/emmm.201707691>
- Yang X, Boehm JS, Yang X et al (2011) A public genome-scale lentiviral expression library of human ORFs. *Nat Methods* 8:659–661. <https://doi.org/10.1038/nmeth.1638>
- Ritz C, Baty F, Streibig JC, Gerhard D (2015) Dose-response analysis using R. *PLoS One* 10:e0146021. <https://doi.org/10.1371/journal.pone.0146021>
- Wintgens JP, Rossner MJ, Wehr MC (2017) Characterizing dynamic protein-protein interactions using the genetically encoded split biosensor assay technique split TEV. *Methods Mol Biol* 1596:219–238. https://doi.org/10.1007/978-1-4939-6940-1_14
- Elkins RC, Davies MR, Brough SJ et al (2013) Variability in high-throughput ion-channel screening data and consequences for cardiac safety assessment. *J Pharmacol Toxicol Methods* 68:112–122. <https://doi.org/10.1016/j.vascn.2013.04.007>
- Song RX, Barnes CJ, Zhang Z et al (2004) The role of Shc and insulin-like growth factor 1 receptor in mediating the translocation of estrogen receptor alpha to the plasma membrane. *Proc Natl Acad Sci USA* 101:2076–2081. <https://doi.org/10.1073/pnas.0308334100>
- Liang Q, Mohan RR, Chen L, Wilson SE (1998) Signaling by HGF and KGF in corneal epithelial cells: Ras/MAP kinase and Jak-STAT pathways. *Invest Ophthalmol Vis Sci* 39:1329–1338

23. Vincent F, Loria P, Pregel M et al (2015) Developing predictive assays: the phenotypic screening “rule of 3”. *Sci Transl Med* 7:293p15. <https://doi.org/10.1126/scitranslmed.aab1201>
24. Rusnak DW, Lackey K, Affleck K et al (2001) The effects of the novel, reversible epidermal growth factor receptor/ErbB-2 tyrosine kinase inhibitor, GW2016, on the growth of human normal and tumor-derived cell lines in vitro and in vivo. *Mol Cancer Ther* 1:85–94
25. Mulvihill MJ, Cooke A, Rosenfeld-Franklin M et al (2009) Discovery of OSI-906: a selective and orally efficacious dual inhibitor of the IGF-1 receptor and insulin receptor. *Future Med Chem* 1:1153–1171. <https://doi.org/10.4155/fmc.09.89>
26. Qian F, Engst S, Yamaguchi K et al (2009) Inhibition of tumor cell growth, invasion, and metastasis by EXEL-2880 (XL880, GSK1363089), a novel inhibitor of HGF and VEGF receptor tyrosine kinases. *Cancer Res* 69:8009–8016. <https://doi.org/10.1158/0008-5472.CAN-08-4889>
27. Davis MI, Hunt JP, Herrgard S et al (2011) Comprehensive analysis of kinase inhibitor selectivity. *Nat Biotechnol* 29:1046–1051. <https://doi.org/10.1038/nbt.1990>
28. Fidanze SD, Erickson SA, Wang GT et al (2010) Imidazo[2,1-b]thiazoles: multitargeted inhibitors of both the insulin-like growth factor receptor and members of the epidermal growth factor family of receptor tyrosine kinases. *Bioorg Med Chem Lett* 20:2452–2455. <https://doi.org/10.1016/j.bmcl.2010.03.015>
29. Wang GT, Mantei RA, Hubbard RD et al (2010) Substituted 4-amino-1H-pyrazolo[3,4-d]pyrimidines as multi-targeted inhibitors of insulin-like growth factor-1 receptor (IGF1R) and members of ErbB-family receptor kinases. *Bioorg Med Chem Lett* 20:6067–6071. <https://doi.org/10.1016/j.bmcl.2010.08.052>
30. Ward RA, Anderton MJ, Ashton S et al (2013) Structure- and reactivity-based development of covalent inhibitors of the activating and gatekeeper mutant forms of the epidermal growth factor receptor (EGFR). *J Med Chem* 56:7025–7048. <https://doi.org/10.1021/jm400822z>
31. Zhou W, Ercan D, Chen L et al (2009) Novel mutant-selective EGFR kinase inhibitors against EGFR T790M. *Nature* 462:1070–1074. <https://doi.org/10.1038/nature08622>
32. Birmingham A, Selfors LM, Forster T et al (2009) Statistical methods for analysis of high-throughput RNA interference screens. *Nat Methods* 6:569–575. <https://doi.org/10.1038/nmeth.1351>
33. Jones RB, Gordus A, Krall JA, MacBeath G (2006) A quantitative protein interaction network for the ErbB receptors using protein microarrays. *Nature* 439:168–174. <https://doi.org/10.1038/nature04177>
34. Oh D, Ogiue-Ikeda M, Jadwin JA et al (2012) Fast rebinding increases dwell time of Src homology 2 (SH2)-containing proteins near the plasma membrane. *PNAS* 109:14024–14029. <https://doi.org/10.1073/pnas.1203397109>
35. Schulze WX, Deng L, Mann M (2005) Phosphotyrosine interactome of the ErbB-receptor kinase family. *Mol Syst Biol* 1(2005):0008. <https://doi.org/10.1038/msb4100012>
36. Ward CW, Gough KH, Rashke M et al (1996) Systematic mapping of potential binding sites for Shc and Grb2 SH2 domains on insulin receptor substrate-1 and the receptors for insulin, epidermal growth factor, platelet-derived growth factor, and fibroblast growth factor. *J Biol Chem* 271:5603–5609. <https://doi.org/10.1074/jbc.271.10.5603>
37. Pawson T (2004) Specificity in signal transduction: from phosphotyrosine-SH2 domain interactions to complex cellular systems. *Cell* 116:191–203. [https://doi.org/10.1016/S0092-8674\(03\)01077-8](https://doi.org/10.1016/S0092-8674(03)01077-8)
38. Hanke S, Mann M (2009) The phosphotyrosine interactome of the insulin receptor family and its substrates IRS-1 and IRS-2. *Mol Cell Proteomics* 8:519–534. <https://doi.org/10.1074/mcp.M800407-MCP200>
39. MacDonald JIS, Gryz EA, Kubu CJ et al (2000) Direct binding of the signaling adapter protein Grb2 to the activation loop tyrosines on the nerve growth factor receptor tyrosine kinase, TrkA. *J Biol Chem* 275:18225–18233. <https://doi.org/10.1074/jbc.M001862200>
40. Galinski S, Wichert SP, Rossner MJ, Wehr MC (2018) Multiplexed profiling of GPCR activities by combining split TEV assays and EXT-based barcoded readouts. *Sci Rep* 8:8137. <https://doi.org/10.1038/s41598-018-26401-9>
41. Roepstorff K, Grandal MV, Henriksen L et al (2009) Differential effects of EGFR ligands on endocytic sorting of the receptor. *Traffic* 10:1115–1127. <https://doi.org/10.1111/j.1600-0854.2009.00943.x>
42. Vasudevan HN, Soriano P (2016) A thousand and one receptor tyrosine kinases: wherein the specificity? *Curr Top Dev Biol* 117:393–404. <https://doi.org/10.1016/bs.ctdb.2015.10.016>
43. Freed DM, Bessman NJ, Kiyatkin A et al (2017) EGFR ligands differentially stabilize receptor dimers to specify signaling kinetics. *Cell* 171:683–695.e18. <https://doi.org/10.1016/j.cell.2017.09.017>
44. Ronan T, Macdonald-Obermann JL, Huelsmann L et al (2016) Different epidermal growth factor receptor (EGFR) agonists produce unique signatures for the recruitment of downstream signaling proteins. *J Biol Chem* 291:5528–5540. <https://doi.org/10.1074/jbc.M115.710087>
45. Zinkle A, Mohammadi M (2018) A threshold model for receptor tyrosine kinase signaling specificity and cell fate determination. *F1000Res*. <https://doi.org/10.12688/f1000research.14143.1>
46. Ghosh I, Hamilton AD, Regan L (2000) Antiparallel leucine zipper-directed protein reassembly: application to the green fluorescent protein. *J Am Chem Soc* 122:5658–5659. <https://doi.org/10.1021/ja994421w>
47. Zhou J, Lin J, Zhou C et al (2011) An improved bimolecular fluorescence complementation tool based on superfolder green fluorescent protein. *Acta Biochim Biophys Sin (Shanghai)* 43:239–244. <https://doi.org/10.1093/abbs/gmq128>
48. Paulmurugan R, Umezawa Y, Gambhir SS (2002) Noninvasive imaging of protein–protein interactions in living subjects by using reporter protein complementation and reconstitution strategies. *PNAS* 99:15608–15613. <https://doi.org/10.1073/pnas.242594299>
49. Petschnigg J, Groisman B, Kotlyar M et al (2014) The mammalian-membrane two-hybrid assay (MaMTH) for probing membrane-protein interactions in human cells. *Nat Methods* 11:585–592. <https://doi.org/10.1038/nmeth.2895>
50. Barnea G, Strapps W, Herrada G et al (2008) The genetic design of signaling cascades to record receptor activation. *Proc Natl Acad Sci USA* 105:64–69. <https://doi.org/10.1073/pnas.0710487105>
51. Jares-Erijman EA, Jovin TM (2003) FRET imaging. *Nat Biotechnol* 21:1387–1395. <https://doi.org/10.1038/nbt896>
52. Pflieger KD, Eidne KA (2006) Illuminating insights into protein–protein interactions using bioluminescence resonance energy transfer (BRET). *Nat Methods* 3:165–174. <https://doi.org/10.1038/nmeth841>
53. Madden R, Kosari S, Peterson GM et al (2018) Lapatinib plus capecitabine in patients with HER2-positive metastatic breast cancer: a systematic review. *Int J Clin Pharmacol Ther* 56:72–80. <https://doi.org/10.5414/CP203123>
54. Petrelli F, Ghidini M, Lonati V et al (2017) The efficacy of lapatinib and capecitabine in HER-2 positive breast cancer with brain metastases: a systematic review and pooled analysis. *Eur J Cancer* 84:141–148. <https://doi.org/10.1016/j.ejca.2017.07.024>
55. Basu D, Richters A, Rauh D (2015) Structure-based design and synthesis of covalent-reversible inhibitors to overcome drug resistance in EGFR. *Bioorg Med Chem* 23:2767–2780. <https://doi.org/10.1016/j.bmc.2015.04.038>

Publisher's Note Springer Nature remains neutral with regard to jurisdictional claims in published maps and institutional affiliations.

Electronic supplementary material

Monitoring activities of receptor tyrosine kinases using a universal adapter in genetically encoded split TEV assays

Jan P. Wintgens^{1,2}, Sven P. Wichert^{1,2}, Luksa Popovic², Moritz J. Rossner¹, Michael C. Wehr^{1,2*}

(1) Department of Psychiatry and Psychotherapy, University Hospital, LMU Munich, Nussbaumstr. 7, 80336 Munich, Germany

(2) Systasy Bioscience GmbH, Adams-Lehmann-Str. 56, 80797 Munich, Germany

(*) Author for correspondence: Dr. Michael C. Wehr, email: Michael.Wehr@med.uni-muenchen.de; phone: +49 (0) 89 4400 53275

Supplementary Figures.....	3
Supplementary Tables.....	20

Supplementary Figures

a SH2(GRB2) – 3xSH2 of GRB2

DNA sequence:

```
atgGTGtggttttttggcaaaatccccagagccaaggcagaagaaatgcttagcaaacagcggcaccgatggggcc
tttcttatccgagagagtgagagcgctcctggggacttctccctctctgtcaagtttgaaacgatgtgcagcac
ttcaaggtgctccgagatggagccggaagtacttctctgggtggtgaagttcaattctttgaatgagctggtg
gattatcacagatctacatctgtctccagaaaccagcagatattcctgcgggacatagaaGGAGGTGGAGGTAGC
ACCGGTGGAGGAGGTAGCtggttttttggcaaaatccccagagccaaggcagaagaaatgcttagcaaacagcgg
caccgatggggcctttcttatccgagagagtgagagcgctcctggggacttctccctctctgtcaagtttgaaac
gatgtgcagcacttcaaggtgctccgagatggagccggaagtacttctctgggtggtgaagttcaattctttg
aatgagctggtggattatcacagatctacatctgtctccagaaaccagcagatattcctgcgggacatagaaGGA
GGTGGAGGTAGCACCGGTGGAGGAGGTAGCtggttttttggcaaaatccccagagccaaggcagaagaaatgctt
agcaaacagcggcaccgatggggcctttcttatccgagagagtgagagcgctcctggggacttctccctctctgtc
aagtttgaaacgatgtgcagcacttcaaggtgctccgagatggagccggaagtacttctctgggtggtgaag
ttcaattctttgaatgagctggtggattatcacagatctacatctgtctccagaaaccagcagatattcctgcgg
gacatagaa
```

Protein sequence:

```
MVWFFGKIPRAKAEEMLSKQRHDGAFLIRESESAPGDFSLSVKFGNDVQHFVKLRDGAGKYFLWVVKFNSLNELV
DYHRSTSVSRNQIIFLRDIEGGGGSTGGGGSWFFGKIPRAKAEEMLSKQRHDGAFLIRESESAPGDFSLSVKFGN
DVQHFVKLRDGAGKYFLWVVKFNSLNELVDYHRSTSVSRNQIIFLRDIEGGGGSTGGGGSWFFGKIPRAKAEEML
SKQRHDGAFLIRESESAPGDFSLSVKFGNDVQHFVKLRDGAGKYFLWVVKFNSLNELVDYHRSTSVSRNQIIFLR
DIE
```

b SH2(SHC1) – 3xSH2 of SHC1

DNA sequence:

```
atgGTGtggttccatgggaagctgagccggcgggaggctgaggcactgctgcagctcaatggggacttctggta
cgggagagcaccgaccacactggccagatgtgctcactggcttgcagagtgggcagcctaagcatttgctactg
gtggaccctgaggggtgtggttcggactaaggatcaccgcttggaaagtgtcagtcaccttatcagctaccacatg
gacaatcacttgcccatcatctctgcgggcagcgaactgtgtctacagcaacctgtgGGAGGTGGAGGTAGCACC
GGTGGAGGAGGTAGCtggttccatgggaagctgagccggcgggaggctgaggcactgctgcagctcaatggggac
ttctggttacgggagagcaccgaccacactggccagatgtgctcactggcttgcagagtgggcagcctaagcat
ttgctactggtggaccctgaggggtgtggttcggactaaggatcaccgcttggaaagtgtcagtcaccttatcagc
taccacatggacaatcacttgcccatcatctctgcgggcagcgaactgtgtctacagcaacctgtgGGAGGTGGA
GGTAGCACCGGTGGAGGAGGTAGCtggttccatgggaagctgagccggcgggaggctgaggcactgctgcagctc
aatggggacttctggttacgggagagcaccgaccacactggccagatgtgctcactggcttgcagagtgggcag
cctaagcatttgctactggtggaccctgaggggtgtggttcggactaaggatcaccgcttggaaagtgtcagtcac
cttatcagctaccacatggacaatcacttgcccatcatctctgcgggcagcgaactgtgtctacagcaacctgtg
```

Protein sequence:

```
MVWFFHGKLSRREAEALLQLNGDFLVRESTTTPGQYVLTGLQSGQPKHLLLVDPGVVVRTKDRHFESVSHLISYHM
DNHLPIISAGSELCLQQPVGGGGSTGGGGSWFFHGKLSRREAEALLQLNGDFLVRESTTTPGQYVLTGLQSGQPKH
LLLVDPEGVVVRTKDRHFESVSHLISYHMDNHLPIISAGSELCLQQPVGGGGSTGGGGSWFFHGKLSRREAEALLQL
NGDFLVRESTTTPGQYVLTGLQSGQPKHLLLVDPGVVVRTKDRHFESVSHLISYHMDNHLPIISAGSELCLQQPV
```

Fig. S1 continued

C SH2(PIK3R1) – 3xSH2 of PIK3R1(SH2a, SH2a, SH2b)

DNA sequence:

```
atgGTGtggtactggggagatatctcgaggaagaagtgaatgaaaaacttcgagatacagcagacgggaccttt
ttggtacgagatgCGTctactaaaatgcatggtgattatactcttacactaaggaaaggggaaataacaaatta
atcaaaatatttcacgagatgggaaatggtcttctcgaccattaaccttcagttctgtggttgaattaata
aaccactaccggaatgaatctctagctcagtataatcccaattggatgtgaaattactttatccagtaGGAGGT
GGAGGTAGCACCGGTGGAGGAGGTAGCtggtactggggagatatctcgaggaagaagtgaatgaaaaacttcga
gatacagcagacgggaccttttgggtacgagatgCGTctactaaaatgcatggtgattatactcttacactaagg
aaagggggaaataacaaattaatcaaaatatttcacgagatgggaaatggtcttctcgaccattaaccttc
agttctgtggttgaattaataaaccactaccggaatgaatctctagctcagtataatcccaattggatgtgaaa
ttactttatccagtaGGAGGTGGAGGTAGCACCGGTGGAGGAGGTAGCtggatggttggagcagcaaccgaaac
aaagctgaaaacctgttgcgagggagcgagatggcacttttctgtccgggagagcagtaaacagggctgctat
gctctgtctgtagtggtggacggcgaaagtaaacattgtgtcataaacaacagcaactggctatggctttgcc
gagccctataactgtacagctctctgaaagaactgggtgtacattaccaacacacctcccttgtgcagcacaac
gactccctcaatgtcacactagcctaccagta
```

Protein sequence:

```
MVWYWGDISREEVNEKLRDTADGTFLVRDASTKMHGDYTLTLRKGGNNKLIKIFHRDGKYGFS DPLTFSSVVELI
NHYRNESLAQYNPKLDVKLLYPVGGGGSTGGGGSWYWGDISREEVNEKLRDTADGTFLVRDASTKMHGDYTLTLR
KGGNNKLIKIFHRDGKYGFS DPLTFSSVVELINHYRNESLAQYNPKLDVKLLYPVGGGGSTGGGGSWNVGSSNRN
KAENLLRGRDGTFLVRESSKQGCYACSVVDGEVVKHCVINKTATGYGFAEPYNLYSSLKELVLHYQHTSLVQHN
DSLNVTLAYPV
```

d SH2(mix) – 1xSH2 of GRB2, 1xSH2 of SHC1, 1xSH2a of PIK3R1

DNA sequence:

```
atgGTGtggttttttggcaaaatccccagagccaaggcagaagaatgcttagcaaacagcggcagatggggcc
tttcttatccgagagagtgagagcgtcctctgggacttctccctctctgtcaagtttgaaacgatgtgcagcac
ttcaaggtgctccgagatggagccgggaagtacttctctgggtggtgaagttcaattctttgaatgagctggtg
gattatcacagatctacatctgtctccagaaccagcagatattcctgcgggacatagaaGGAGGTGGAGGTAGC
GGAGGTGGAGGTAGCtggttccatgggaagctgagccggcgggaggctgaggcactgctgcagctcaatggggac
ttctggtacgggagagcagaccacacctggccagatgtgctcactggcttgcaagatgggcagcctaagcat
ttgctactgggtggacctgaggtgtggttcggactaaggatcaccgctttgaaaggtcagtcacctatcagc
taccacatggacaatcacttgccatcatctctgcccagcgaactgtgtctacagcaacctgtgGGAGGTGGA
GGTAGCGGAGGTGGAGGTAGCtggtactggggagatatctcgaggaagaagtgaatgaaaaacttcgagataca
gcagacgggaccttttgggtacgagatgCGTctactaaaatgcatggtgattatactcttacactaaggaaaggg
ggaaataacaaattaatcaaaatatttcacgagatgggaaatggtcttctcgaccattaaccttcagttct
gtggttgaattaataaaccactaccggaatgaatctctagctcagtataatcccaattggatgtgaaattactt
tatccagta
```

Protein sequence:

```
MVWFFGKIPRAKAEEMLSKQRHDGAF LIRESESAPGDFSLSVKFGNDVQHFKVLRD GAGKYFLWVVKFNSLNELV
DYHRSTSVSRNQIIFLRDI EGGGSGGGGSWFHGKLSRREAEALLQLNGDFLVRESTTTPGQYVLTGLQSGQPKH
LLLVDPEGVVRTKDRHFESVSHLISYHMDNHLPIISAGSELCLQQPVGGGSGGGGSWYWGDISREEVNEKLRDT
ADGTFLVRDASTKMHGDYTLTLRKGGNNKLIKIFHRDGKYGFS DPLTFSSVVELINHYRNESLAQYNPKLDVKLL
YPV
```

Fig. S1. DNA and protein sequences of concatenated SH2 domain adapters.

SH2 domains are highlighted in cyan (for DNA sequences) and green (for protein sequences). SH2 domains are spaced by flexible linkers (with protein sequence GGGGSTGGGGS). **(a)** Three concatenated SH2 domains of human GRB2; denoted as SH2(GRB2). **(b)** Three concatenated SH2 domains of human SHC1; denoted as SH2(SHC1). **(c)** Three concatenated SH2 domains of human PIK3R1, using twice the N-terminal SH2 domain (SH2-N) of PIK3R1, and once the C-terminal SH2 domain (SH2-C) of PIK3R1; denoted as SH2(PIK3R1). **(d)** Three concatenated SH2 domains of human GRB2, human SHC1, and the N-terminal SH2 domain (SH2-N) of human PIK3R1; denoted as SH2(mix).

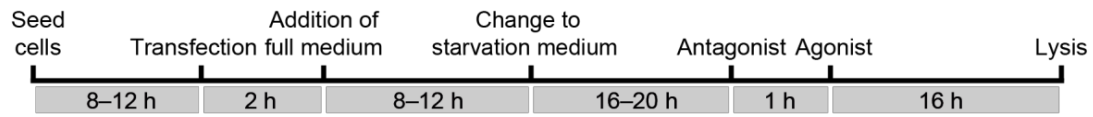


Fig. S2. Experimental time line for agonist and antagonist ERBB split TEV recruitment assays.

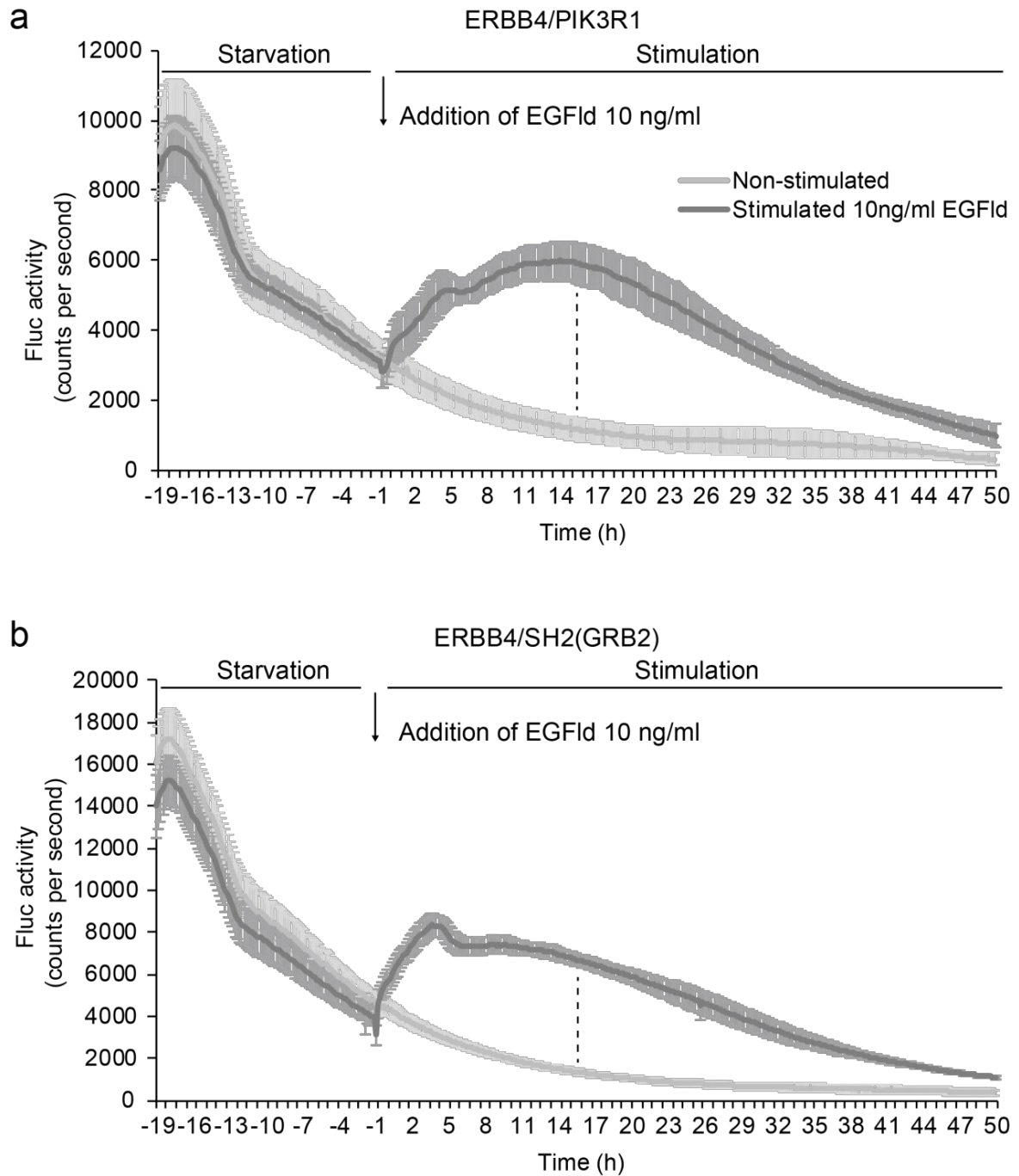


Fig. S3. Split TEV ERBB4 recruitment assays optimally respond after 16 h of stimulation.

The ERBB4-NTEV-tcs-GV (ERBB4) receptor plasmid was transfected into PC12 cells together with a firefly luciferase (Fluc) reporter plasmid, and either a plasmid encoding the full-length adapter PIK3R1-CTEV (assay: ERBB4/PIK3R1) (a) or the SH2-domain adapter SH2(GRB2)-CTEV (assay: ERBB4/SH2(GRB2)) (b). Luciferase activity was measured every 10 minutes. Time point at 0 h denotes the start of the stimulation phase at which 10 ng/mL EGF-like domain (EGFlD) were added to the medium. The dashed line at 16 h represents the highest ratio of stimulation to baseline activity. An average of three samples is shown, error bars represent SD.

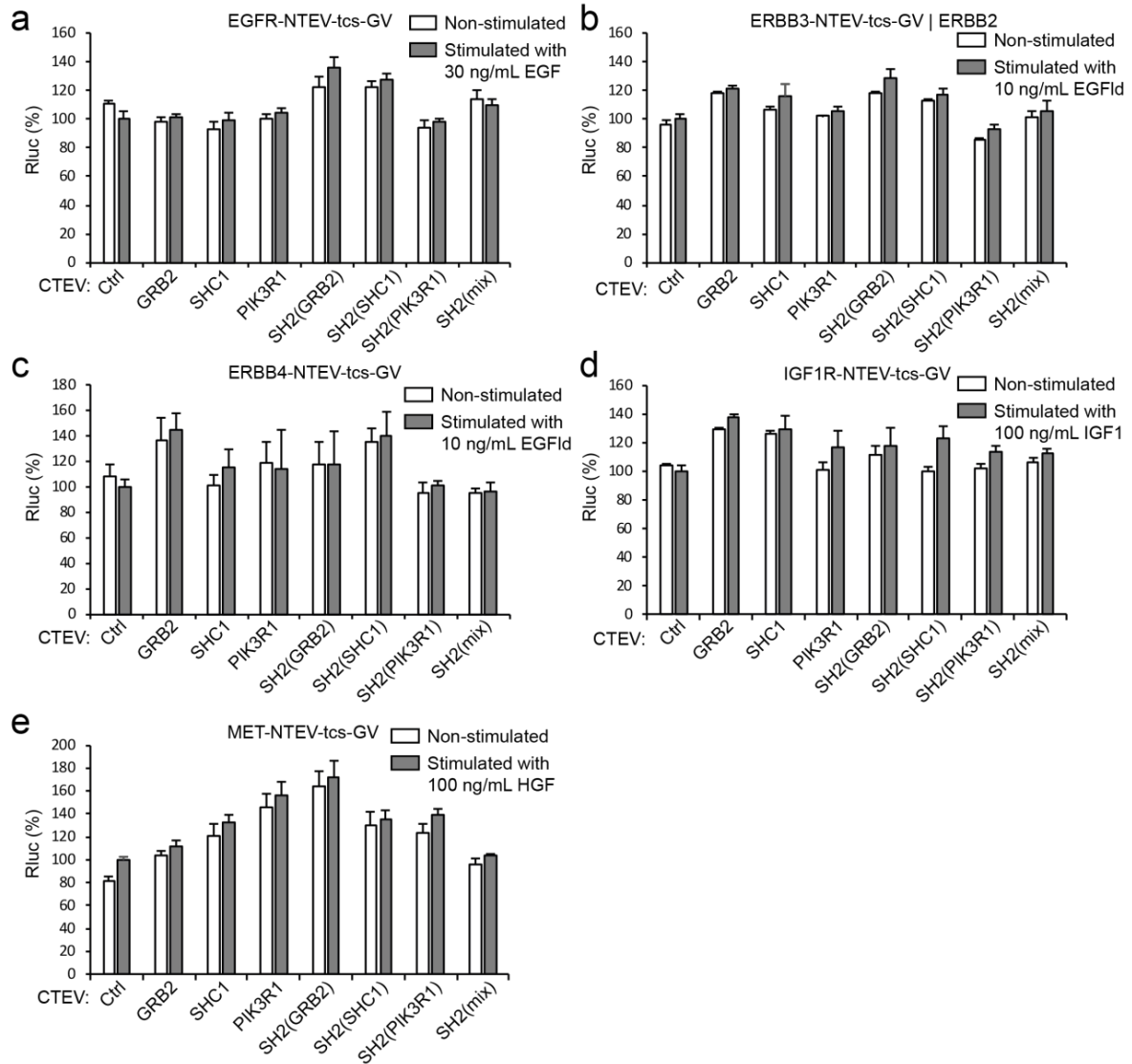


Fig. S4. Constitutive *Renilla* luciferase readings are stable in growth factor stimulated RTK split TEV recruitment assays.

Thymidine kinase-driven *Renilla* luciferase signals were assessed in EGFR (**a**), ERBB2/ERBB3 (**b**), ERBB4 (**c**), IGF1R (**d**), and MET (**e**) split TEV recruitment assays under control and stimulated conditions in PC12 cells. EGF was applied to stimulate EGFR, EGF-like domain (EGFlid) to stimulate ERBB3 and ERBB4, IGF1 to stimulate IGF1R and HGF to stimulate MET. The indicated receptor fusions were transfected together with indicated adapters that were fused to the CTEV moiety. Note that for the ERBB2/ERBB3 assay (**b**), ERBB2 is co-transfected to allow heterodimerisation and thus ERBB3 phosphorylation, which is required for the recruitment of adapters. Assays were stimulated for 16 h, lysed and analysed for *Renilla* activity. Non-stimulated samples are shown as open bars and stimulated once as grey bars. Error bars represent SD, with 6 replicates per condition. Fig. S5 correlates to Figs. 2 and 3.

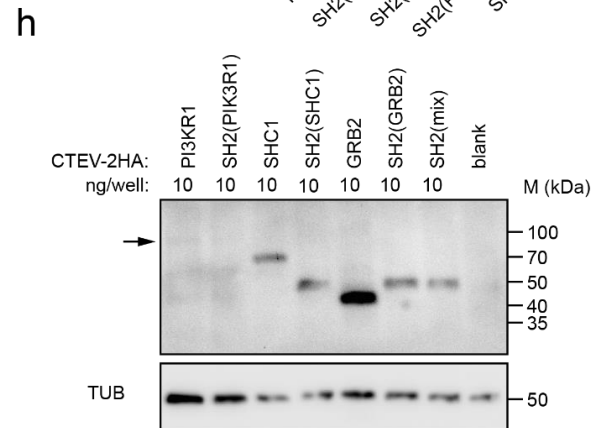
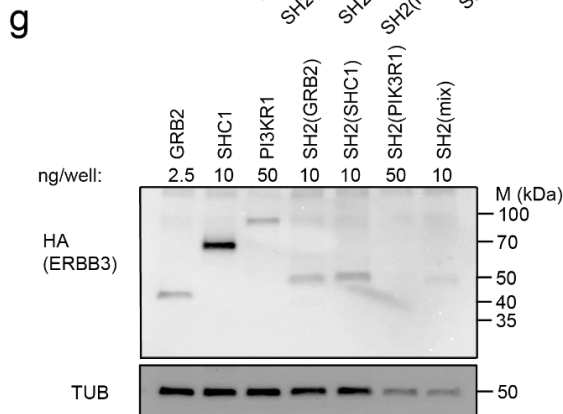
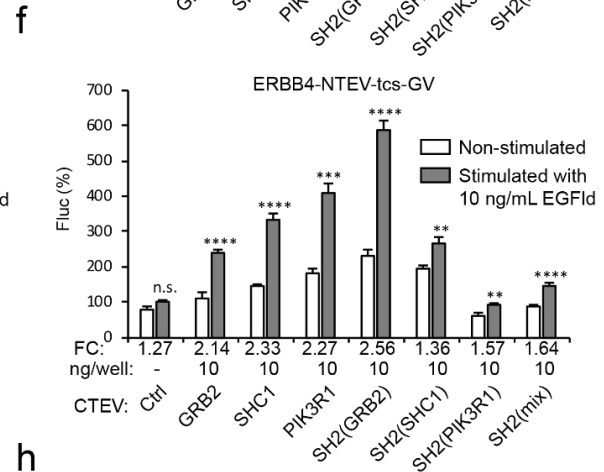
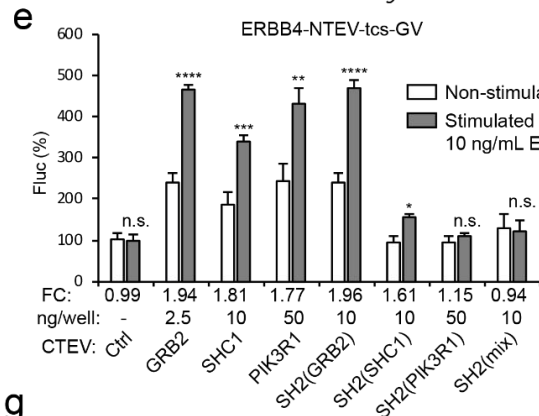
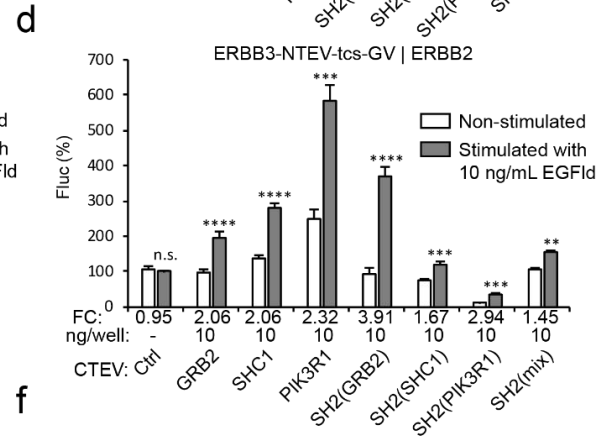
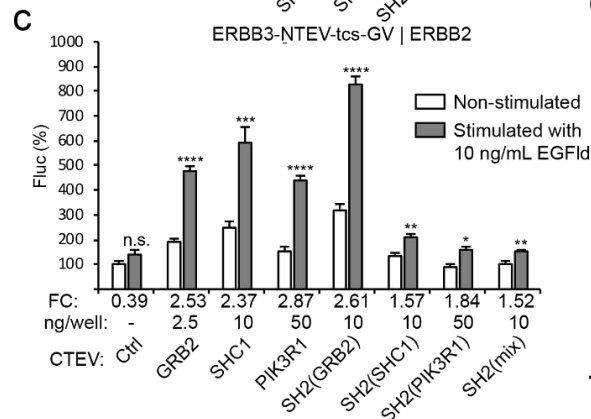
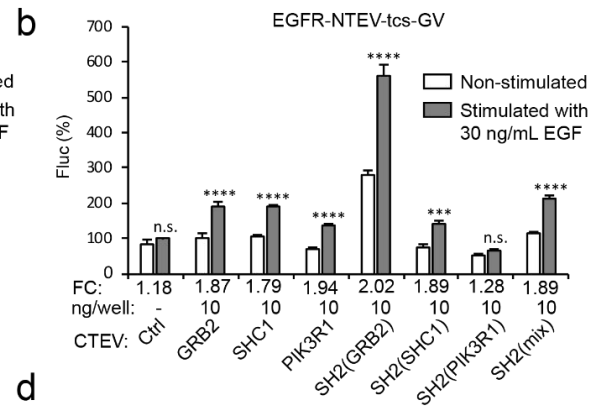
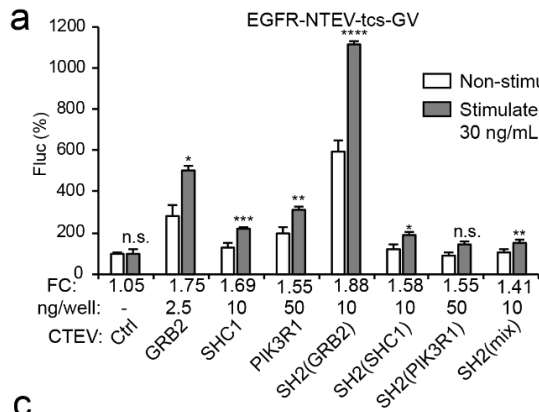


Fig. S5. Transient RTK split TEV recruitment assays tolerate differences in transfected adapter plasmids.

a–f Split TEV recruitment assays for EGFR (**a, b**), ERBB2/ERBB3 (**c, d**), and ERBB4 (**e, f**). Note that for the ERBB2/ERBB3 assay (**c**), ERBB2 is co-transfected to allow heterodimerisation and thus ERBB3 phosphorylation, which is required for the recruitment of adapters. Assays were stimulated for 16 h, and analysed by a firefly luciferase assay. Non-stimulated samples are shown as open bars and stimulated once as grey bars. Ctrl, control (no adapter transfected). Non-stimulated samples are shown as open bars and stimulated once as grey bars. FC, fold change; Ctrl, control (no adapter transfected). Results are shown as average of 6 samples, error bars are shown as SEM. Significance was calculated using the unpaired t-test, with **, $p \leq 0.01$; ***, $p \leq 0.001$; ****, $p \leq 0.0001$; *n.s.* not significant.

g, h Biochemical validation of the expression of titrated (**g**) vs. non-titrated (**h**) adapters. Plasmids encoding adapter proteins (all tagged with CTEV-2HA) were transiently transfected into PC12 cells, allowed to express for 16 h, and lysed. Lysates were subjected to Western blotting using the indicated antibodies. Note that PIK3R1 is very low expressed in (**g**), whereas GRB2 is strongly expressed in (**h**). SH2(PIK3R1) is below detection limit in (**h**). Calculated sizes of fusion proteins are provided in Table S1.

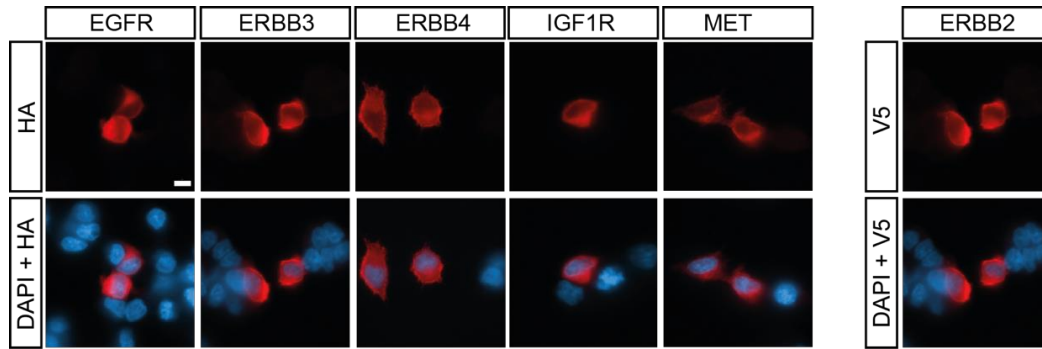


Fig. S6. RTK split TEV fusions are expressed at the cell membrane in PC12 cells.

RTK fusions are expressed at the cell membrane. Plasmids encoding EGFR, ERBB3, ERBB4, IGF1R, and MET (all tagged with NTEV-tcs-GV-2HA), ERBB2-V5, and adapter proteins (all tagged with CTEV-2HA) were transiently transfected into PC12 cells and fixed 20 h later for immunocytochemistry stainings. Receptor expression is displayed for EGFR-, ERBB3-, ERBB4-, IGF1R-, and MET-NTEV-tcs-GV-2HA (red, HA staining) as well as for ERBB2-V5 (red, V5 staining). Nuclei are displayed in blue (Dapi staining). Scale bar represents 5 μ M.

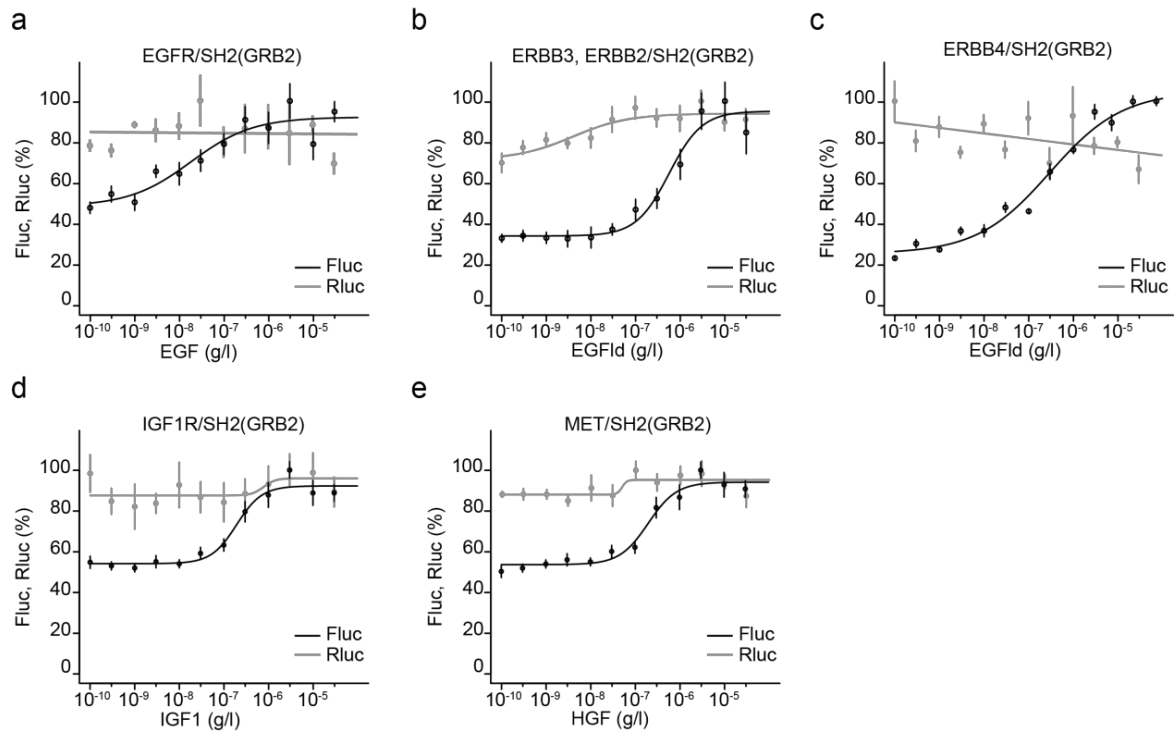


Fig. S7. Constitutive *Renilla* luciferase readout is stable at increasing ligand concentrations.

Split TEV recruitment assays monitoring the activity of EGFR (a), ERBB2/ERBB3 (b), ERBB4 (c), IGF1R (d), and MET (e). Each receptor fusion (NTEV-tcs-GV tag for EGFR, ERBB3, ERBB4, IGF1R, and MET; V5-tagged ERBB2) plasmid is co-transfected with the universal SH2(GRB2) CTEV adapter plasmid into PC12 cells. Depicted are dose-response curves, with agonists applied at increasing concentrations as indicated (EGF, EGFlid, IGF1, HGF). Firefly luciferase is shown in black (as in Fig. 4), the constitutive *Renilla* luciferase signal is shown in grey. Error bars are shown as SEM, with 6 replicates per condition.

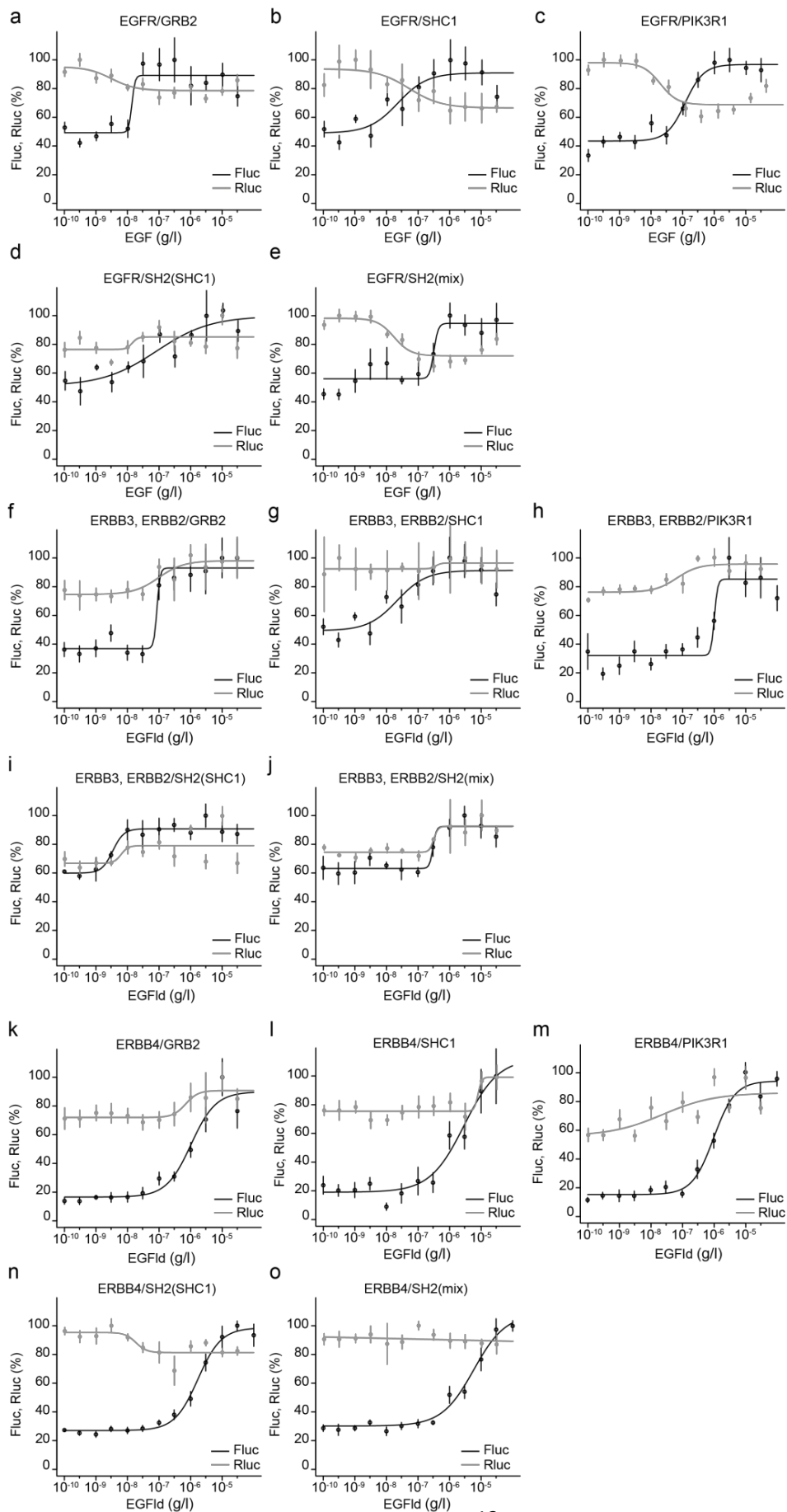


Fig. S8. Agonist dose–response data of split TEV recruitment assays for EGFR, ERBB2/ERBB3, and ERBB4 using full length and concatenated SH2 domain adapters.

EGFR (**a–e**), ERBB2/ERBB3 (**f–j**) and ERBB4 (**k–o**) split TEV recruitment assays were performed as dose–response assays in PC12 cells using full-length adapters of GRB2 (**a, f, k**), SHC1 (**b, g, l**), PIK3R1 (**c, h, m**), as well as SH2 domain adapters SH2(SHC1) (**d, i, n**) and SH2(mix) (**e, j, o**). Agonists EGF and EGF-like domain (EGF_{ld}) were applied at increasing concentrations as indicated. For each assay, plasmids encoding a receptor and an adapter, were co-transfected with a 10xUAS-minCMVp-driven firefly luciferase (Fluc) reporter plasmid shown in black and the constitutive *Renilla* luciferase is shown in grey, as follows:

- (a) EGFR-NTEV-tcs-GV, GRB2-CTEV
- (b) EGFR-NTEV-tcs-GV, SHC1-CTEV
- (c) EGFR-NTEV-tcs-GV, PIK3R1-CTEV
- (d) EGFR-NTEV-tcs-GV, SH2(SHC1)-CTEV
- (e) EGFR-NTEV-tcs-GV, SH2(mix)-CTEV
- (f) ERBB3-NTEV-tcs-GV, ERBB2, GRB2-CTEV
- (g) ERBB3-NTEV-tcs-GV, ERBB2, SHC1-CTEV
- (h) ERBB3-NTEV-tcs-GV, ERBB2, PIK3R1-CTEV
- (i) ERBB3-NTEV-tcs-GV, ERBB2, SH2(SHC1)-CTEV
- (j) ERBB3-NTEV-tcs-GV, ERBB2, SH2(mix)-CTEV
- (k) ERBB4-NTEV-tcs-GV, GRB2-CTEV
- (l) ERBB4-NTEV-tcs-GV, SHC1-CTEV
- (m) ERBB4-NTEV-tcs-GV, PIK3R1-CTEV
- (n) ERBB4-NTEV-tcs-GV, SH2(SHC1)-CTEV
- (o) ERBB4-NTEV-tcs-GV, SH2(mix)-CTEV

Error bars represent SEM, with 6 replicates per condition.

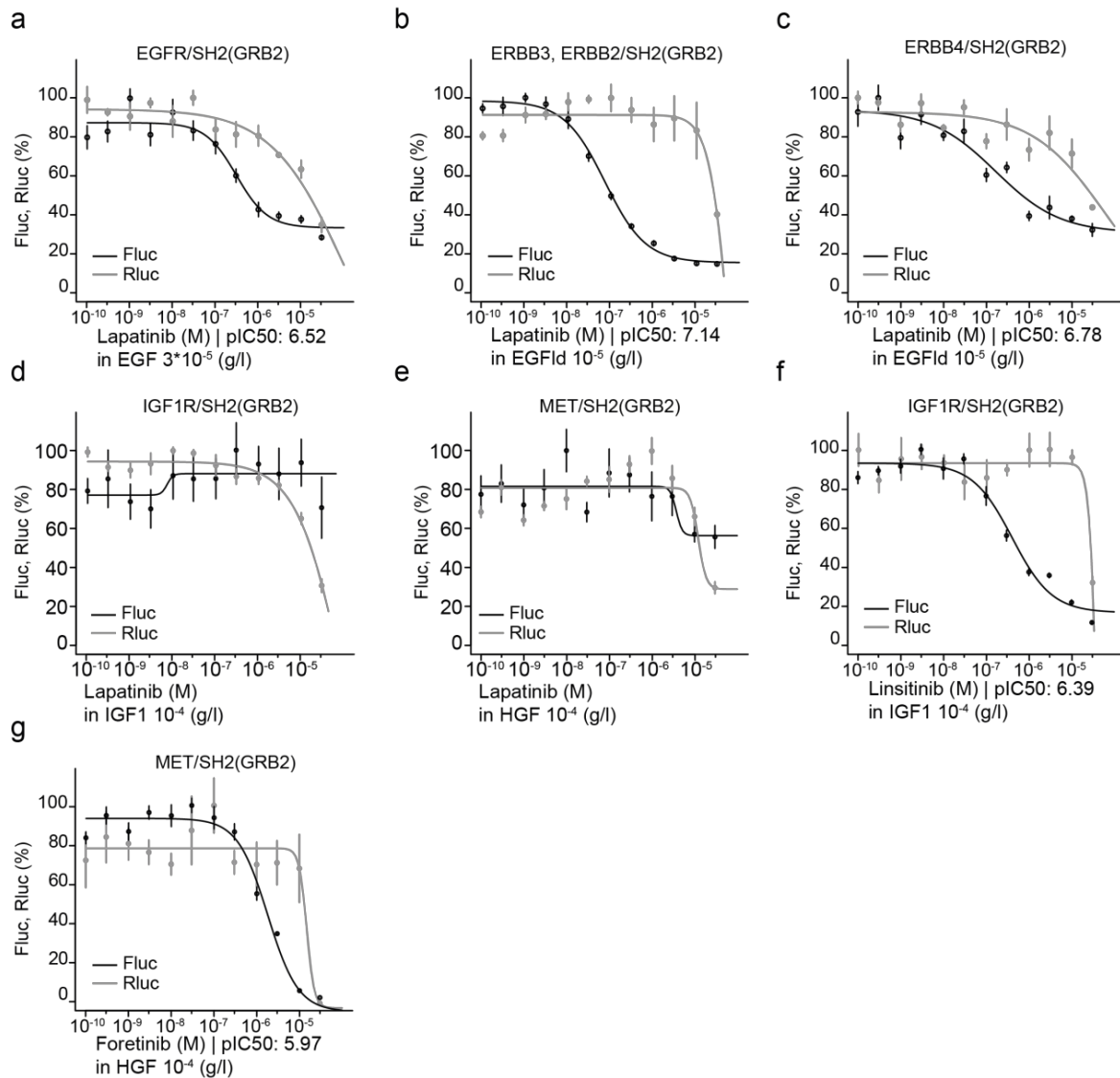


Fig. S9. Antagonists lapatinib, linsitinib and foretinib inhibit their cognate RTK targets.

a–d Split TEV recruitment assays monitoring the lapatinib-mediated inhibition of EGFR (**a**), ERBB2/ERBB3 (**b**), and ERBB4 (**c**), but not IGF1R (**d**) nor MET (**e**). **f, g** Linsitinib-mediated inhibition of IGF1R (**d**), and foretinib-mediated inhibition of MET (**e**). Each receptor fusion (NTEV-tcs-GV tag for EGFR, ERBB3, ERBB4, IGF1R, and MET; V5-tagged ERBB2) plasmid is co-transfected with the universal SH2(GRB2)-CTEV adapter plasmid into PC12 cells as indicated. Depicted are dose–response curves with a constant agonist (EGF, EGFld, IGF1, HGF) and increasing concentrations of lapatinib (**a–d**), linsitinib (**e**) and foretinib (**g**). Firefly luciferase is shown in black (as in Fig. 5), the constitutive *Renilla* luciferase is shown in grey. Note that the constitutive *Renilla* luciferase readout indicates toxicity of lapatinib, linsitinib, and foretinib at 30 μ M. Error bars are shown as SEM, with 6 replicates per condition.

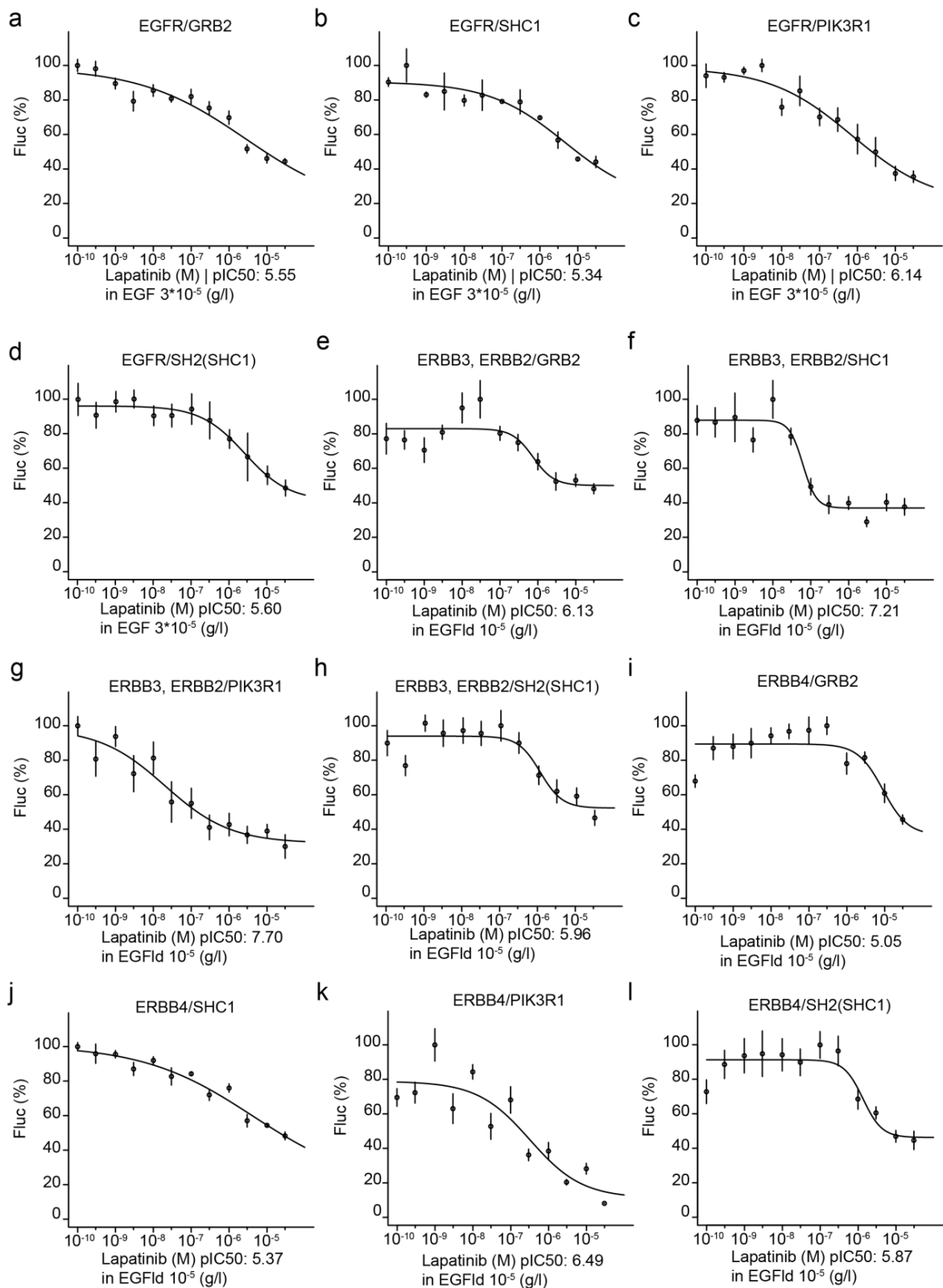


Fig. S10. Dose–response data of ERBB family split TEV recruitment assays using full length and concatenated SH2 domain adapters testing lapatinib inhibition.

EGFR (**a–d**), ERBB2/ERBB3 (**e–h**) and ERBB4 (**i–l**) split TEV recruitment assays were performed as dose–response assays in PC12 cells using full-length adapters of GRB2 (**a, e, i**), SHC1 (**b, f, j**), PIK3R1 (**c, g, k**), and the SH2 domain adapter SH2(SHC1) (**d, h, l**). The ERBB family antagonist lapatinib was applied at increasing concentrations as indicated. Agonists EGF and EGF-like domain (EGF_{ld}) were applied at constant concentrations as indicated. For each assay, plasmids encoding a receptor and an adapter, were co-transfected with a 10xUAS-minCMVp-driven firefly luciferase (Fluc) reporter plasmid, as follows:

- (a) EGFR-NTEV-tcs-GV, GRB2-CTEV
- (b) EGFR-NTEV-tcs-GV, SHC1-CTEV
- (c) EGFR-NTEV-tcs-GV, PIK3R1-CTEV
- (d) EGFR-NTEV-tcs-GV, SH2(SHC1)-CTEV
- (e) ERBB3-NTEV-tcs-GV, ERBB2, GRB2-CTEV
- (f) ERBB3-NTEV-tcs-GV, ERBB2, SHC1-CTEV
- (g) ERBB3-NTEV-tcs-GV, ERBB2, PIK3R1-CTEV
- (h) ERBB3-NTEV-tcs-GV, ERBB2, SH2(SHC1)-CTEV
- (i) ERBB4-NTEV-tcs-GV, GRB2-CTEV
- (j) ERBB4-NTEV-tcs-GV, SHC1-CTEV
- (k) ERBB4-NTEV-tcs-GV, PIK3R1-CTEV
- (l) ERBB4-NTEV-tcs-GV, SH2(SHC1)-CTEV

Error bars represent SEM, with 6 replicates per condition.

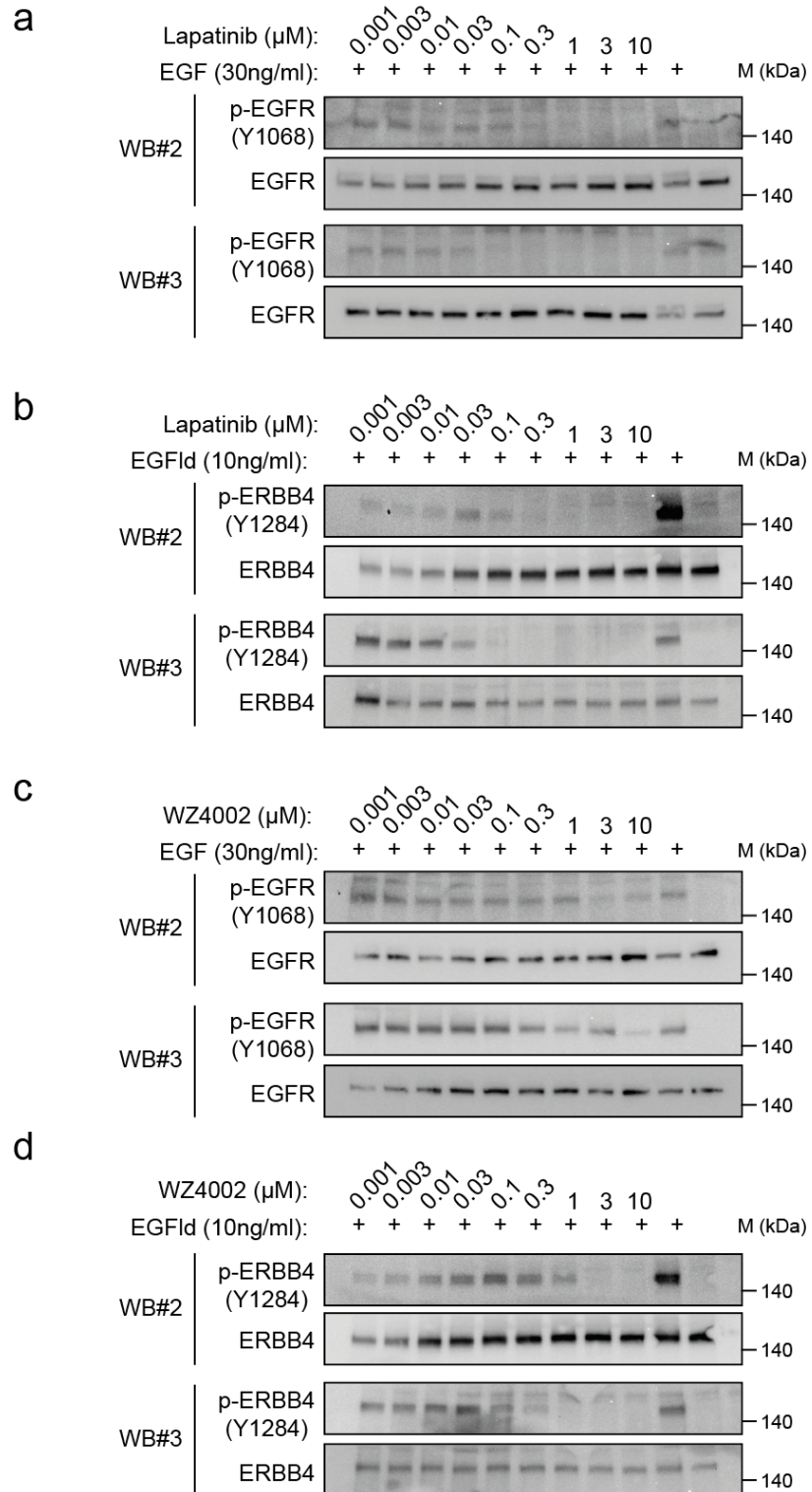


Fig. S11. Lapatinib and WZ4002 reduce p-EGFR (Y1068) and p-ERBB4 (Y1284) levels in A549 cells and T-47D cells.

Starved cells were treated for 1 h with increasing concentrations of lapatinib (**a, b**) or WZ4002 (**c, d**) and stimulated for 5 mins with 30 ng/ml EGF (**a, c**) or 10 ng/ml EGFId (**b, d**) where indicated. Lysates were subjected to Western blotting and probed with indicated antibodies.

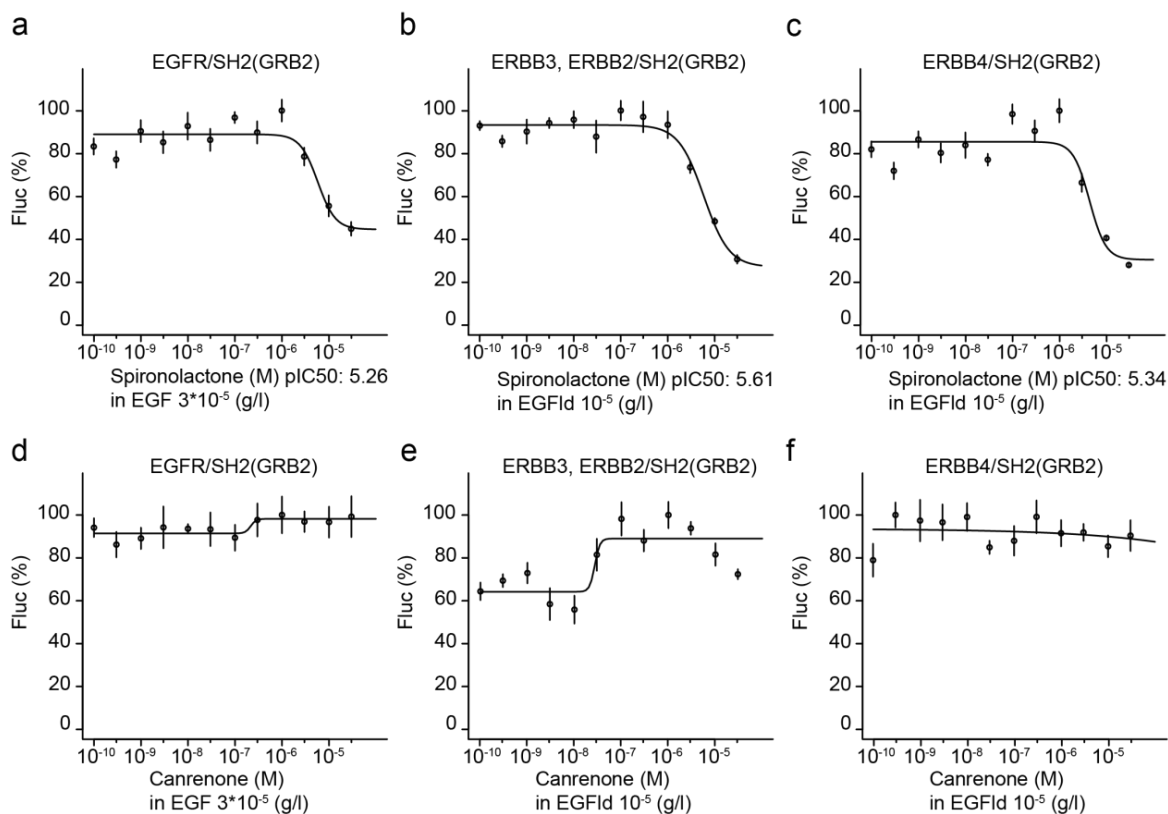


Fig. S12. Spironolactone inhibits ERBB receptor activities using the universal SH2 domain adapter in the split TEV recruitment assay.

Antagonist dose–response split TEV recruitment assays using spironolactone (**a–c**) and canrenone (**d–f**), which were both applied at increasing concentrations as indicated. EGFR (**a, d**), ERBB2/ERBB3 (**b, e**), and ERBB4 (**c, f**) split TEV recruitment assays were performed in PC12 cells using the SH2 domain adapter SH2(GRB2). Agonists EGF and EGF-like domain (EGFlid) were applied at constant concentrations as indicated. For each assay, plasmids encoding a receptor and an adapter, were co-transfected with a 10xUAS-minCMVp-driven firefly luciferase (Fluc) reporter plasmid, as follows:

- (a) EGFR-NTEV-tcs-GV, SH2(GRB2)-CTEV
- (b) ERBB3-NTEV-tcs-GV, ERBB2, SH2(GRB2)-CTEV
- (c) ERBB4-NTEV-tcs-GV, SH2(GRB2)-CTEV
- (d) EGFR-NTEV-tcs-GV, SH2(GRB2)-CTEV
- (e) ERBB3-NTEV-tcs-GV, ERBB2, SH2(GRB2)-CTEV
- (f) ERBB4-NTEV-tcs-GV, SH2(GRB2)-CTEV

Error bars represent SEM, with 6 replicates per condition.

Supplementary Tables

Table S1. Calculation of p-values using an unpaired t-test for assay data shown in Fig. 2.

Receptor-NTEV-tcs-GV Adapter-CTEV	EGFR	ERBB2/ ERBB3	ERBB4	IGF1R	MET
Control	0.4756	0.1443	0.9645	0.790	0.3153
GRB2	0.0137	<0.0001	<0.0001	0.0016	0.0002
SHC1	0.0005	0.0003	0.0006	0.0004	0.0406
PIK3R1	0.0032	<0.0001	0.0064	<0.0001	0.0017
SH2(GRB2)	<0.0001	<0.0001	<0.0001	<0.0001	0.0004
SH2(SHC1)	0.0390	0.0048	0.0182	0.0716	0.0009
SH2(PIK3R1)	0.1228	0.0207	0.1822	0.0042	0.0897
SH2(mix)	0.0079	0.0088	0.7840	0.0224	0.8422

The unpaired t-test was run using GraphPad Prism (version 5).

Table S2. Calculated sizes of fusion proteins.

Fusion protein	Size (kDa)
EGFR-NTEV-tcs-GV-2HA	187.4
ERBB2-V5	141.2
ERRB3-NTEV-tcs-GV-2HA	201.3
ERBB4-NTEV-tcs-GV-2HA	200.1
IGF1R-NTEV-tcs-GV-2HA	208
MET-NTEV-tcs-GV-2HA	210.9
SHC1-CTEV-2HA	67.4
PIK3R1-CTEV-2HA	99.3
GRB2-CTEV-2HA	40.9
SH2(GRB2)-CTEV-2HA	49.9
SH2(SHC1)-CTEV-2HA	48.4
SH2(PIK3R1)-CTEV-2HA	50.3
SH2(mix)-CTEV-2HA	49.5

Receptors were fused to NTEV-tcs-GV-2HA, adapters to CTEV-2HA.

kDa kilodaltons

Table S3. IC₅₀ and pIC₅₀ values for lapatinib obtained from dose–response split TEV recruitment assays as indicated.

Receptor-NTEV-tcs-GV Adapter-CTEV	EGFR		ERBB2/ERBB3		ERBB4	
	IC ₅₀ [μM]	pIC ₅₀	IC ₅₀ [μM]	pIC ₅₀	IC ₅₀ [μM]	pIC ₅₀
GRB2	2.791	5.55	0.747	6.13	9,005	5.05
SHC1	4.561	5.34	0.062	7.21	4.275	5.37
PIK3R1	0.730	6.14	0.020	7.70	0.321	6.49
SH2(GRB2)	0.305	6.52	0.072	7.14	0.166	6.78
SH2(SHC1)	2.511	5.60	1.091	5.96	1.356	5.87

Perspective and discussion

In the first publication, we developed an assay system to monitor ERBB4 activity relevant for NRG1-ERBB4 signaling, which is implicated in SZ. In a drug repurposing screening approach, spironolactone was identified as ERBB4 antagonist. Its efficacy to reduce ERBB4 activity was validated biochemically by means of phosphorylation in heterologous human cells and in transgenic mice *in vivo*. Functionally, spironolactone's antagonistic effect was validated using electrophysiology. The study provides a proof of principle for targeting the NRG1-ERBB4 pathway and using a drug repurposing screen, a strongly demanded strategy for drug development in psychiatric diseases (Insel, 2012). Currently, spironolactone is evaluated in a clinical trial as a novel treatment option for patients with schizophrenia mainly targeting the cognitive alterations (Hasan et al., 2020).

In the second publication, we developed a universal RTK adapter for the cell based split TEV assay. The new adapter consists of three concatenated SH2 domains from GRB2 termed SH2(GRB2), a well-characterized RTK adapter protein. The SH2(GRB2) showed a higher signal-to-noise ratio and performed best in dose response assays using agonists and antagonists. Dose response assays, especially when cell-based, are important to validate the concentration needed for a drug to be effective. The potency of an antagonist is mostly shown as inhibitory concentration of 50% (IC_{50}), the resembling the concentration of a compound where it inhibits 50% of the stimulated signal. The agonist counterpart is called excitatory concentration 50% (EC_{50}).

When different targets are monitored the selectivity of a tested drug can be compared using the IC_{50} and IC_{80} values. During drug development, efficacy, selectivity, and safety reasons are major objectives for drug discovery campaigns. Within a cell the drug has a variety of potential interaction partners, with unintended interactions leading to undesired and effects of the compound (Huggins et al., 2012). The selectivity a drug shows towards its intended target compared to related and non-related targets contributes to its efficacy. Cell-based assay with a baseline reporter control can be used as a toxicity screen within an assay, giving additional information about the cell viability when a certain compound concentration is present. In cell-

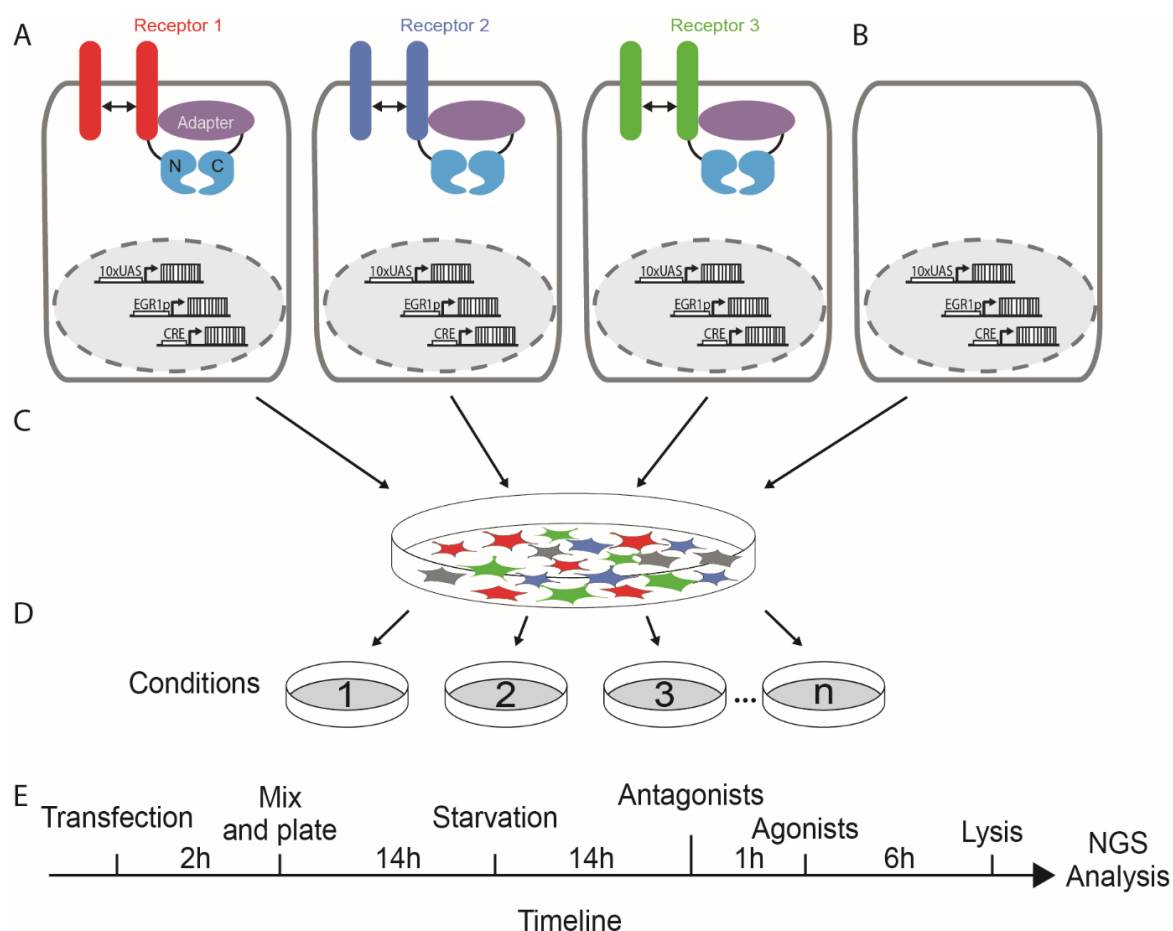
based multiplexed profiling assays efficacy, selectivity and toxicity can therefore be addressed within one assay.

Multiplexed assays for profiling receptor activities and physiological signaling

To test the selectivity of ERBB4 antagonists on other members of the ERBB receptor family, the split TEV assay was newly designed to use the same universal adapter for all ERBB receptor assays. However, instead of using a luciferase read-out, a molecular barcode as an RNA reporter that is transcribed upon GV binding was introduced. (Fig. T5). This made it possible to measure multiple receptor activities in parallel, making the result more comparable and vastly reducing the number of samples used, as multiple assays are combined within one well. Additionally, related (e.g. the ERBB family) and non-related (e.g. HTR2A) receptors can be tested in one measurement, comparing selectivity between various potential targets within the cell.

In more detail, individual cell populations were transfected with one receptor (NTEV) construct, the SH2(GRB2) CTEV construct, and three barcode reporters, which therefore indicate the activity of one given receptor. For each receptor one cell population was transfected using a different set of barcodes (Fig. T5 A). Furthermore, one cell population was transfected with a set of reporters only to control for cell viability and other effects that the experiment conditions might have on barcode reporter expression (Fig. T5 B). Additionally, all cell populations were transfected with pathway sensors encoding an early growth response protein 1 promoter (EGR1p) and the cAMP response element (CRE), both linked to unique barcode reporters. These pathway sensors respond to altered mitogen-activated protein kinase (MAPK) (EGR1p sensor) and cAMP/calcium signaling (CRE sensor) and were described in more detail in (Herholt et al., 2018). The transfected cell populations are mixed and plated (Fig. T5 C), testing conditions are thus applied to all cell populations at once, reducing sample numbers and increasing the amount of data obtained from one sample (Fig. T5 D). The activity of each receptor and relevant physiological cellular signaling is measured simultaneously and therefore allows for assessing compound selectivity and potential detrimental cellular effects, including toxicity. Figure T5 E shows the timeline of a typical profiling experiment, starting with individual transfections similar to the transfection in (Wintgens et al., 2019) per receptor, cell populations are subsequently mixed and plated together. Cells are allowed to attach to the plate over night for about 14 hours and are then starved (2%FCS instead of 10% in the

maintenance medium) for another 14 hours. After the starvation phase antagonists are added as a pretreatment, followed by the agonists one hour later. Finally, the cells are lysed, the RNA



is purified, and then subjected by next generation sequencing. Barcode frequency is then bioinformatically analyzed and graphically visualized.

Figure T5: Schematic overview of the profiler experiment. (A) Individual cell populations are transfected with a receptor (NTEV), an adapter (CTEV), 10xUAS barcode reporters, and the pathway sensors EGR1p and CRE. (B) 10xUAS barcode reporters and pathway sensor are transfected only to serve as cell population control. (C) Mix and plate approach for multiplexing: individual cell populations with one receptor each are mixed, plated into wells, and treated under defined conditions (D). (E) Timeline of a profiler experiment.

Agonist treatment of the ERBB family and HTR2A

Receptor activation was tested in PC12 cells by applying the ERBB agonists EGF (specific for EGFR) and EGF-like domain (EGFId, specific for ERBB3 and ERBB4) as well as the HTR2A agonist serotonin within a concentration range of 0.1 pM to 30 nM (Fig. T6) to the transfected receptors EGFR, ERBB3 (co-transfected with ERBB2 for heterodimer formation), ERBB4, and HTR2A. As described, the pathway sensors ERG1p and CRE were also transfected into each cell

population. The panel is completed by the 10xUAS only control for monitoring cell viability and for normalizing barcode expression among individual wells. (Fig. T5B). When EGF was applied to the cells in this multiparametric assay, only the EGFR is activated (Fig. T6). Conversely, when the cells were treated with EGFd, ERBB3 and ERBB4 was activated, but EGFR was not. The results of individual dose response assays using molecular barcode reporters are consistent with the data obtained with luciferase assays shown in my previous work (Wintgens et al., 2019). For both EGF and EGFd treatments, the EGR1p sensor is activated, which is also consistent with the literature, as all ERBB receptors are known to activate the MAPK pathway (Nakakuki et al., 2008). As expected, neither the HTR2A receptor nor the CRE sensor responded to EGF or EGFd treatment. However, when the cells were stimulated with serotonin only CRE and HTR2A responded. The non-responsive control 10xUAS verified that the activities monitored in this multiplex assay are due to specific activation of targets (i.e. receptors) and pathways. In conclusion, the multiplexed assay setup presented allows that multiple receptor activities and downstream physiological signaling can be simultaneously monitored at dose response. Notably, I did not observe any cross activation of receptors by non-cognate stimuli, nor any side effects at the level of pathway sensors.

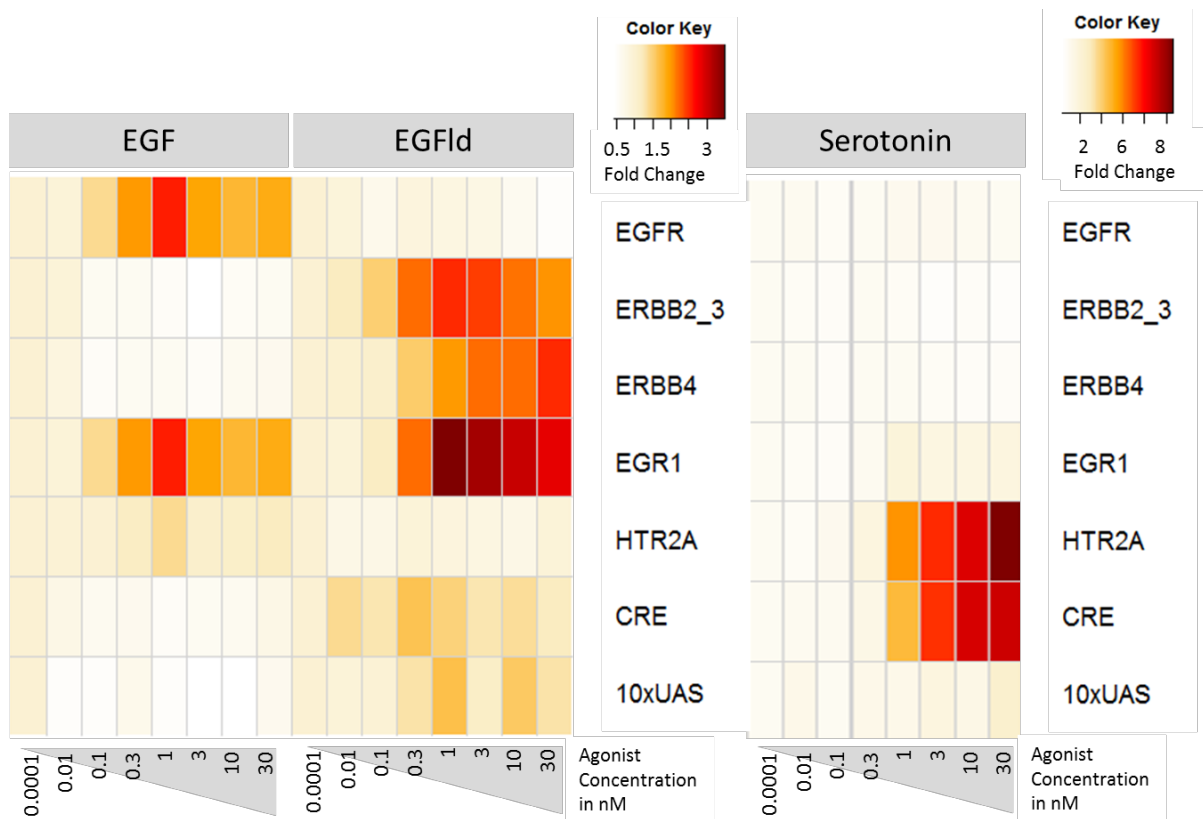


Figure T6: Profiles of agonist induced receptor activities obtained from multiplexed assays. Heatmaps of barcoded assays monitoring receptor and pathway sensor activities. PC12 cells were stimulated for 6h with EGF, EGFlid, and serotonin in a concentration range of 0.1pM to 30nM respectively. Plotted are fold changes referenced to a non-stimulated condition. Note that both heatmaps are based on data from one experiment. The heatmaps were split to better indicate the different fold changes for serotonin vs. EGF and EGFlid treatments.

Antagonist treatment of the ERBB family and HTR2A

Next, the multiplexed receptor profiler was tested with known antagonists to demonstrate the feasibility of the approach. To do this, PC12 cells were transfected with the described receptor and pathways sensor panel. Cells were then treated with increasing concentrations from 0.1 pM to 30 nM of lapatinib, afatinib, WZ4002, erlotinib, AG1478, and gefitinib, all known inhibitors of the ERBB receptor family. After 1 hour of antagonist pretreatment, cells were stimulated using a mixed stimulation of 30 ng/mL EGF, 10 ng/mL EGFlid, and 0.7 μ M serotonin (Fig. T7). The results for lapatinib and WZ4002 are highly consistent with previously obtained data from standard luciferase assays (Wintgens et al., 2019). In general, all ERBB receptors respond to the treatment, while, as expected, the HTR2A receptor was not inhibited by any of the ERBB antagonists. Afatinib, the only covalently binding antagonist, showed an inhibition already at very low concentrations, but induces toxicity at higher concentrations from 3nM and over, a finding that can be seen in the 10xUAS control panel. Thus, suggestive inhibition by afatinib at higher concentrations is linked to cellular toxicity rather than reduced receptor activity. Most inhibitors tested in this multiparametric assay system showed selectivity for ERBB3 or ERBB4. Thus, it was important to test whether the readout of this assay system is not biased towards these two receptors but can also reliably indicate a compound's selectivity for EGFR. Therefore, we included AG1478, which was previously reported to be an EGFR selective antagonist (Levitzki and Gazit, 1995), a result that we were able to reproduce here.

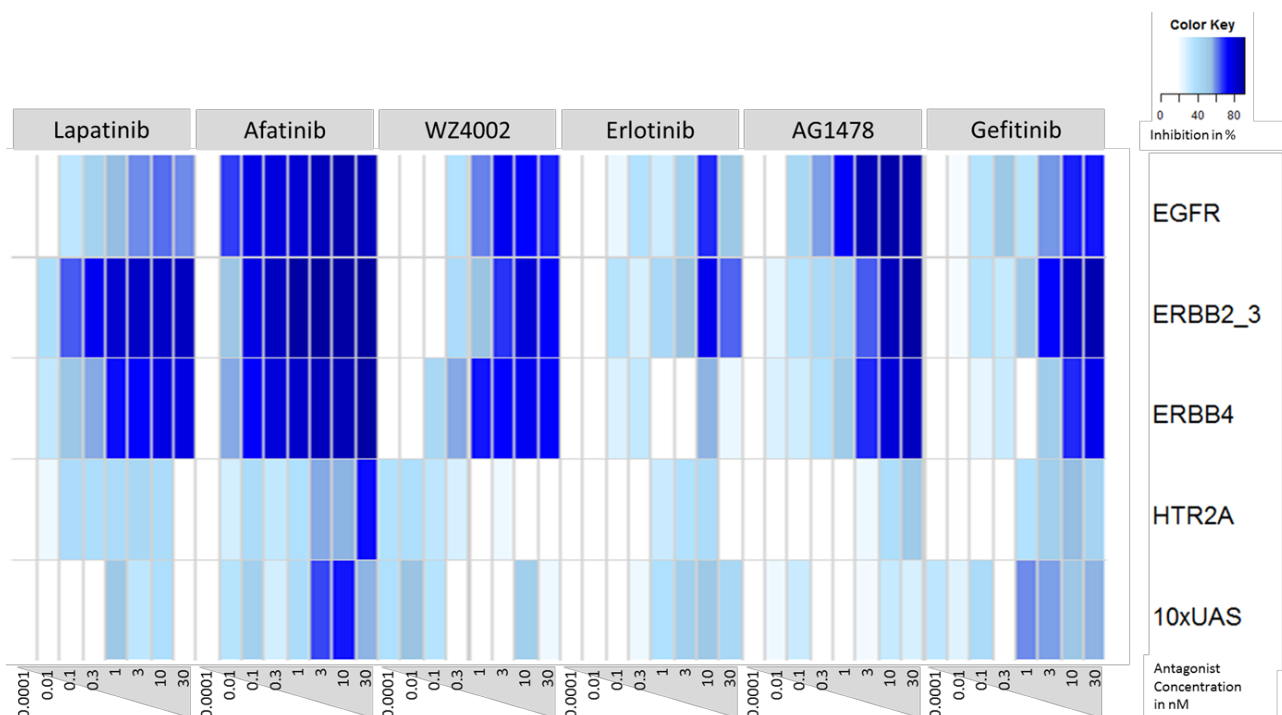


Figure T7: Profiles of antagonist induced receptor activities obtained from multiplexed assays. Heatmaps of multiplexed barcode-based measurement of receptor activity stimulated with EGF (30ng/mL), EGFlid (10ng/mL), and serotonin (0.7 μ M). ERBB family antagonists lapatinib, afatinib, WZ4002, erlotinib, AG1478, and gefitinib were applied in increasing concentrations from 0.1pM to 30nM. The inhibition of receptors is shown in percent referenced to fully stimulated samples.

Extracted from the previous data set of ERBB antagonists, the results of lapatinib and AG1478 mediated inhibition are shown as dose response curves to clearly display the selectivity (Fig. T8). Lapatinib is selective for ERBB3 and ERBB4, with a 5-fold selectivity over EGFR. The inhibition varies for lower concentrations and in the total reduction of activity. AG1478, however, inhibits EGFR with an IC_{50} value of 0.122 μ M, while ERBB3 and ERBB4 show 122-fold and 80-fold higher IC_{50} , supporting the notion that AG1478 is selective for EGFR.

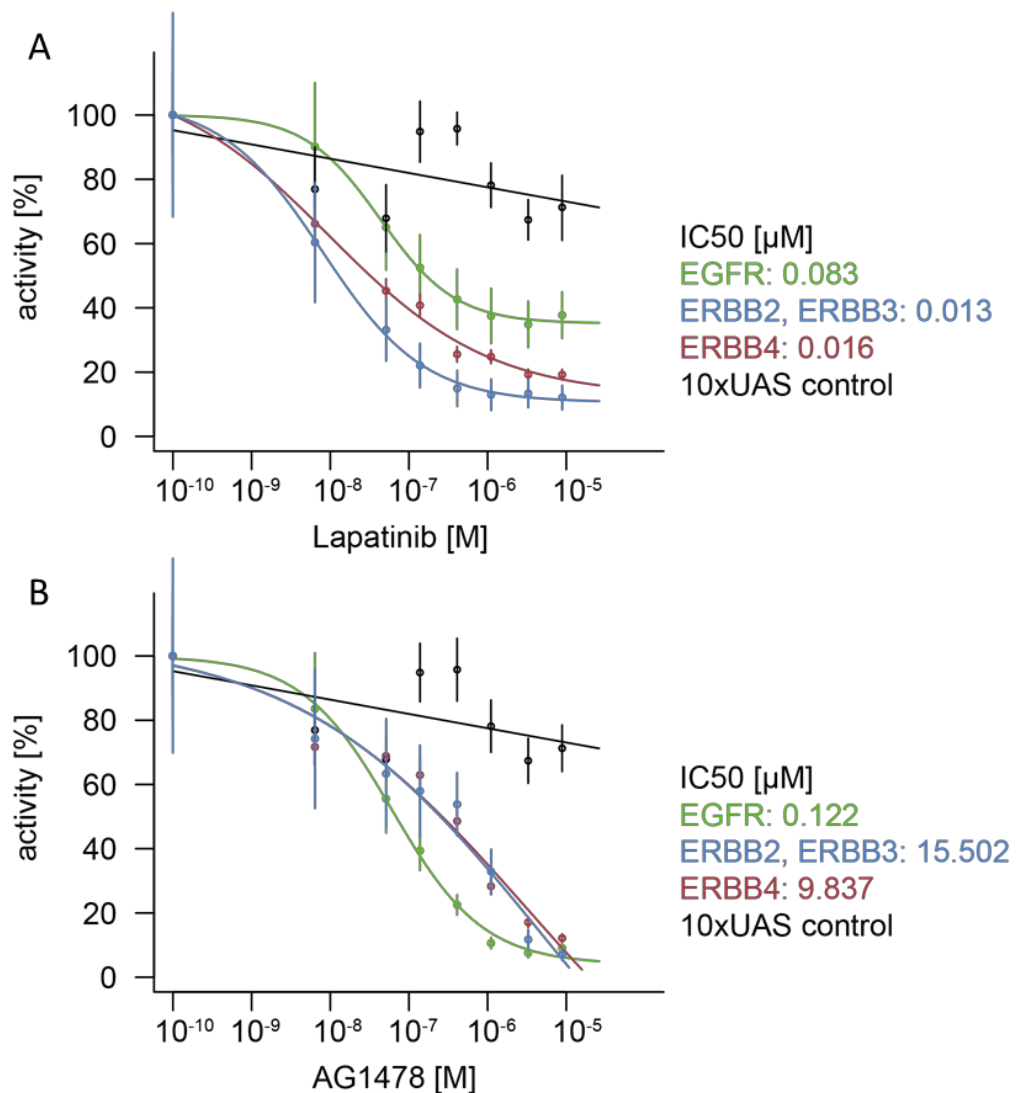


Figure T8: Barcoded reporter assays using split TEV for a dose response analysis of lapatinib (A) and AG1478 (B) using a constant stimulus mix EGF (30ng/mL), EGfId (10ng/mL), and serotonin (0.7μM). Data for EGFR are plotted in green, for ERBB2 and ERBB3 in blue, and ERBB4 in red. Dose response curves were calculated using the R script published in (Wintgens et al., 2019). Error bars are shown as SEM, with six replicates per condition.

Pathway sensor responses to antagonist treatments

The pathway sensors monitor the physiological signaling of the cell by means of transcription factor activities that represent endpoint of cellular signaling cascades. In detail, MAPK pathway and cAMP signaling pathway activities are assessed by the EGR1p sensor and the CRE sensor, respectively (Fig. T9). Inhibition of ERBB family receptor leads to a reduced MAPK signaling, which is in line with the data for all antagonists applied. Again, afatinib showed a

reduction in the signal already at low concentrations, consistent with the results obtained for monitoring receptor activity (Fig. T7). As all samples were also treated with 0.7 μ M serotonin that was present in the stimulation mix, the CRE sensor was activated to baseline levels. Notably, the signal was further increased by adding ERBB3 and ERBB4 selective inhibitors. However, EGFR selective AG1478 did not increase the signal of the CRE sensor further.

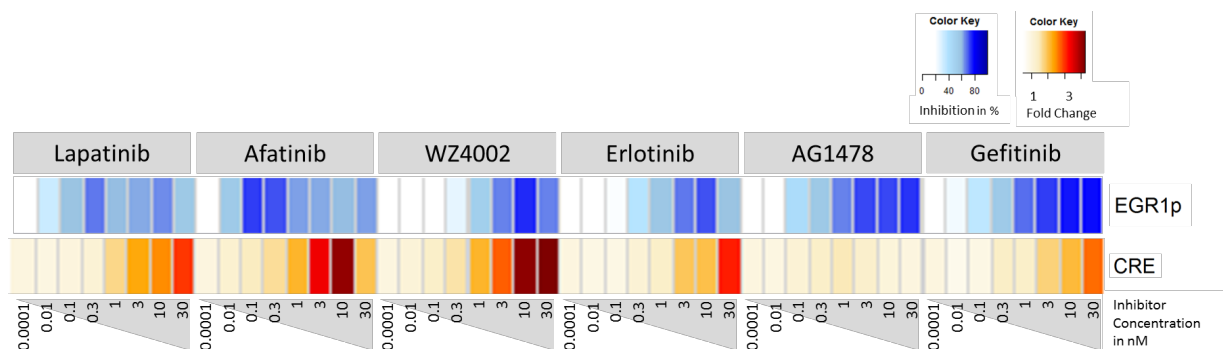


Figure T9: Heatmap of pathway responses of EGR1p and CRE sensors upon antagonist treatment. Lapatinib, afatinib, WZ4002, erlotinib, AG1478, and gefitinib were applied in increasing concentrations from 0.1pM to 30nM. Inhibition of EGR1p is plotted in blue as percent referenced to EGF (30ng/mL), EGFId (10ng/mL) and serotonin (0.7 μ M) stimulated samples. Activation of CRE is plotted in orange as log₂ transformed fold changes referenced to the same stimulated samples.

Discussion

Using this multiparametric profiler approach it is possible to measure activities of multiple receptors and downstream pathway activities in one experiment by using barcode reporters as a read out. The stimulation was demonstrated to be selective for the respective receptors (Fig. T6). Additionally, the pathway sensors that are either clustered cis elements to monitor cAMP/calcium signaling (CRE sensor) or an enhancer sequence of a MAPK pathway-indicative gene (EGR1p sensor) are activated accordingly. Previously reported inhibition of the ERBB receptor family was reproduced, with selectivity according to literature (Fig. T7) (Davis et al., 2011; Levitzki and Gazit, 1995; Wintgens et al., 2019). The EGR1p sensor showed that the MAPK pathway is downregulated by all ERBB inhibitors. The CRE sensor, however, was upregulated by all antagonists applied, but not by the EGFR selective antagonist AG1478 (Fig. T9). As the CRE sensor is already induced to baseline levels by the 0.7 μ M serotonin that is present in the stimulation mix, which is therefore also present in the reference samples, the detected increase in CRE activity is on top of the initial serotonin induction. As all receptor

transfections contain the same 3 CRE barcode reporters it is not possible to distinguish the signals induced by the various receptors. Therefore, future profiler experiments should be equipped with individual barcodes for each receptor transfected into a cell population. For example, when using three receptors and one control (as depicted in Fig. T5), three barcode reporters each for CRE and EGR1p sensors will be needed for every receptor.

The profiling approach presented here provides several benefits: (I) within one experiment activities of various targets and pathways can be measured in a cell-based assay format. The effects of several ligands and antagonistic compounds can be simultaneously studied in this multiparametric assay approach. The barcoded reporter system produces large data sets from multiple wells, which contrasts the separate measurement for each receptor compound combination in standard luciferase assays. Therefore, the profiler approach may provide an advantage in early drug discovery where compounds have to be screened against multiple targets and in multiple conditions (i.e. varying concentrations). (II) The mix and plate platform described in figure T5 is highly scalable and flexible regarding receptors, pathway reporters, and the ligands used in each experimental setup. Additionally, a unique identifier is part of every primer sequence given to each well to extract the RNA, subsequently the samples can be processed together, reducing workload and costs further. When sequencing, the unique identifier makes it possible to discriminate which barcode was extracted from what well. (III) The system could be further improved with respect to robustness and sensitivity by using cell lines that stably express the equivalent of the shown individual transfected cell populations. Especially, expression levels of targets, e.g. applying closer to endogenous expression levels, could be better controlled by using an inducible and stable cell line system. These stable cell lines then could also be mixed and plated as described. (IV) The profiler may also be performed in primary cells or human disease models derived from human induced pluripotent stem cells. To do this, the components of the assay, i.e. the receptor-NTEV-tcs-GV, adapter-CTEV, and barcoded reporters need to be made available as lentiviruses to guarantee efficient infection of target cells. (V) Many cancer mutations lead to a distorted signaling of certain receptors. To inhibit the signaling of the mutated, but not the still needed non-mutated version of these receptors selectively would lower side-effects of cancer drugs (Arteaga and Engelman, 2014). With our assay this comparison can be done within one measurement, additionally screening the cell viability.

(VI) Physiological signaling of the cell, either regular or altered, can be measured simultaneously when using the pathway sensors described above. The panel of pathway sensors can be expanded, for example to sensors of calcium signaling, proliferation, and immune pathways (Herholt et al., 2018). Additionally, pathway sensors may be assigned through their barcode reporters to single receptors (individual cell populations) to also track cellular pathway signatures induced by each receptor. Finally, the panel of receptors screened is flexible and thus could cover a greater variety of biological targets. Many compound campaigns fail late in the process due to unexpected side effects of the drug impacting important cellular targets. Expanding the profiler to cover a panel of these targets could help discover compounds that are at risk of a late stage drop out (Bowes et al., 2012).

In summary, the flexible and robust profiler technology and the combined acquisition of receptor activity and pathway signatures modulated by compounds may provide a valuable tool to promote early drug discovery. The selectivity, efficacy and toxicity of drug candidates could be pre-assessed before going into the animal model. The approach would therefore be complementing the biochemical, computational approaches, and transcriptomic approaches used in drug discovery to date (Chen et al., 2017; González-Maeso et al., 2003; Subramanian et al., 2017).

Bibliography

Abe, Y., Namba, H., Kato, T., Iwakura, Y., and Nawa, H. (2011). Neuregulin-1 Signals from the Periphery Regulate AMPA Receptor Sensitivity and Expression in GABAergic Interneurons in Developing Neocortex. *J. Neurosci.* *31*, 5699–5709.

Agarwal, A., Zhang, M., Trembak-Duff, I., Unterbarnscheidt, T., Radyushkin, K., Dibaj, P., Martins de Souza, D., Boretius, S., Brzózka, M.M., Steffens, H., et al. (2014). Dysregulated Expression of Neuregulin-1 by Cortical Pyramidal Neurons Disrupts Synaptic Plasticity. *Cell Rep.*

Andrews, G., Sanderson, K., Corry, J., Issakidis, C., and Lapsley, H. (2003). Cost-effectiveness of current and optimal treatment for schizophrenia. *Br. J. Psychiatry* *183*, 427–435.

Arteaga, C.L., and Engelman, J.A. (2014). ERBB Receptors: From Oncogene Discovery to Basic Science to Mechanism-Based Cancer Therapeutics. *Cancer Cell* *25*, 282–303.

Badowska, D. (2015). Schizophrenia risk factor Tcf4 and gene-environment interaction in mice. *Gött. Niedersächsische Staats- Univ. Gött.*

Balu, D.T., and Coyle, J.T. (2011). Neuroplasticity signaling pathways linked to the pathophysiology of schizophrenia. *Neurosci. Biobehav. Rev.* *35*, 848–870.

Bayer, T.A., Falkai, P., and Maier, W. (1999). Genetic and non-genetic vulnerability factors in schizophrenia: the basis of the “two hit hypothesis.” *J. Psychiatr. Res.* *33*, 543–548.

Bowes, J., Brown, A.J., Hamon, J., Jarolimek, W., Sridhar, A., Waldron, G., and Whitebread, S. (2012). Reducing safety-related drug attrition: the use of in vitro pharmacological profiling. *Nat. Rev. Drug Discov.* *11*, 909–922.

Britsch, S. (2007). *The Neuregulin-I/ErbB signaling system in development and disease* (Berlin: Springer).

Brzózka, M.M., Radyushkin, K., Wichert, S.P., Ehrenreich, H., and Rossner, M.J. (2010). Cognitive and sensorimotor gating impairments in transgenic mice overexpressing the schizophrenia susceptibility gene Tcf4 in the brain. *Biol. Psychiatry* *68*, 33–40.

Bugarski-Kirola, D., Blaettler, T., Arango, C., Fleischhacker, W.W., Garibaldi, G., Wang, A., Dixon, M., Bressan, R.A., Nasrallah, H., Lawrie, S., et al. (2017). Bitopertin in Negative Symptoms of Schizophrenia—Results From the Phase III FlashLyte and DayLyte Studies. *Biol. Psychiatry* *82*, 8–16.

Bygrave, A.M., Kilonzo, K., Kullmann, D.M., Bannerman, D.M., and Kätzel, D. (2019). Can N-Methyl-D-Aspartate Receptor Hypofunction in Schizophrenia Be Localized to an Individual Cell Type? *Front. Psychiatry* *10*.

- Cardin, J.A., Carlén, M., Meletis, K., Knoblich, U., Zhang, F., Deisseroth, K., Tsai, L.-H., and Moore, C.I. (2009). Driving fast-spiking cells induces gamma rhythm and controls sensory responses. *Nature* 459, 663–667.
- Carlsson, A., and Lindqvist, M. (1963). Effect of Chlorpromazine or Haloperidol on Formation of 3-Methoxytyramine and Normetanephrine in Mouse Brain. *Acta Pharmacol. Toxicol. (Copenh.)* 20, 140–144.
- Chen, B., Ma, L., Paik, H., Sirota, M., Wei, W., Chua, M.-S., So, S., and Butte, A.J. (2017). Reversal of cancer gene expression correlates with drug efficacy and reveals therapeutic targets. *Nat. Commun.* 8.
- Clark, A. (2013). Whatever next? Predictive brains, situated agents, and the future of cognitive science. *Behav. Brain Sci.* 36, 181–204.
- Coyle, J.T. (2012). NMDA Receptor and Schizophrenia: A Brief History. *Schizophr. Bull.* 38, 920–926.
- Creese, I., Burt, D., and Snyder, S. (1976). Dopamine receptor binding predicts clinical and pharmacological potencies of antischizophrenic drugs. *Science*.pdf.
- Davis, K., Kahn, R., Ko, G., and Davidson, M. (1991). Dopamine in schizophrenia: a review and reconceptualization. *Am. J. Psychiatry* 148, 1474–1486.
- Davis, M.I., Hunt, J.P., Herrgard, S., Ciceri, P., Wodicka, L.M., Pallares, G., Hocker, M., Treiber, D.K., and Zarrinkar, P.P. (2011). Comprehensive analysis of kinase inhibitor selectivity. *Nat. Biotechnol.* 29, 1046–1051.
- Dayan, P., Hinton, G.E., Neal, R.M., and Zemel, R.S. (1995). The Helmholtz Machine. *Neural Comput.* 7, 889–904.
- Deakin, I.H., Law, A.J., Oliver, P.L., Schwab, M.H., Nave, K.A., Harrison, P.J., and Bannerman, D.M. (2009). Behavioural characterization of neuregulin 1 type I overexpressing transgenic mice. *Neuroreport* 20, 1523–1528.
- Deakin, I.H., Nissen, W., Law, A.J., Lane, T., Kanso, R., Schwab, M.H., Nave, K.-A., Lamsa, K.P., Paulsen, O., Bannerman, D.M., et al. (2012). Transgenic Overexpression of the Type I Isoform of Neuregulin 1 Affects Working Memory and Hippocampal Oscillations but not Long-term Potentiation. *Cereb. Cortex* 22, 1520–1529.
- del Pino, I., García-Frigola, C., Dehorter, N., Brotons-Mas, J.R., Alvarez-Salvado, E., Martínez de Lagrán, M., Ciceri, G., Gabaldón, M.V., Moratal, D., Dierssen, M., et al. (2013). *ErbB4* Deletion from Fast-Spiking Interneurons Causes Schizophrenia-like Phenotypes. *Neuron* 79, 1152–1168.
- E. McCullumsmith, R., Hammond, J., Funk, A., and H. Meador-Woodruff, J. (2012). Recent Advances in Targeting the Ionotropic Glutamate Receptors in Treating Schizophrenia. *Curr. Pharm. Biotechnol.* 13, 1535–1542.
- Elert, E. (2014). Aetiology: Searching for schizophrenia’s roots. *Nature* 508, S2–S3.

Fazzari, P., Paternain, A.V., Valiente, M., Pla, R., Lujan, R., Lloyd, K., Lerma, J., Marin, O., and Rico, B. (2010). Control of cortical GABA circuitry development by Nrg1 and ErbB4 signalling. *Nature* 464, 1376–1380.

Flames, N., Long, J.E., Garratt, A.N., Fischer, T.M., Gassmann, M., Birchmeier, C., Lai, C., Rubenstein, J.L.R., and Marín, O. (2004). Short- and long-range attraction of cortical GABAergic interneurons by neuregulin-1. *Neuron* 44, 251–261.

Friston, K., Kilner, J., and Harrison, L. (2006). A free energy principle for the brain. *J. Physiol.-Paris* 100, 70–87.

Friston, K., Brown, H.R., Siemerikus, J., and Stephan, K.E. (2016). The dysconnection hypothesis (2016). *Schizophr. Res.* 176, 83–94.

Funk, A.J., Rumbaugh, G., Harotunian, V., McCullumsmith, R.E., and Meador-Woodruff, J.H. (2009). Decreased expression of NMDA receptor-associated proteins in frontal cortex of elderly patients with schizophrenia: *NeuroReport* 20, 1019–1022.

Gonzalez-Burgos, G., Hashimoto, T., and Lewis, D.A. (2010). Alterations of cortical GABA neurons and network oscillations in schizophrenia. *Curr. Psychiatry Rep.* 12, 335–344.

González-Maeso, J., Yuen, T., Ebersole, B.J., Wurmbach, E., Lira, A., Zhou, M., Weisstaub, N., Hen, R., Gingrich, J.A., and Sealton, S.C. (2003). Transcriptome Fingerprints Distinguish Hallucinogenic and Nonhallucinogenic 5-Hydroxytryptamine 2A Receptor Agonist Effects in Mouse Somatosensory Cortex. *J. Neurosci.* 23, 8836–8843.

Hahn, C.-G., Wang, H.-Y., Cho, D.-S., Talbot, K., Gur, R.E., Berrettini, W.H., Bakshi, K., Kamins, J., Borgmann-Winter, K.E., Siegel, S.J., et al. (2006). Altered neuregulin 1–erbB4 signaling contributes to NMDA receptor hypofunction in schizophrenia. *Nat. Med.* 12, 824–828.

Hammond, J.C., Shan, D., Meador-Woodruff, J.H., and McCullumsmith, R.E. (2014). Evidence of Glutamatergic Dysfunction in the Pathophysiology of Schizophrenia. In *Synaptic Stress and Pathogenesis of Neuropsychiatric Disorders*, M. Popoli, D. Diamond, and G. Sanacora, eds. (New York, NY: Springer New York), pp. 265–294.

Hasan, A., Roeh, A., Leucht, S., Langguth, B., Hansbauer, M., Oviedo-Salcedo, T., Kirchner, S.K., Papazova, I., Löhrs, L., Wagner, E., et al. (2020). Add-on spironolactone as antagonist of the NRG1-ERBB4 signaling pathway for the treatment of schizophrenia: study design and methodology of a multicenter randomized, placebo-controlled trial. *Contemp. Clin. Trials Commun.* 100537.

Hashimoto, R., Straub, R.E., Weickert, C.S., Hyde, T.M., Kleinman, J.E., and Weinberger, D.R. (2004). Expression analysis of neuregulin-1 in the dorsolateral prefrontal cortex in schizophrenia. *Mol. Psychiatry* 9, 299–307.

Hashimoto, T., Nguyen, Q.L., Rotaru, D., Keenan, T., Arion, D., Beneyto, M., Gonzalez-Burgos, G., and Lewis, D.A. (2009). Protracted Developmental Trajectories of GABA_A Receptor α 1 and α 2 Subunit Expression in Primate Prefrontal Cortex. *Biol. Psychiatry* 65, 1015–1023.

He, H., and Cline, H.T. (2019). What Is Excitation/Inhibition and How Is It Regulated? A Case of the Elephant and the Wisemen. *J. Exp. Neurosci.* *13*, 117906951985937.

Helmholtz, H. von (1866). Concerning the perceptions in general.

Hengen, K.B., Lambo, M.E., Van Hooser, S.D., Katz, D.B., and Turrigiano, G.G. (2013). Firing Rate Homeostasis in Visual Cortex of Freely Behaving Rodents. *Neuron* *80*, 335–342.

Herholt, A., Brankatschk, B., Kannaiyan, N., Papiol, S., Wichert, S.P., Wehr, M.C., and Rossner, M.J. (2018). Pathway sensor-based functional genomics screening identifies modulators of neuronal activity. *Sci. Rep.* *8*, 17597.

Horváth, S., and Mirnics, K. (2015). Schizophrenia as a Disorder of Molecular Pathways. *Biol. Psychiatry* *77*, 22–28.

Howes, O.D., and Kapur, S. (2014). A neurobiological hypothesis for the classification of schizophrenia: type a (hyperdopaminergic) and type B (normodopaminergic). *Br. J. Psychiatry* *205*, 1–3.

Huggins, D.J., Sherman, W., and Tidor, B. (2012). Rational Approaches to Improving Selectivity in Drug Design. *J. Med. Chem.* *55*, 1424–1444.

Humphries, C., Mortimer, A., Hirsch, S., and de Bellerocche, J. (1996). NMDA receptor mRNA correlation with antemortem cognitive impairment in schizophrenia_Humphries_1996.pdf.

lascone, D.M., Li, Y., Sümbül, U., Doron, M., Chen, H., Andreu, V., Goudy, F., Segev, I., Peng, H., and Polleux, F. (2018). Whole-neuron synaptic mapping reveals local balance between excitatory and inhibitory synapse organization. *BioRxiv*.

Insel, T.R. (2010). Rethinking schizophrenia. *Nature* *468*, 187–193.

Insel, T.R. (2012). Next-generation treatments for mental disorders. *Sci. Transl. Med.* *4*, 155ps19.

Janssen, M.J., Leiva-Salcedo, E., and Buonanno, A. (2012). Neuregulin Directly Decreases Voltage-Gated Sodium Current in Hippocampal ErbB4-Expressing Interneurons. *J. Neurosci.* *32*, 13889–13895.

Javitt, D.C. (2010). Glutamatergic theories of schizophrenia. *Isr. J. Psychiatry Relat. Sci.* *47*, 4–16.

Kato, T., Kasai, A., Mizuno, M., Fengyi, L., Shintani, N., Maeda, S., Yokoyama, M., Ozaki, M., and Nawa, H. (2010). Phenotypic characterization of transgenic mice overexpressing neuregulin-1. *PloS One* *5*, e14185.

Kenny, E.M., Cormican, P., Furlong, S., Heron, E., Kenny, G., Fahey, C., Kelleher, E., Ennis, S., Tropea, D., Anney, R., et al. (2014). Excess of rare novel loss-of-function variants in synaptic genes in schizophrenia and autism spectrum disorders. *Mol. Psychiatry* *19*, 872–879.

- Kotzadimitriou, D., Nissen, W., Paizs, M., Newton, K., Harrison, P.J., Paulsen, O., and Lamsa, K. (2018). Neuregulin 1 Type I Overexpression Is Associated with Reduced NMDA Receptor-Mediated Synaptic Signaling in Hippocampal Interneurons Expressing PV or CCK. *Eneuro* 5, ENEURO.0418-17.2018.
- Law, A.J., Lipska, B.K., Weickert, C.S., Hyde, T.M., Straub, R.E., Hashimoto, R., Harrison, P.J., Kleinman, J.E., and Weinberger, D.R. (2006). Neuregulin 1 transcripts are differentially expressed in schizophrenia and regulated by 5' SNPs associated with the disease. *Proc. Natl. Acad. Sci. U. S. A.* 103, 6747–6752.
- Lee, T.S., and Mumford, D. (2003). Hierarchical Bayesian inference in the visual cortex. *J. Opt. Soc. Am. A* 20, 1434.
- Lemmon, M.A., and Schlessinger, J. (2010). Cell Signaling by Receptor Tyrosine Kinases. *Cell* 141, 1117–1134.
- Lencz, T., and Malhotra, A.K. (2015). Targeting the schizophrenia genome: a fast track strategy from GWAS to clinic. *Mol. Psychiatry* 20, 820–826.
- Levitzki, A., and Gazit, A. (1995). Tyrosine kinase inhibition: an approach to drug development. *Science* 267, 1782–1788.
- Lewis, D.A., and González-Burgos, G. (2008). Neuroplasticity of Neocortical Circuits in Schizophrenia. *Neuropsychopharmacology* 33, 141–165.
- Li, H., Chou, S.-J., Hamasaki, T., Perez-Garcia, C.G., and O'Leary, D.D. (2012a). Neuregulin repellent signaling via ErbB4 restricts GABAergic interneurons to migratory paths from ganglionic eminence to cortical destinations. *Neural Develop.* 7, 10.
- Li, K.-X., Lu, Y.-M., Xu, Z.-H., Zhang, J., Zhu, J.-M., Zhang, J.-M., Cao, S.-X., Chen, X.-J., Chen, Z., Luo, J.-H., et al. (2012b). Neuregulin 1 regulates excitability of fast-spiking neurons through Kv1.1 and acts in epilepsy. *Nat Neurosci* 15, 267–273.
- Lichtenstein, P., Yip, B.H., Björk, C., Pawitan, Y., Cannon, T.D., Sullivan, P.F., and Hultman, C.M. (2009). Common genetic determinants of schizophrenia and bipolar disorder in Swedish families: a population-based study. *373*, 6.
- Liu, B.A., Jablonowski, K., Raina, M., Arcé, M., Pawson, T., and Nash, P.D. (2006). The Human and Mouse Complement of SH2 Domain Proteins—Establishing the Boundaries of Phosphotyrosine Signaling. *Mol. Cell* 22, 851–868.
- Lundgaard, I., Luzhynskaya, A., Stockley, J.H., Wang, Z., Evans, K.A., Swire, M., Volbracht, K., Gautier, H.O.B., Franklin, R.J.M., French-Constant, C., et al. (2013). Neuregulin and BDNF Induce a Switch to NMDA Receptor-Dependent Myelination by Oligodendrocytes. *PLoS Biol.* 11, e1001743.
- Luo, X., He, W., Hu, X., and Yan, R. (2014). Reversible overexpression of bace1-cleaved neuregulin-1 N-terminal fragment induces schizophrenia-like phenotypes in mice. *Biol. Psychiatry* 76, 120–127.

- Marenco, S., Geramita, M., van der Veen, J.W., Barnett, A.S., Kolachana, B., Shen, J., Weinberger, D.R., and Law, A.J. (2011). Genetic association of ErbB4 and human cortical GABA levels in vivo. *J. Neurosci. Off. J. Soc. Neurosci.* *31*, 11628–11632.
- Margraf, J., and Schneider, S. (2016). From neuroleptics to neuroscience and from Pavlov to psychotherapy: more than just the “emperor’s new treatments” for mental illnesses? *EMBO Mol. Med.* *8*, 1115–1117.
- Maynard, T.M., Sikich, L., Lieberman, J.A., and LaMantia, A.S. (2001). Neural development, cell-cell signaling, and the “two-hit” hypothesis of schizophrenia. *Schizophr. Bull.* *27*, 457–476.
- Mcguire, P., Howes, O., Stone, J., and Fusarpoli, P. (2008). Functional neuroimaging in schizophrenia: diagnosis and drug discovery. *Trends Pharmacol. Sci.* *29*, 91–98.
- Mei, L., and Nave, K.-A. (2014). Neuregulin-ERBB Signaling in the Nervous System and Neuropsychiatric Diseases. *Neuron* *83*, 27–49.
- Meltzer, H.Y., and Stahl, S.M. (1976). the dopamine hypothesis of schizophrenia: a review •[^] M A I # • A I I f A. *Schizophr. Bull.* *2*, 58.
- Miller, D.W., and Abercrombie, E.D. (1996). Effects of MK-801 on spontaneous and amphetamine-stimulated dopamine release in striatum measured with in vivo microdialysis in awake rats. *Brain Res. Bull.* *40*, 57–62.
- Miller, E.K., and Cohen, J.D. (2001). An Integrative Theory of Prefrontal Cortex Function. *Annu. Rev. Neurosci.* *24*, 167–202.
- Monfils, M.-H., and Teskey, G.C. (2004). Induction of long-term depression is associated with decreased dendritic length and spine density in layers III and V of sensorimotor neocortex. *Synapse* *53*, 114–121.
- Nakakuki, T., Yumoto, N., Naka, T., Shirouzu, M., Yokoyama, S., and Hatakeyama, M. (2008). Topological Analysis of MAPK Cascade for Kinetic ErbB Signaling. *PLoS ONE* *3*, e1782.
- Nestler, E.J., and Hyman, S.E. (2010). Animal models of neuropsychiatric disorders. *Nat. Neurosci.* *13*, 1161–1169.
- van Os, J., and Kapur, S. (2009). Schizophrenia. *Lancet* *374*, 635–645.
- Pardiñas, A.F., Holmans, P., Pocklington, A.J., Escott-Price, V., Ripke, S., Carrera, N., Legge, S.E., Bishop, S., Cameron, D., Hamshere, M.L., et al. (2018). Common schizophrenia alleles are enriched in mutation-intolerant genes and in regions under strong background selection. *Nat. Genet.* *50*, 381–389.
- Powell, S.B., Sejnowski, T.J., and Behrens, M.M. (2012). Behavioral and neurochemical consequences of cortical oxidative stress on parvalbumin-interneuron maturation in rodent models of schizophrenia. *Neuropharmacology* *62*, 1322–1331.

- Raabe, F.J., Galinski, S., Papiol, S., Falkai, P.G., Schmitt, A., and Rossner, M.J. (2018). Studying and modulating schizophrenia-associated dysfunctions of oligodendrocytes with patient-specific cell systems. *NPJ Schizophr.* 4.
- Radua, J., Surguladze, S.A., Marshall, N., Walshe, M., Bramon, E., Collier, D.A., Prata, D.P., Murray, R.M., and McDonald, C. (2013). The impact of CACNA1C allelic variation on effective connectivity during emotional processing in bipolar disorder. *Mol. Psychiatry* 18, 526–527.
- Rakic, P., Bourgeois, J., Eckenhoff, M., Zecevic, N., and Goldman-Rakic, P. (1986). Concurrent overproduction of synapses in diverse regions of the primate cerebral cortex. *Science* 232, 232–235.
- Rapoport, J.L., Giedd, J.N., and Gogtay, N. (2012). Neurodevelopmental model of schizophrenia: update 2012. *Mol. Psychiatry* 17, 1228–1238.
- Rauss, K., and Pourtois, G. (2013). What is Bottom-Up and What is Top-Down in Predictive Coding? *Front. Psychol.* 4.
- Rossi, F., Charlton, C.A., and Blau, H.M. (1997). Monitoring protein-protein interactions in intact eukaryotic cells by beta-galactosidase complementation. *Proc. Natl. Acad. Sci. U. S. A.* 94, 8405–8410.
- Saha, S., Chant, D., Welham, J., and McGrath, J. (2005). A systematic review of the prevalence of schizophrenia. *PLoS Med.* 2, e141.
- Santos, R., Ursu, O., Gaulton, A., Bento, A.P., Donadi, R.S., Bologa, C.G., Karlsson, A., Al-Lazikani, B., Hersey, A., Oprea, T.I., et al. (2017). A comprehensive map of molecular drug targets. *Nat. Rev. Drug Discov.* 16, 19–34.
- Schizophrenia Working Group of the Psychiatric Genomics Consortium (2014). Biological insights from 108 schizophrenia-associated genetic loci. *Nature* 511, 421–427.
- Schizophrenia Working Group of the Psychiatric Genomics Consortium, Sekar, A., Bialas, A.R., de Rivera, H., Davis, A., Hammond, T.R., Kamitaki, N., Tooley, K., Presumey, J., Baum, M., et al. (2016). Schizophrenia risk from complex variation of complement component 4. *Nature* 530, 177–183.
- Schmitt, A., Hasan, A., Gruber, O., and Falkai, P. (2011). Schizophrenia as a disorder of disconnectivity. *Eur. Arch. Psychiatry Clin. Neurosci.* 261 Suppl 2, S150-154.
- Schwartz, T.L., Sachdeva, S., and Stahl, S.M. (2012). Glutamate Neurocircuitry: Theoretical Underpinnings in Schizophrenia. *Front. Pharmacol.* 3.
- Seeman, P., and Lee, T. (1975). Antipsychotic drugs direct correlation between clinical potency and presynaptic action on dopamine neurons. *Science.* 1975;.pdf.
- Shaw, P., Lerch, J.P., Pruessner, J.C., Taylor, K.N., Rose, A.B., Greenstein, D., Clasen, L., Evans, A., Rapoport, J.L., and Giedd, J.N. (2007). Cortical morphology in children and adolescents with different apolipoprotein E gene polymorphisms: an observational study. *Lancet Neurol.* 6, 494–500.

- Shew, W.L., Yang, H., Yu, S., Roy, R., and Plenz, D. (2011). Information Capacity and Transmission Are Maximized in Balanced Cortical Networks with Neuronal Avalanches. *J. Neurosci.* *31*, 55–63.
- Sin, W.C., Haas, K., Ruthazer, E.S., and Cline, H.T. (2002). Dendrite growth increased by visual activity requires NMDA receptor and Rho GTPases. *Nature* *419*, 475–480.
- Sohal, V.S., and Rubenstein, J.L.R. (2019). Excitation-inhibition balance as a framework for investigating mechanisms in neuropsychiatric disorders. *Mol. Psychiatry* *24*, 1248–1257.
- Sohal, V.S., Zhang, F., Yizhar, O., and Deisseroth, K. (2009). Parvalbumin neurons and gamma rhythms enhance cortical circuit performance. *Nature* *459*, 698–702.
- Sokolov, B.P. (2002). Expression of NMDAR1, GluR1, GluR7, and KA1 Glutamate Receptor mRNAs Is Decreased in Frontal Cortex of “Neuroleptic-Free” Schizophrenics: Evidence on Reversible Up-Regulation by Typical Neuroleptics. *J. Neurochem.* *71*, 2454–2464.
- Stephan, K.E., Friston, K.J., and Frith, C.D. (2009). Dysconnection in Schizophrenia: From Abnormal Synaptic Plasticity to Failures of Self-monitoring. *Schizophr. Bull.* *35*, 509–527.
- Stone, J.M., Morrison, P.D., and Pilowsky, L.S. (2007). Review: Glutamate and dopamine dysregulation in schizophrenia — a synthesis and selective review. *J. Psychopharmacol. (Oxf.)* *21*, 440–452.
- Subramanian, A., Narayan, R., Corsello, S.M., Peck, D.D., Natoli, T.E., Lu, X., Gould, J., Davis, J.F., Tubelli, A.A., Asiedu, J.K., et al. (2017). A Next Generation Connectivity Map: L1000 Platform and the First 1,000,000 Profiles. *Cell* *171*, 1437-1452.e17.
- Sullivan, P.F., Kendler, K.S., and Neale, M.C. (2003). Schizophrenia as a complex trait: evidence from a meta-analysis of twin studies. *Arch. Gen. Psychiatry* *60*, 1187–1192.
- Tan, G.-H., Liu, Y.-Y., Hu, X.-L., Yin, D.-M., Mei, L., and Xiong, Z.-Q. (2012). Neuregulin 1 represses limbic epileptogenesis through ErbB4 in parvalbumin-expressing interneurons. *Nat Neurosci* *15*, 258–266.
- Ting, A.K., Chen, Y., Wen, L., Yin, D.-M., Shen, C., Tao, Y., Liu, X., Xiong, W.-C., and Mei, L. (2011). Neuregulin 1 promotes excitatory synapse development and function in GABAergic interneurons. *J. Neurosci. Off. J. Soc. Neurosci.* *31*, 15–25.
- Tinti, M., Kiemer, L., Costa, S., Miller, M.L., Sacco, F., Olsen, J.V., Carducci, M., Paoluzi, S., Langone, F., Workman, C.T., et al. (2013). The SH2 domain interaction landscape. *Cell Rep.* *3*, 1293–1305.
- Vullhorst, D., Neddens, J., Karavanova, I., Tricoire, L., Petralia, R.S., McBain, C.J., and Buonanno, A. (2009). Selective Expression of ErbB4 in Interneurons, But Not Pyramidal Cells, of the Rodent Hippocampus. *J. Neurosci.* *29*, 12255–12264.
- Vullhorst, D., Mitchell, R.M., Keating, C., Roychowdhury, S., Karavanova, I., Tao-Cheng, J.-H., and Buonanno, A. (2015). A negative feedback loop controls NMDA receptor function in cortical interneurons via neuregulin 2/ErbB4 signalling. *Nat. Commun.* *6*.

- Vullhorst, D., Ahmad, T., Karavanova, I., Keating, C., and Buonanno, A. (2017). Structural Similarities between Neuregulin 1–3 Isoforms Determine Their Subcellular Distribution and Signaling Mode in Central Neurons. *J. Neurosci.* *37*, 5232–5249.
- Wehr, M.C., and Rossner, M.J. (2016). Split protein biosensor assays in molecular pharmacological studies. *Drug Discov. Today* *21*, 415–429.
- Wehr, M., Reinecke, L., Botvinnik, A., and Rossner, M. (2008). Analysis of transient phosphorylation-dependent protein-protein interactions in living mammalian cells using split-TEV. *BMC Biotechnol.* *8*, 55.
- Wehr, M.C., Laage, R., Bolz, U., Fischer, T.M., Grünewald, S., Scheek, S., Bach, A., Nave, K.-A., and Rossner, M.J. (2006). Monitoring regulated protein-protein interactions using split TEV. *Nat. Methods* *3*, 985–993.
- Weickert, C.S., Tiwari, Y., Schofield, P.R., Mowry, B.J., and Fullerton, J.M. (2012). Schizophrenia-associated HapICE haplotype is associated with increased NRG1 type III expression and high nucleotide diversity. *Transl. Psychiatry* *2*, e104.
- Wintgens, J.P., Wichert, S.P., Popovic, L., Rossner, M.J., and Wehr, M.C. (2019). Monitoring activities of receptor tyrosine kinases using a universal adapter in genetically encoded split TEV assays. *Cell. Mol. Life Sci.* *76*, 1185–1199.
- Yaffe, M.B. (2002). Phosphotyrosine-binding domains in signal transduction. *Nat. Rev. Mol. Cell Biol.* *3*, 177–186.
- Yin, D.-M., Chen, Y.-J., Lu, Y.-S., Bean, J.C., Sathyamurthy, A., Shen, C., Liu, X., Lin, T.W., Smith, C.A., Xiong, W.-C., et al. (2013). Reversal of Behavioral Deficits and Synaptic Dysfunction in Mice Overexpressing Neuregulin 1. *Neuron* *78*, 644–657.

Acknowledgment

First of all, I want to thank to Prof. Moritz Rossner, for the knowledge, the support and experience I gained from him. I am thankful for the open and honest work relationship, the discussions and insights and for the opportunity of being a member in his lab.

My thanks also go Dr. Michael Wehr, I am very grateful that I had the opportunity to work with such a supportive, patient supervisor who was always open for my questions, short or long discussions, and generally helping me enjoying science, maybe even as much as he does.

I want to thank Dr. Ben Brankatschk for the detailed discussions about any experiment, for being a role model critical thinking scientist, and for always having the time and motivation of thinking it through one more time.

I am also thankful to Dr. Sabrina Galinski for all the profiling knowledge she so willingly shared, for answering all those little or big questions I shot at her from the side of the desk, and for being a very pleasant office roomie.

Thank you also to Dr. Sven Wichert for teaching me robotics, for being supportive throughout my project and for being the good soul and positive human being he is.

Additionally, I want to thank Nadia Gabellini, Karin Neumeier, Monika Rübekel, Barbara Meisel, and Johanna Zach for their excellent technical support, their patience when teaching me in the beginning of the project and for the always friendly and productive relationship.

Finally, thank you to all members of MNB and the connected labs.